Journal of the
HYDRAULICS DIVISION
Proceedings of the American Society of Civil Engineers

CONTENTS

June, 1956

Papers

Paper 1004 HY 3

Journal of the
HYDRAULICS DIVISION
Proceedings of the American Society of Civil Engineers

VISUAL ACCUMULATION TUBE FOR SIZE ANALYSIS OF SANDS

B. C. Colby[1] and R. P. Christensen[2]
(Proc. Paper 1004)

SYNOPSIS

The visual-accumulation-tube method was developed primarily for making size analyses of the sand fractions of suspended-sediment and bed-material samples. Because the fundamental property governing the motion of a sediment particle in a fluid is believed to be its fall velocity, the analysis is designed to determine the fall-velocity-frequency distribution of the individual particles of the sample. The analysis is based on a stratified sedimentation system in which the sample is introduced at the top of a transparent settling tube containing distilled water. The procedure involves the direct visual tracing of the height of sediment accumulation in a contracted section at the bottom of the tube. A pen records the height on a moving chart. The method is simple and fast, provides a continuous and permanent record, gives highly reproducible results, and accurately determines the fall-velocity characteristics of the sample.

The apparatus, procedure, results, and accuracy of the visual-accumulation-tube method for determining the sedimentation-size distribution of sands are presented in this paper.

INTRODUCTION

The visual-accumulation-tube method for the size analysis of sands was developed as a part of a general series of investigations entitled "A Study of Methods Used in Measurement and Analysis of Sediment Loads in Streams" and sponsored by the Subcommittee on Sedimentation, Inter-Agency Committee on Water Resources (formerly Federal Inter-Agency River Basin

Note: Discussion open until November 1, 1956. Paper 1004 is part of the copyrighted Journal of the Hydraulics Division of the American Society of Civil Engineers, Vol. 82, No. HY 3, June, 1956.

1. Hydr. Engr., Geological Survey, U. S. Dept. of the Interior, Minneapolis, Minn.
2. Hydr. Engr., Corps of Engrs., U. S. Dept. of the Army, Minneapolis, Minn.

Committee[3]). The developmental work was carried on at the St. Anthony Falls Hydraulic Laboratory, University of Minnesota, by the active cooperation of the U. S. Geological Survey and the Corps of Engineers, U. S. Army; financial assistance was given by the U. S. Bureau of Reclamation.

Size analyses of sands have been made for many years. With recent added attention to sediment-transport problems in streams, the emphasis has shifted toward the determination of fall velocity or sedimentation size instead of physical size or volume of the individual grains. In fluvial sediment problems, the fall velocity of an individual particle in water appears to be the most significant and fundamental measurement of particle size.[4,5] None of the size-analysis methods previously available for sands were sufficiently economical and at the same time sufficiently accurate in establishing the fall velocity distribution that would be found if each particle of the sample was dropped individually. The many sedimentation-size analysis methods that did determine the rate of fall of the sample actually indicated a settling velocity that was affected by concentrations of material, space limitations, and other influences inherent in the combination of sample, fluid, and apparatus.

The VA-tube method for analysis of sands was developed to meet two principal requirements:

1) The method must be fast, inexpensive, and adaptable for use by personnel having little scientific training.
2) Results must be based on the fall velocity of the individual particles composing the sample.

Direct measurement of the fall velocity of the individual particles was not practical for routine size analyses. However, a velocity-frequency distribution may be obtained by allowing a sand sample to settle through a definite length of water column. Sediment is introduced at the top of a column of distilled water, and the rate of sediment accumulation is measured at the bottom. This general settling-velocity method is not new; Benningsen,[6] Kennedy,[7] Werner,[6] Emery,[6] Travis,[8] and others[6] have used similar sedimentation-

3. "Measurement and Analysis of Suspended Sediment Loads in Streams," by M. E. Nelson and P. C. Benedict, Trans., ASCE, Vol. 116, 1951, pp. 917-918.
4. "Development of a Stratified-Suspension Technique for Size-Frequency Analysis," by H. J. Skidmore, Thesis, Dept. of Mechanics and Hydraulics, Iowa State University, 1948, p. 2.
5. "A Study of Methods Used in Measurement and Analysis of Sediment Loads in Streams," Subcommittee on Sedimentation, Inter-Agency Committee on Water Resources, Report No. 7, Corps of Engrs., U. S. Dept. of the Army, St. Paul District, St. Paul, Minn., 1943, pp. 14-15.
6. "A Study of Methods Used in Measurement and Analysis of Sediment Loads in Streams," Subcommittee on Sedimentation, Inter-Agency Committee on Water Resources, Report No. 4, Corps of Engrs., U. S. Dept. of the Army, St. Paul District, St. Paul, Minn., 1941, pp. 74-76, 144-146.
7. "Report on the Deposit, and Scour of Silt in the Main Line, Sirhind Canal, and on the Silt Experiments 1893-1898," by R. G. Kennedy, Punjab Public Works Dept. of Irrigation Br. Paper No. 9.
8. "Measurement of Average Particle Size by Sedimentation and Other Physical Means," by P. M. Travis, Am. Soc. for Testing Materials, Bull. No. 102, 1940, pp. 29-32.

size methods. Their analyses determined the quantities of sediment that settled the length of the water column within given intervals of time, and each time interval corresponded to a definite settling velocity.

The velocity-frequency distributions obtained by the general settling-velocity method differed from those for the fall velocity of the individual particles for three reasons: (1) The sample could not be introduced at the top of the water column so that all particles would start to settle from the same elevation at the same time and without mutual interference. (2) The rate of fall of each particle was affected by the nearness of the tube walls, the influence of adjacent particles, and the density currents set up in the fluid. In addition, the effects varied because of the contracting and contracted sections of sedimentation tube which were a part of most systems of this type. (3) Whether the accumulation of sediment was measured in place at the bottom of the sedimentation tube or was removed for measurement, inaccuracies were inherent in determining the quantity settled out of suspension at given time intervals.

Usually the velocities obtained in any of the many sedimentation systems have been accepted without critical investigation as equal to, or at least representative of, the fundamental fall velocity of the particles. Emery[9] calibrated his fall velocity apparatus with quartz sands of established sieve-size distributions. This procedure does not meet the needs of the present investigation of fall velocity. His calibration showed that quartz particles of the smaller sand sizes fell much faster in the Emery tube than would quartz spheres of the same sieve sizes. The coarse sand particles did not show the same degree of difference.

A more exacting study of fall velocity was made for the VA-tube development. For the finer sand sizes, in the range 62 to 125 microns, the velocities in the VA-tube were about 40% greater than those of the same particles falling along. The difference between rates of fall under the two conditions gradually reduced to zero at the coarse or very coarse sand sizes.

For the VA-tube development the fall velocity of the individual particle in water has been accepted as the fundamental measurement of particle size. "Standard fall velocity" may be defined as the terminal uniform settling velocity of the particle falling alone in quiescent distilled water of infinite extent and at a standard temperature of 24°C. This is the ideal fall velocity for the VA-tube development. However, a standard temperature is not generally accepted, and not all determinations of fall velocity can be made at 24°C. The settling velocity of a sand particle may be determined at another temperature and converted to that at 24°C by the relation for quartz spheres.[10] Unpublished data[11] support theoretical considerations which indicate that determinations within normal ranges of laboratory temperatures, if converted by the relation for spheres, will yield fall velocities essentially the same as

9. "Rapid Method of Mechanical Analysis of Sand," by K. O. Emery, Jour. Sed. Petrology, Vol. 8, No. 3, pp. 105-110.
10. "A Study of Methods Used in Measurement and Analysis of Sediment Loads in Streams," Subcommittee on Sedimentation, Inter-Agency Committee on Water Resources, Report No. 4, Corps of Engrs., U. S. Dept. of the Army, St. Paul District, St. Paul, Minn., 1941, Fig. 5.
11. "Preliminary Report on the Fall Velocity of Missouri River Sand" by L. C. Fowler, Missouri River Div., Corps of Engineers, U. S. Army.

those in water at 24°C. "Fall velocity" will be used herein as the terminal uniform settling velocity of a particle falling alone in quiescent distilled water of infinite extent. A quantitative expression for fall velocity must be accompanied by a statement of the temperature at which it applies.

The actual settling velocity of particles in the VA-tube was not the same as the fall velocity of the individual particles. Sedimentation theory was inadequate to define the relation between the two. Therefore, a calibration procedure was substituted for theoretical definition so that the effects of mutual interference of particles, size limitations of the system, and volume-weight relations did not require separate determinations.

The instrumentation and techniques for the VA-tube method possess several advantages over previous processes of the same type, but the really significant improvement lies in this calibration which makes possible the direct determination of the fall-velocity distribution of the sample. The calibration was accomplished by analyzing hundreds of sand samples for which the fall-velocity characteristics had previously been established. The preparation of such samples was made possible by new techniques for determining the fall-velocity frequency distribution of sand samples.

As a concession to those accustomed to a linear-size designation, the term "fall diameter" is introduced. The fall diameter of a particle is the diameter of a sphere that has a specific gravity of 2.65 and also has the same terminal uniform settling velocity as the particle when each is allowed to settle alone in quiescent distilled water of infinite extent and at a temperature of 24°C. The temperature qualification in the definition is necessary only for precision; within the normal range of laboratory temperatures the effect of temperature on fall diameters is usually negligible.

Twelve sets of the VA-tube apparatus were delivered to various sedimentation laboratories in 1954. In some of these laboratories, the method has been in routine use for several months and has been considered satisfactory. Improvements in apparatus and technique can undoubtedly be made as the result of further field experience.

Visual-Accumulation-Tube Method

Samples Suitable for Analysis

Samples whose particles are mainly in the range of sand sizes are suitable for analysis in the VA-tube. The weight of the samples may be as small as 0.05 gm for fine sands and as large as 15 gm for samples with a normal size distribution. If many coarse particles, larger than a sieve diameter of 1 or 2 mm, are present in a sample, they are removed by sieving. If any clay or much silt (sizes under 62 microns) is contained in a sample, it is removed before VA-tube analysis. Some coarse silt does not affect the accuracy of results, but appreciable quantities of silt require additional time for making the analysis. The clay and silt fractions should be separated from the sand by sieving or by sedimentation processes, but the division need not be at a precise size.

Samples for analysis should be relatively free of organic matter and in such condition that the grains will fall as individual particles and not in aggregates. The sand particles should be thoroughly soaked in water before analysis so that every particle is completely wetted; they should be contained in not more than 40 ml of water at a temperature no lower than that of the water in the sedimentation tube.

Visual-Accumulation Tube

The apparatus for the VA-tube method of analysis consists of the following main parts as shown in Fig. 1:

1) A glass funnel, or tube-and-funnel combination, about 10 in. long.
2) A rubber tube that connects the funnel and the main sedimentation tube and that together with a special clamping mechanism serves as a valve.
3) A glass sedimentation tube. Tubes are of 2 lengths. A 180-cm tube has a 140-cm section of 2-in. inside diameter, a 20-cm contracting section, and a 20-cm accumulation section of 10-mm inside diameter. This long tube is used for the analysis of bed, beach, or other sands of coarse sizes when a sufficient quantity of the material is available. A 120-cm tube has an 80-cm section of 1-in. inside diameter; a 20-cm contracting section; and a 20-cm accumulation section with an inside diameter of 2.1, 3.4, 5.0, or 7.0 mm. The short tube is suitable for the analysis of suspended-sediment samples that contain only small quantities of sand that is mostly less than 1 mm in diameter. An elastic plug is inserted in the lower end of the accumulation section to close the tube.
4) An electrically operated tapping mechanism that strikes against the glass tube and helps keep the accumulation of sediment uniformly packed and level on top.
5) A special VA-tube recorder which consists of: (1) A carriage that can be moved vertically by a hand-operated mechanism and on which are mounted a recording pen and an optical instrument consisting of a 2-power telescope eyepiece with a horizontal cross hair. (2) A cylinder that carries a chart and rotates at a constant rate during the analysis.
6) The recorder chart is a printed form on which the pen draws a continuous record of the accumulation.

Plans and specifications are available for all items of the visual-tube equipment. The cost of the complete visual-tube apparatus is about $500, or approximately that of a set of sieves and sieve shaker.

Selection of Tube Size

A necessary preliminary to analysis is the choice of the proper tube size for a given sample. Frequently, two sizes or more would be satisfactory. The quantity of sand and the upper particle-size limit in a sample are used as guides in selecting the tube size. Table 1 indicates the limitations on sand samples suitable for analysis in each size of tube. If the pertinent characteristics of samples are not known from previous experience with the sampled stream, the sample to be analyzed may be compared with a set of synthetic samples. For instance, a sample may be analyzed in a 2.1-mm tube if it does not exceed in quantity or particle size a synthetic sample containing about 0.8 gm of sand with a maximum particle size of 250 microns.

The maximum particle sizes shown in Table 1 are those that should not be exceeded by a significant percentage of the sample. The percentage of excess may be greater if the sample is small in relation to the capacity of the tube or if the analysis of the coarser portion is not highly important.

Normally, the best results are obtained if the total height of accumulation in the bottom of the tube is between 1 and 4 in. If a sample has a very limited size range or the material is predominantly coarse, better results are obtained with maximum heights less than 4 in. If a satisfactory tube size is not selected the first time, the sample can be rerun in another size of tube.

Table 1.--Guide to Selection of Tube Size

Sample		Maximum particle size		Sedimentation tube	
Dry weight (gm)	Volume of sand (ml)	Fall diameter (microns)	Sieve diameter (microns)	Length (cm)	Size (mm)
0.05- 0.8	0.03-0.5	250	250	120	2.1
0.4 - 2.0	0.2 -1.2	350	400	120	3.4
0.8 - 4.0	0.5 -2.4	500	600	120	5.0
1.6 - 6.0	1.0 -4.0	700	1,000	120	7.0
5.0 -15.0	3.0 -9.0	--	2,000	180	10.0

However, the choice of a suitable tube is not difficult because the usable limits of the respective tubes overlap considerably.

Methods of Analysis

The authors and their assistants have analyzed many samples with the visual-accumulation tube. These analyses required less than 10 minutes if the particles in the sample had fall diameters greater than 62 microns. More samples could be analyzed per hour than by sieving. If silt was present, the analysis took a longer time. For those who might be interested, the step-by-step procedure used by the authors is as follows:

1) The proper chart for the chosen length of tube is selected and, after notes to identify the sample, operator, and analysis are written on the chart, it is placed on the drum. (The 180-cm tube requires a different chart than the 120-cm tubes because of the greater distance through which the sample must settle.)
2) The recorder pen is oriented on the zero-accumulation and zero-time lines of the chart.
3) The recorder is adjusted to bring the horizontal hair in the eyepiece level with the top of the tube plug where the accumulation of sediment begins.
4) When the apparatus, including the proper sedimentation section, is assembled, the tube is filled with distilled water to just above the valve. The temperature of the water in the tube is recorded, and the valve is closed. The water need not be changed for succeeding analyses.
5) The electrical tapping mechanism is started; this operation also closes the electrical circuit to a switch at the valve so that opening the valve starts rotation of the cylinder.
6) The sand sample is washed into the funnel above the closed valve and is stirred briskly for 10 seconds.
7) The valve is immediately and fully opened. Because opening the valve automatically starts the cylinder, the chart time and the settling of the particles in the tube begin simultaneously.
8) The operator watches through the eyepiece and, as soon as the first particles reach the bottom of the tube, he moves the carriage vertically at a rate that keeps the horizontal hair on a level with the top of the accumulation of sediment. This procedure continues until the pen has passed the 62-micron size on the chart. Then rotation of the cylinder automatically stops. If material is still falling, the tracking operation is continued, at least intermittently, until the maximum height of accumulation is determined.

9. While the pen stands at the maximum height of accumulation, the cylinder is rotated by hand to extend the line of maximum accumulation across the chart.
10. After the valve is closed, the sample is drained into a beaker by removing the tube plug. If necessary, the valve is opened slightly to drain out the sample. The plug is replaced.
11. The chart is removed from the recorder.

Calibration

The settling velocity of sediment particles varies with many factors including the size of sedimentation column, the presence of other particles, and the manner of introducing the sample. In the VA-tube method, the finer sands fall as much as 40% faster than individual particles, while the coarser sizes are affected to a lesser degree. A fall diameter of 250 microns corresponds to a fall velocity of 3.44 cm/sec when the particle falls alone in distilled water at 24°C and corresponds to a settling velocity of about 4.4 cm/sec when the particle falls in the visual tube in the presence of other particles in water at 24°C. Results expressed in terms of the fall diameter of the individual particles were, therefore, obtainable only by calibration of the VA-tube method. A satisfactory calibration required analysis of hundreds of sand samples for each of which the fall-diameter distribution had been previously determined.

Determination of Fall-Diameter Distribution

Test samples of known fall-diameter distribution were needed for calibrating the VA-tube method. There was no available method for satisfactorily compositing samples having known fall-diameter distributions; therefore, one was developed that was based on the fall velocities of the individual particles. The primary concept was simple and obvious, and other investigators had pointed the way. Carey and Stairmand[12] had developed a photographic method for determining the fall velocity of individual grains in samples composed of particles smaller than 100 microns. Serr[13] had determined the sedimentation-diameter distribution for sands of sizes larger than about 140 microns by an individual dropping of many representative particles from each of several sieve fractions.

The essentials of the procedure developed for determining the fall-diameter distribution for sands were as follows: A bulk sample of sand was sieved, 10 gm at a time, until the desired quantity of material of each sieve fraction had been obtained. The sieve-size distribution based on the total weight of each fraction was recorded. Then each sieve fraction was carefully split and resplit until about 100 representative particles remained. The particles from a sieve fraction were dropped individually in distilled water, and the fall velocity of each was determined and converted into fall diameter

12. "Size Analysis by Photographic Sedimentation," by W. F. Carey and C. J. Stairmand, Inst. of Chem. Engr., London, Trans., Vol. 16, 1938, pp. 57-62.
13. "A Comparison of the Sedimentation Diameter and the Sieve Diameter for Various Types of Natural Sands," by E. F. Serr, III, Thesis in Irrigation Engr., Colorado A & M College, Fort Collins, Colo., 1948.

by using the relation of the diameter of a quartz sphere to its settling velocity in water.[10] The fall diameters of the particles were cubed to approximate their relative volumes and weights. A fall diameter was chosen at about the median division of a summation of the cubed diameters arranged in order of size. A summation was made of all cubed diameters smaller than the median, and this sum was expressed as a percentage of the total of all the cubed diameters. For example, assume that the sum for particles smaller than 305 microns was 48% of the sum for the sieve fraction 250 to 350 microns. If, in the recorded sieve size distribution for the bulk sample, 50% was finer than 250 microns and 10% was in the 250 to 350 fraction, then 50 plus 4.8 or 54.8% of the total sample had fall diameters smaller than 305 microns. Extending this process to all the sieve fractions completed the fall-diameter distribution for the sample.

Fig. 2 shows the fall-diameter distribution and the sieve-diameter distribution for a sand sample. A sieve-size distribution curve is defined only at the sizes of sieves actually used. A fall-diameter distribution curve, obtained by the method above is defined only at the approximately median sizes chosen to divide the fractions. Common practices which introduce errors are (1) the use of average or mean figures between defined points on size-distribution curves, and (2) the substitution of particle counts that are unweighted for distributions by weight.

Four comments that pertain to the method of determining fall-diameter distributions are justified.

1) The cube of the fall diameter was assumed to be proportional to the weight of the particle. This relationship is not always exact, but for a a group of particles, the cube more adequately represents the volume and weight than would the first power of the fall diameter. Even use of the first power of the fall diameter would not seriously alter the results if the range of sizes for a fraction was small.
2) The previously cited process for computing the size distribution required modification if a significant percentage of material in the sieve fractions coarser than 350 microns had fall diameters less than 305 microns or if a significant percentage of material in the sieve fractions finer than 250 microns had fall diameters greater than 305 microns. The necessity for modification was readily apparent and was infrequent except for very coarse sieve fractions. By extra computations the weight equivalent of offending material was transferred from the original sieve fraction to the proper side of the 305-micron size.
3) Splits of 100 particles from each of about 8 sieve fractions were generally adequate to determine the fall-diameter distribution. The fall-diameter distribution curve should have a shape similar to that for the sieve-diameter distribution, and any inconsistency in the results of a split was immediately obvious from a plot of the size distribution. If inconsistencies were minor, the results for adjacent sieve fractions were averaged when drawing the final distribution curve; but, if any large discrepancy was found, the split was rechecked or repeated. In the example cited, if the 48% smaller than the cube of 305 microns should actually have been 40% (an extreme variation) the percentage finer would have been changed only from 54.8% to 54.0%. Errors in individual splits (1) were independent of those for other splits, (2) were not subject to cumulative errors, and (3) generally applied to small fractions of the total sample.

4) Within the temperature range from 20°C to 30°C, the effect of temperature on the settling velocity of a particle of sediment in water was considered to be essentially the same as that on the velocity of a sphere that has a specific gravity of 2.65.

Test Samples of Known Fall-Diameter Distribution

The process for determining the fall-diameter distribution of a sand is a laborious one, and applying it directly to many sands in order to calibrate the visual-tube method would not have been feasible. However, many test samples could be composited from the sieve fractions of any one sand for which the fall-diameter distribution had been determined. In this manner a large supply and variety of test samples were obtained.

The original relative weights of the various sieve fractions were composited into samples having the same sieve- and fall-diameter distributions as those in the original sand. These samples were made up in a variety of total weights, and duplicate samples could be compounded in any or all of the weights. Different relative weights of the various sieve fractions were used to obtain test samples of different size-frequency distributions. The fall-diameter distribution was readily computed for each of these samples by the same methods used for the original sand. In the former illustration 48% of the sieve fraction 250 to 350 microns was finer than a fall diameter of 305 microns. If a test sample was made up in which 60% of the sample was from sieve sizes finer than 250 microns and 20% was from the 250 to 350 sieve fraction, then 60 plus (48 x 20/100) or 69.6% of the test sample was finer than a fall-diameter of 305 microns. Extending the process to the other sieve fractions completed the fall-diameter distribution for the test sample, and percentages finer than desired division sizes could be determined from a plotting of the distribution.

Method of Calibration

Nearly 300 analyses of samples with predetermined fall-diameter distributions were available for the calibration of the VA-tube method. The calibration was incorporated in two charts, one for the 120-cm tubes and one for the 180-cm tubes.

Each analysis produced a curve of sediment accumulation with time. (See Fig. 3.) Because the percentage finer than each division size was already known for a calibration sample, the percentage of the total accumulation that should occur at each division size was known. The point on the chart at which the proper percentage of the accumulation occurred for a given division size indicated the location at which the division-size line must be placed to divide the accumulation at the proper percentage. Assume that 40% of a calibration sample was finer than 125 microns. Then the intersection of the pen trace with the elevation for 60% of the total accumulation fixed the distance from the time origin at which the proper percentage for the 125 micron size was obtained. Consequently, for the temperature of analysis, each analysis established a point on the chart for each division size in the sample. A series of analyses of known samples supplied a group of points tending to define the proper location of each division-size line. The distance of a division-size line from the time origin of the chart is a measure of the time for that division size of particle to fall in the VA-tube.

Analyses at other temperatures provided information for adjustments for temperature. Actually there were not enough analyses to define completely the effect of temperature on the time of fall, but the effect of changes in

temperature was considered proportional to the effect on the fall velocities of spheres--an assumption that could not be much in error for the relatively narrow range of temperatures encountered in the analyses.

Average times from all analyses in the 120-cm tube could be satisfactorily combined into one chart provided that the previously stated limits (Table 1) of sample quantity and particle size were regarded. The chart for the 120-cm tubes is shown in Fig. 4. A second chart was prepared for the 180-cm tube.

The calibrated charts show analyses directly in the desired terms of fall-diameter distribution by weight, which is equivalent to fall-velocity distributions by weight. Therefore, the calibration automatically covers the effects of such conditions as particle concentration and size, methods of introducing the sample, size limitations of the system, and the fact that accumulation is measured in terms of height or volume instead of weight.

The charts were designed to give the best average results for sands similar to those used in calibration. If much work is to be done with a given sand, especially one that may have highly unusual qualities, then a check calibration should be made for that sand if extremely accurate results are required.

Results from Analysis

Size Distribution from the Chart

In the VA-tube analytical procedure, the pen trace on the chart is a curve for which time is the abscissa and height of accumulated sediment is the ordinate. The curve is a continuous record of the size distribution of the sample. According to custom, analytical results are expressed as percentages of the sample finer (or coarser) than specified division sizes; one common series of these sizes is shown on the chart for the 120-cm tube in Fig. 4. The various temperature lines and the spread between them are required by, and indicate the magnitude of, temperature effects on the analyses. These temperature effects are in proportion to those for spheres of specific gravity 2.65.

The percentages finer than those sizes shown on the recorder chart were found from the chart by use of a scale that when placed at a convenient angle would divide the total accumulation into 100 equal parts. (See Fig. 4.) Briefly, the procedure is as follows: The intersections of the accumulation curve and the division-size lines for the temperature of analysis are marked. Points are interpolated along the curve for temperatures between the positions of the plotted size lines. The zero percent of the scale is placed on the total-accumulation line, and the 100% on the zero-accumulation line. The scale is moved horizontally to the intersection of the curve with the size-temperature line. The percentage finer that the division size is represented by the portion of the total accumulation that lies above the curve and may be read directly on the scale.

Several modifications of the method for reading percentages from the chart are possible. Horizontal lines may be drawn through the intercepts on the curve, and all percentages may be read from one position of the scale. If 10% of material coarser than that analyzed in the visual tube was removed from the sample prior to analysis, then the 90% mark may be used on the zero-accumulation line to show readings directly in percentages of the total sample. Similarly, if 40% of the original sample was removed as silt and

clay before visual-tube analysis, the 40% mark may be used on the total-accumulation line to obtain direct readings in percentages of the total sample. The scale may be reversed to show readings in percentages coarser.

Accuracy of Method

The fall-diameter distributions of the samples analyzed for calibration of the visual-tube method were predetermined from individual particle drops. The fall-diameter distributions obtained from the visual-tube analyses were compared with the predetermined fall-diameter distributions to define the accuracy summary shown in Table 2. The data are in terms of differences in percentage finer figures. If, for example, the known amount finer than 125 microns was 40% by weight and the analysis showed 38%, then the difference is -2% and any percentage between 38 and 42 would be within 2% accuracy. Over 75% of the results for all division sizes were within 2% of the known distribution. The accuracy is shown for the various tube sizes, for different sand mixtures classified according to predominant size, and for several fall diameters.

Analyses in the various sizes of tube were about equally accurate except that the accuracy in tubes having a 2.1-mm accumulation section was comparatively low. The reduction in accuracy may have been due to the restricted size, but it probably reflected difficulties in compounding duplicate samples and in analyzing the small quantities of the samples for this small tube.

The accuracy differed somewhat for the various sand mixtures that were analyzed. The very coarse sands contained only a small range of sizes and, consequently, had high concentrations of material at some of the division sizes; the accuracy was lower for these sands. Any small difference in chart time, fall velocity, or calibration produced much greater errors in percentage of the total sample if the concentration of particles was high at a division size.

Variations in accuracy at the different fall diameters were probably not significant except that the high concentrations of material at the 1000-micron size resulted in lower accuracy. At other division sizes the proportion of samples having high concentrations was small. The accuracy at the 62-micron size tended to be high because in many samples the concentration at this size was rather low.

Although Table 2 was based on a large number of analyses there may be occasional samples that can not be analyzed with the same accuracy. The effect of specific gravities much different from 2.65 has not been evaluated, except that samples containing some relatively light-weight material showed no identifiable reduction in accuracy. Several samples composed of one or two sieve fractions have been analyzed but no general evaluation of accuracy has been made for these samples. Analysis of a single sieve fraction produces problems of high and rapidly changing concentrations which are undesirable.

SUMMARY

The visual-accumulation-tube method is rapid, economical, and accurate for obtaining the sedimentation-size distribution of sand samples. The significant technical advance is the development and calibration of an instrument that records results in terms of the fall velocity of the individual particles of the sample.

The fall velocity of the individual particles is one of the most fundamental properties governing the action of sediment in a fluid. The VA-tube method is an improved means of establishing this fundamental property of sands.

An average calibration for the VA-tube was based on analyses of hundreds of samples of known fall-diameter distribution by weight. The calibration provided for normal variations in sand samples; in extremely unusual circumstances, the calibration should be rechecked.

For samples containing only sand sizes, the VA-tube method is a faster means of determining size distribution than the standard sieving method. Therefore, it may justify consideration outside the field of purely sedimentation problems.

The method has been used satisfactorily by several laboratories over a period of many months.

A 16-mm film is available for showing the apparatus and for demonstrating the analytical procedures of the VA-tube method.

ACKNOWLEDGMENTS

The development of the visual-accumulation-tube method was under the general supervision of P. C. Benedict, M. ASCE (U. S. Geological Survey), and M. E. Nelson, M. ASCE (Corps of Engineers, U. S. Army). G. M. Watts, J. M. ASCE, and C. O. Johnson, J. M. ASCE, (U. S. Geological Survey) contributed valuable assistance in the development.

Table 2.--Accuracy of the visual-tube method

Qualification	Observations within given limits, %					Total observations
	Within 1%	Within 2%	Within 3%	Within 5%	Within 10%	
SEDIMENTATION TUBE						
Diameter of accumulation section, mm:						
2.1	36.9	64.2	81.0	95.5	100.0	179
3.4	56.8	80.5	92.4	99.7	100.0	384
5	54.2	75.7	90.7	99.3	100.0	432
7	62.0	84.3	95.2	100.0	100.0	166
a 10	50.9	77.0	88.7	98.1	100.0	318
b 4 and 9	59.4	82.1	95.1	100.0	100.0	224
All observations	53.8	77.5	90.7	98.9	100.0	1,703
SAND MIXTURE						
Predominant size:						
Very coarse sand	44.4	61.1	77.7	94.4	100.0	18
Do	33.3	52.8	63.9	86.1	100.0	36
Coarse sand	50.0	81.2	92.2	100.0	100.0	64
Do	48.2	83.9	92.9	100.0	100.0	56
Do	51.7	81.7	93.3	100.0	100.0	60
Do	52.3	75.0	93.8	100.0	100.0	128
Medium sand	59.4	81.2	95.0	100.0	100.0	160
Do	55.2	79.6	92.5	99.6	100.0	496
Fine sand	62.0	87.5	96.0	99.5	100.0	200
Do	44.3	63.0	82.1	98.0	100.0	246
Very fine sand	53.3	82.2	91.1	98.5	100.0	135
Do	62.5	76.9	89.4	98.1	100.0	104
All observations	53.8	77.5	90.7	98.9	100.0	1,703
FALL DIAMETER						
Division size, microns:						
1,400	72.2	80.6	88.9	97.2	100.0	36
1,000	25.0	58.3	75.0	86.1	100.0	36
700	56.6	79.2	89.3	100.0	100.0	159
500	46.4	75.2	94.1	100.0	100.0	153
350	45.4	70.3	87.6	99.5	100.0	185
250	53.8	78.8	93.9	100.0	100.0	212
175	50.4	80.7	92.9	98.7	100.0	238
125	49.2	75.6	88.2	99.2	100.0	238
88	56.5	74.4	87.9	98.2	100.0	223
62	71.3	87.0	95.1	99.1	100.0	223
All observations	53.8	77.5	90.7	98.9	100.0	1,703

a 180-cm sedimentation tube; other sizes refer to 120-cm tubes.
b Experimental tube not used for routine analyses.

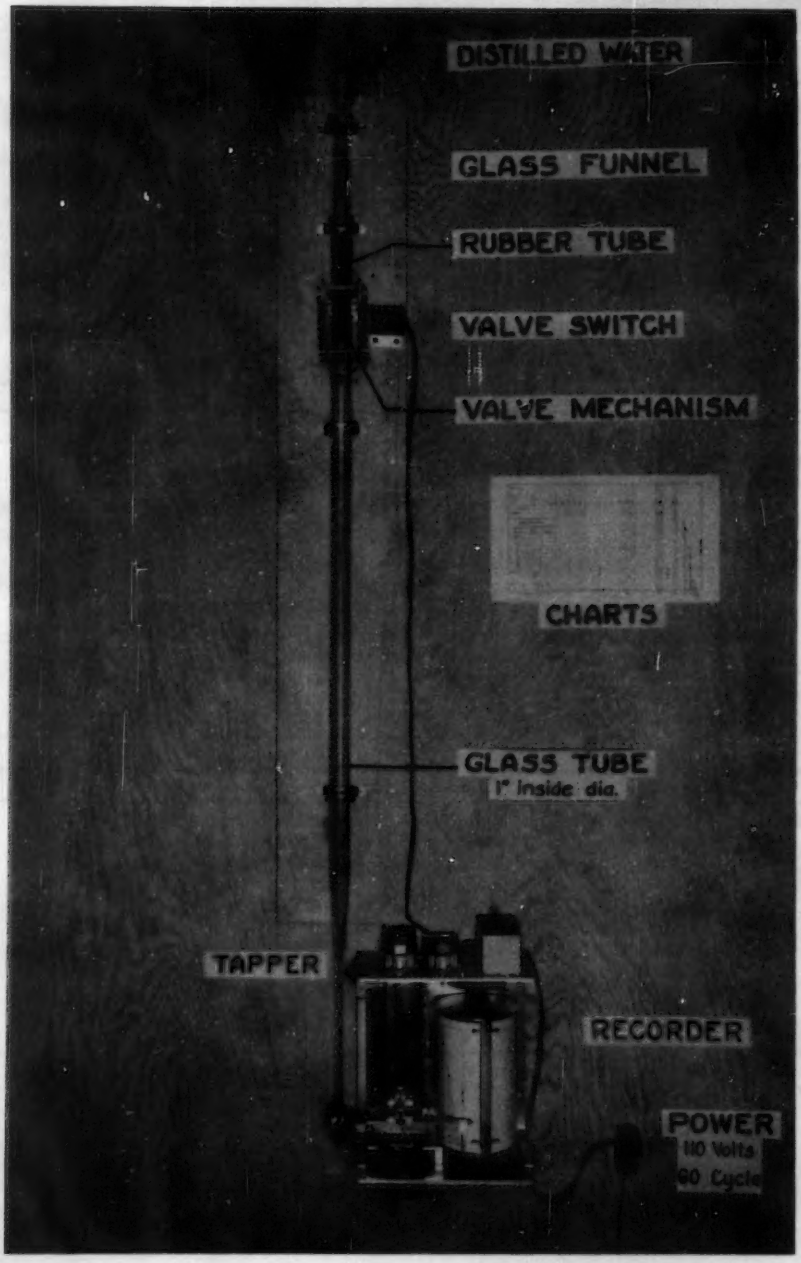

Fig. 1--Visual-Accumulation-Tube Apparatus

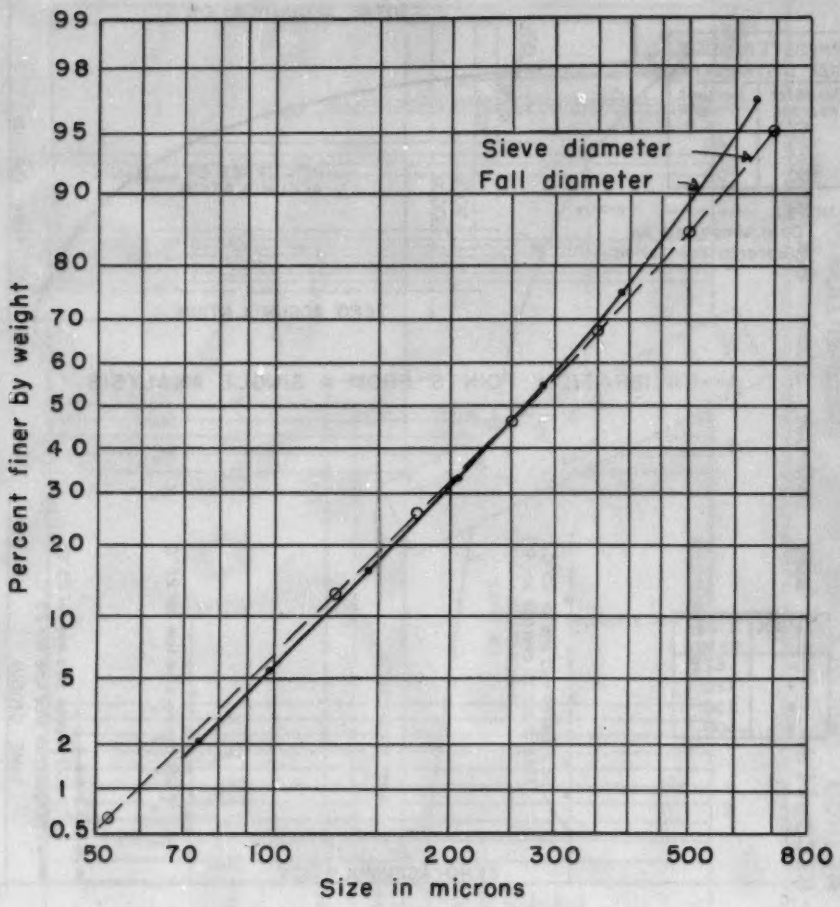

FIG. 2 — FALL- AND SIEVE-DIAMETER DISTRIBUTION

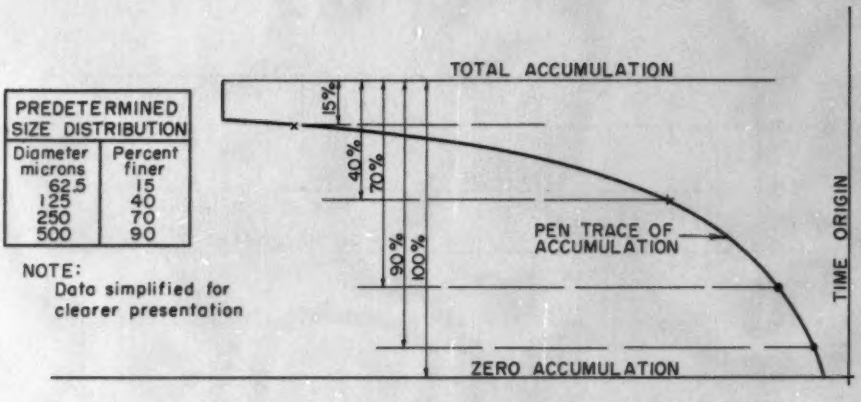

A--CALIBRATION POINTS FROM A SINGLE ANALYSIS

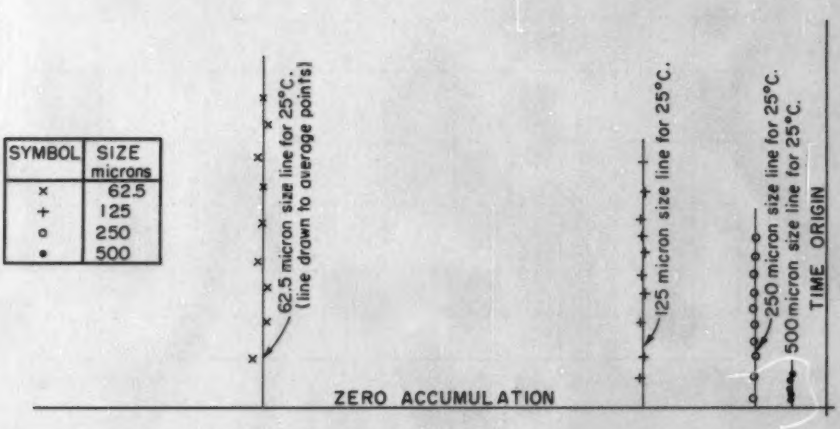

B--CALIBRATION POINTS FROM SEVERAL ANALYSES AT 25°C

FIG. 3--FUNDAMENTALS OF CALIBRATION METHOD

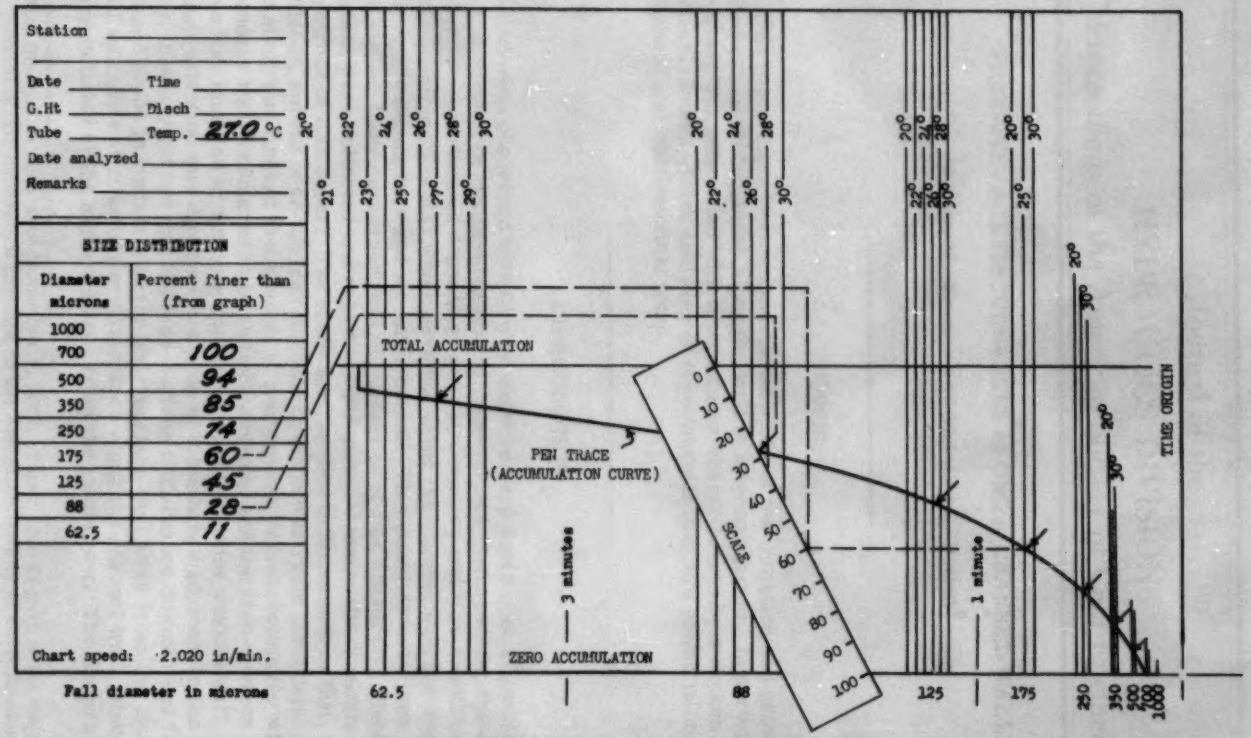

FIG. 4 — RECORDER CHART FOR 120-CM TUBE SHOWING METHOD OF READING SIZE DISTRIBUTION

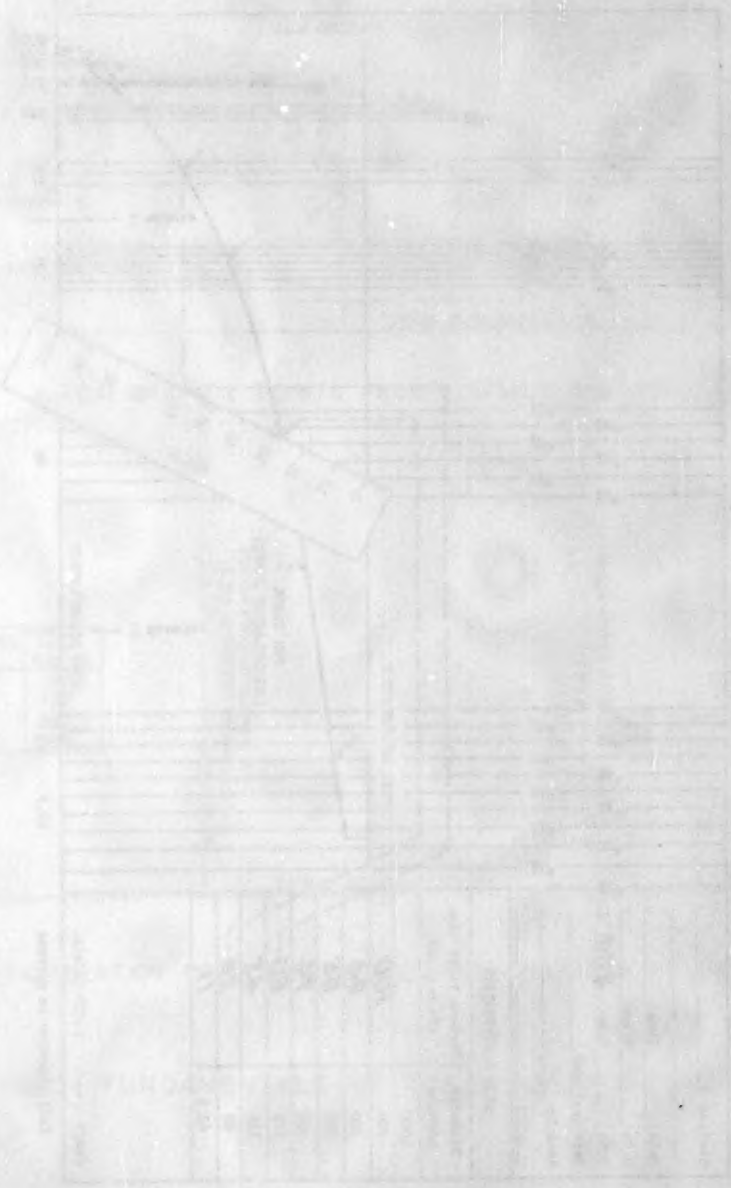

Paper 1005 HY 3

Journal of the
HYDRAULICS DIVISION
Proceedings of the American Society of Civil Engineers

FREE-SURFACE DISTURBANCES ALONG A CHANNEL WALL

Amein M. Amein[1] and Melville S. Priest[2]
(Proc. Paper 1005)

SYNOPSIS

This paper reports an experimental study of the initiation and growth of free-surface disturbances along the wall of a steep channel. In particular, the study was concerned with disturbances characterized by a broken liquid surface. Results from analyses of experimental data are shown in both graphical and mathematical form.

INTRODUCTION

Problems concerned with flow of water in very steep open channels may be complicated by the development of free-surface disturbances, the character of the disturbances depending upon the boundary and flow conditions. One such disturbance is that which develops along the channel wall and results in a broken watersurface and air entrainment. This paper summarizes an experimental study concerned with disturbances of this character. Experimental data were collected and reported by Amein,(1) under the direction of his co-author of this paper. The study was devoted to disturbances that, once initiated, spread over the free-surface in the downstream direction. Further, the study was limited to a channel of rectangular cross-section for which the boundary was considered to be initially smooth, and the free-surface disturbance was initiated by fixing a thin wire to the otherwise smooth wall. Although attention was directed to a zone of disturbance adjacent to the channel wall, it was observed that the free-surface disturbance downstream from a pointed probe in contact with the watersurface well away from the channel wall was quite similar to the disturbance along the channel wall, when both were initiated at the same distance from the inlet crest. The disturbance

Note: Discussion open until November 1, 1956. Paper 1005 is part of the copyrighted Journal of the Hydraulics Division of the American Society of Civil Engineers, Vol. 82, No. HY 3, June, 1956.

1. School of Civ. Eng., Cornell Univ., Ithica, N. Y.
2. Prof. of Civ. Eng., Alabama Polytechnic Inst., Auburn, Ala.

studied might best be described as exhibiting the characteristics of a wake. The conditions associated with initiation and growth of the free-surface disturbances are presented through relations of dimensionless parameters.

Equipment and Procedure

The experiment was conducted with equipment operated by the Department of Hydraulics, Cornell University. The channel is a glass-walled, tilting flume with a width of 18 inches and a plane-bottom length of 12 feet. Water flows from a reservoir, over a curved bottom, and into the flume. Discharge was determined by means of a Venturi meter installed in the supply pipeline. Inclination of the channel bottom to the horizontal was determined by means of an engineer's level and metal tape. Depth of flow in the flume was measured with a micrometer screw used as a point gage. The characteristics of the free-surface disturbances were observed by placing a light source at the upstream end of the flume and viewing the watersurface from such a position that reflection of light made the disturbance clearly visible.

For each angle of inclination of the channel bottom, data were collected for several different discharges. For each discharge, a thin wire was moved, from some distance downstream from the crest, step by step in the upstream direction along the channel wall to find the upstream limit at which it was possible to initiate the free-surface disturbance. The wire extended from the channel bottom to well above the free watersurface, with the longitudinal axis normal to the channel bottom. Having established the limiting location at which the disturbance could be initiated, the discharge, length from the inlet crest, depth of flow at the limiting cross-section, and water temperature were determined.

For each particular inclination of the channel bottom and discharge, growth of the free-surface disturbance was studied. The disturbance was initiated by fixing the thin wire to the channel wall. The resulting free-surface disturbance was periodic in nature such that the outer edge of the disturbance is a wave form that is progressive in the downstream direction. Coordinates describing growth of the disturbance were measured to the outer limit or envelope of the wave form. Also, discharge, depth of flow at the cross-section of initiation, and water temperature were determined. The disturbance was initiated at several different locations along the channel wall, and coordinates measured, for each discharge. Data were collected for several different discharges for each inclination of the channel bottom.

The overall experimental limits were: angle of inclination of the channel bottom to the horizontal, from 10° to 45°; discharge, from 0.0177 to 0.0730 cfs; and water temperature, from 38.0 to 44.0°F.

Experimental data are shown in Appendices 1 and 2.

Analysis

Quantities pertinent to conditions that are just sufficient for initiation of the free-surface disturbance may be related through the dimensionless parameters of the function

$$\delta/x = 0.00686\,(U\delta/\nu)^{0.237}$$

where U is mean velocity of flow across the cross-section of initiation, L is length from the inlet crest to the cross-section of initiation, ν is kinematic viscosity of the water, and D is depth of flow at the cross-section of initiation. The relation between the parameters of the above function is shown graphically in Fig. 1. Fitting the experimental data to a power function, the relation may be expressed as

$$U\delta/\nu = 0.00146\,(Ux/\nu)^{1.31} \qquad (1)$$

This relation is represented by the curve in Fig. 1.

Quantities pertinent to growth of the free-surface disturbance may be related through the dimensionless parameters of the function

$$\psi(U\delta/\nu, Ux/\nu) = 0 ,$$

where x and δ are coordinates of points on the outer envelope of the disturbance, the origin of coordinates being at the point of initiation and the x and δ-axes being, respectively, along and normal to the channel wall. Other quantities are as previously defined. The relation between the parameters of the above function is shown graphically in Fig. 2. The advantage in the choice of parameters shown is that, for particular values of U and ν, Fig. 2 indicates the shape of the outer envelope of the disturbance, subject to distortion due to choice of scales. Fitting the experimental data to a power function, the relation may be expressed as

$$UL/\nu = 2{,}750\,(D/L)^{-0.800} . \qquad (2)$$

This relation is represented by the curve in Fig. 2. From Eq. 2, other forms such as those commonly used in connection with turbulent boundary layers and wakes may be easily derived. As an example,

$$\phi(UL/\nu, D/L) = 0 ,$$

CONCLUSION

The study was conducted under laboratory conditions and was limited to a prismatic channel of rectangular cross-section, plane bottom for test reach, and smooth boundaries, and to discharges such that the flow was at relatively shallow depths. However, it is believed that the study makes a substantial contribution to knowledge of the initiation and growth of free-surface disturbances.

The free-surface disturbances were initiated by fixing a thin wire to an otherwise smooth channel wall. For prototype channels which have walls that may be considered as rough, it seems likely that the disturbance will be initiated as soon as flow conditions are sufficient.

As mentioned in the Introduction, the disturbance exhibited the characteristics of a wake and could be initiated well away from the channel wall as well

as at the wall. Also, the depth of flow enters directly into the description of conditions just sufficient for initiation of the disturbance. Thus, such disturbances are not exclusively wall effects.

With flow conditions at initiation of the disturbance known, it appears that growth or spread of the disturbance over the free-surface in the downstream direction may be described through parameters similar in form to those used in describing boundary layers and wakes.

The primary interest of this study was in free-surface disturbances associated with air entrainment within a zone along the channel wall. It is possible, particularly with relatively narrow channels and substantial depths of flow, that zones of air entrainment along the two channel walls may join, resulting in air entrainment across the entire width. It is also possible, particularly with relatively wide channels and shallow depths of flow, that zones of air entrainment along the channel walls may join a zone of air entrainment which results from boundary layer growth along the channel bottom. In this connection, this study is a companion to a study reported by Priest and Baligh.(2)

Within the limitations of this study, it is believed that Fig. 1 and Eq. 1 adequately describe conditions just sufficient for initiation of the free-surface disturbance at the channel wall and that Fig. 2 and Eq. 2 adequately describe growth of such a disturbance, as evidenced by a broken free-surface. The scatter of data shown in Figures 1 and 2 is believed to be largely the result of experimental error associated with difficulties in measurement. The extents to which the results may have been influenced by the use of mean velocity, rather than free-surface velocity, and by nonuniformity of flow have not been determined.

REFERENCES

1. Amein, A. M., Free surface disturbances initiated at the sides in steep open channels, doctoral thesis, Cornell University, 1955 (unpublished).

2. Priest, M. S. and Baligh, A., Free-surface instability of liquids in steep channels, Transactions, American Geophysical Union, 35, pp. 133-135, 1954.

Appendix 1

Experimental data for conditions just sufficient for initiation of the disturbance.

θ	Q	D	L	Temp.
deg.	cfs	mm	ft.	deg. F
10	0.0188	1.94	1.47	41.3
	0.0292	2.38	1.39	40.0
	0.0376	2.86	0.81	40.5
	0.0460	5.37	0.10	40.3
	0.0547	6.08	0.59	40.2
	0.0618	7.57	0.58	40.1
15	0.0186	1.70	0.96	41.0
	0.0290	3.27	0.17	40.7
	0.0372	3.47	0.07	40.5
	0.0445	4.99	0.18	40.4
	0.0534	7.21	0.12	40.2
	0.0610	8.77	0.08	40.2
20	0.0177	1.64	0.73	41.5
	0.0294	3.01	0.17	40.9
	0.0378	4.37	0.12	40.7
	0.0460	5.76	0.10	40.2
	0.0540	6.77	0.06	40.1
	0.0625	8.04	0.06	40.0
25	0.0273	2.97	0.27	42.2
	0.0368	3.63	0.27	42.0
	0.0458	5.06	0.24	40.8
	0.0567	6.04	0.24	40.7
	0.0515	5.64	0.16	40.7
30	0.0274	2.25	0.74	42.0
	0.0207	1.90	0.74	41.2
	0.0385	3.13	0.74	41.1
	0.0350	2.97	0.74	41.3
	0.0453	4.25	0.08	40.8
	0.0590	5.96	0.04	41.0
35	0.0180	1.98	0.11	41.1
	0.0280	2.77	0.10	41.3
	0.0352	3.36	0.23	41.0
	0.0440	4.01	0.11	41.0
	0.0545	4.67	0.11	41.0
	0.0730	6.13	0.11	41.0
40	0.0190	1.71	0.33	41.8
	0.0294	2.56	0.25	41.2
	0.0365	3.47	0.21	41.0
	0.0456	4.58	0.18	41.0
	0.0533	5.19	0.18	41.0
45	0.0202	1.69	0.25	40.7
	0.0282	2.34	0.24	40.2
	0.0365	3.53	0.18	40.0
	0.0461	4.81	0.09	40.0
	0.0490	4.26	0.26	40.0
	0.0621	4.77	0.26	39.9

Appendix 2

Experimental data describing growth of the disturbance.

θ	Q	D_i^*	L_i^*	δ	x	Temp.
deg.	cfs	mm	ft.	ft.	ft.	deg. F
10	0.0292	1.95	2.93	0.094	1.47	41.0
				0.182	2.48	
		2.23	1.84	0.115	1.89	
	0.0376	2.58	2.20	0.125	1.61	40.7
				0.182	2.18	
		2.32	3.37	0.161	1.69	40.6
				0.213	2.19	
	0.0460	2.60	3.03	0.187	2.04	40.4
				0.260	2.56	
		3.26	1.77	0.156	2.02	40.3
				0.213	2.58	
	0.0547	3.16	2.46	0.166	1.89	
				0.244	2.58	40.2
		4.20	1.14	0.166	2.24	
15	0.0186	1.43	2.33	0.078	1.08	41.5
				0.130	2.14	
		1.46	1.83	0.099	1.62	41.2
				0.146	2.68	
	0.0290	1.75	2.25	0.104	1.72	40.8
				0.140	2.19	
		1.90	1.57	0.156	2.39	
	0.0372	2.09	2.25	0.130	1.71	40.6
				0.177	2.18	
		2.26	1.79	0.151	2.17	
	0.0445	2.43	2.25	0.140	1.73	40.5
				0.187	2.18	
		3.00	1.04	0.114	1.90	
				0.208	2.91	40.3
	0.0534	2.91	1.79	0.172	2.16	
				0.224	2.62	40.2
		3.30	1.19	0.114	1.77	
				0.208	2.77	
	0.0610	3.59	0.98	0.125	1.91	
				0.213	2.92	
20	0.0378	1.82	2.27	0.141	1.73	40.7
				0.187	2.16	
		2.14	1.23	0.171	2.29	
	0.0460	1.96	2.29	0.161	1.71	40.5
				0.197	2.16	
		2.51	1.23	0.129	1.73	40.3
				0.223	2.74	
	0.0540	2.32	2.29	0.155	1.70	40.2
				0.217	2.16	

* The subscript "i" refers to conditions at the initiation of disturbance.

Appendix 2
(Continued)

θ	Q	D_1	L_1	δ	x	Temp.
deg.	cfs	mm	ft.	ft.	ft.	deg. F
20	0.0540	3.14	1.19	0.145	1.96	40.2
				0.186	2.53	
	0.0625	3.54	0.99	0.140	1.97	40.0
				0.233	2.96	
25	0.0273	1.31	2.39	0.135	1.72	42.6
				0.172	2.18	
		1.53	1.42	0.120	1.66	42.4
				0.198	2.67	
	0.0368	1.60	2.39	0.161	1.71	
				0.230	2.18	42.0
		1.95	1.33	0.135	1.75	
				0.234	2.92	
	0.0458	1.86	2.38	0.156	1.72	41.0
				0.198	2.18	
	0.0567	2.12		0.167	1.71	40.8
				0.224	2.17	
		2.72	1.33	0.135	1.73	40.7
				0.240	2.74	
	0.0315	2.02	2.36	0.167	1.73	
				0.229	2.19	
		2.51	1.34	0.130	1.72	
				0.230	2.27	
30	0.0207	1.11	2.59	0.070	1.11	44.0
				0.073	1.15	
		1.20	1.90	0.078	1.34	43.0
				0.060	1.14	
	0.0385	1.49	3.25	0.333	3.00	41.0
				0.187	1.88	
		1.51	2.50	0.208	2.08	
				0.313	2.92	
	0.0350	1.47	3.05	0.182	1.92	41.3
				0.141	1.51	
		1.50	2.25	0.214	2.33	
				0.141	1.66	
	0.0463	1.63	3.62	0.146	1.50	38.0
				0.166	1.78	
				0.208	2.09	
				0.375	3.33	
	0.0453	1.76	2.70	0.302	2.74	40.9
				0.182	1.84	
		2.00	1.58	0.270	3.00	40.8
				0.229	2.45	
	0.0590	2.85	1.17	0.324	3.34	41.5
				0.156	1.85	
		3.50	0.80	0.161	2.22	41.2
				0.094	1.52	

Appendix 2
(Continued)

θ	Q	D_i	L_i	δ	x	Temp.
deg.	cfs	mm	ft.	ft.	ft.	deg. F
35	0.0281	1.25	3.08	0.130	1.53	41.1
				0.083	1.00	
		1.29	2.34	0.177	2.26	41.2
				0.130	1.75	
		1.40	1.50	0.068	0.88	
				0.120	1.58	
	0.0352	1.41	3.08	0.088	1.00	41.3
				0.141	1.51	
		1.62	1.71	0.109	1.36	41.2
				0.208	2.36	
	0.0440		1.46	0.167	1.71	41.0
				0.062	0.69	
		1.98	3.08	0.073	1.02	
				0.135	1.72	
	0.0545	2.16	1.50	0.140	1.51	40.8
				0.213	2.14	
	0.0522	2.13	1.71	0.291	2.83	38.2
				0.192	1.75	
				0.286	2.52	
		1.73	3.38	0.062	0.88	
				0.125	1.59	
	0.0730	4.66	1.54	0.089	1.24	40.8
				0.271	2.96	
				0.220	2.49	
				0.573	5.41	
40	0.0190	0.99	2.50	0.104	1.66	41.8
				0.136	2.18	
		1.10	1.43	0.062	1.02	
				0.094	1.73	
	0.0294	1.27	2.46	0.146	1.66	
				0.183	2.16	42.5
		1.33	1.49	0.125	1.66	
	0.0365	1.38	2.44	0.161	1.73	41.9
				0.218	2.18	
		1.59	1.55	0.130	1.61	41.2
				0.224	2.61	
	0.0456	1.53	2.46	0.156	1.72	41.1
				0.219	2.18	
		1.86	1.43	0.141	1.72	41.0
				0.239	2.73	
	0.0533	1.75	2.46	0.172	1.71	
				0.218	2.17	
		2.03	1.56	0.136	1.58	
				0.239	2.59	
45	0.0277	1.15	3.50	0.083	1.06	38.2
				0.125	1.61	
				0.167	2.13	
		1.19	2.06	0.125	1.86	

Appendix 2
(Continued)

θ	Q	D_1	L_1	δ	x	Temp.
deg.	cfs	mm	ft.	ft.	ft.	deg. F
45	0.0277	1.19	2.06	0.177	2.41	38.2
	0.0365	1.35	2.50	0.151	1.71	40.3
				0.208	2.17	
		1.47	1.78	0.208	2.44	
				0.255	2.88	
	0.0461	1.48	1.97	0.136	1.47	39.9
				0.166	1.77	
	0.0453	1.60	2.06	0.250	2.48	38.2
				0.156	1.46	
				0.248	2.32	
		1.50	1.94	0.214	2.25	
				0.266	2.70	
	0.0490	2.05	1.42	0.271	2.81	40.0
				0.323	3.26	
	0.0621	2.16	1.51	0.151	1.69	39.9
				0.260	2.70	

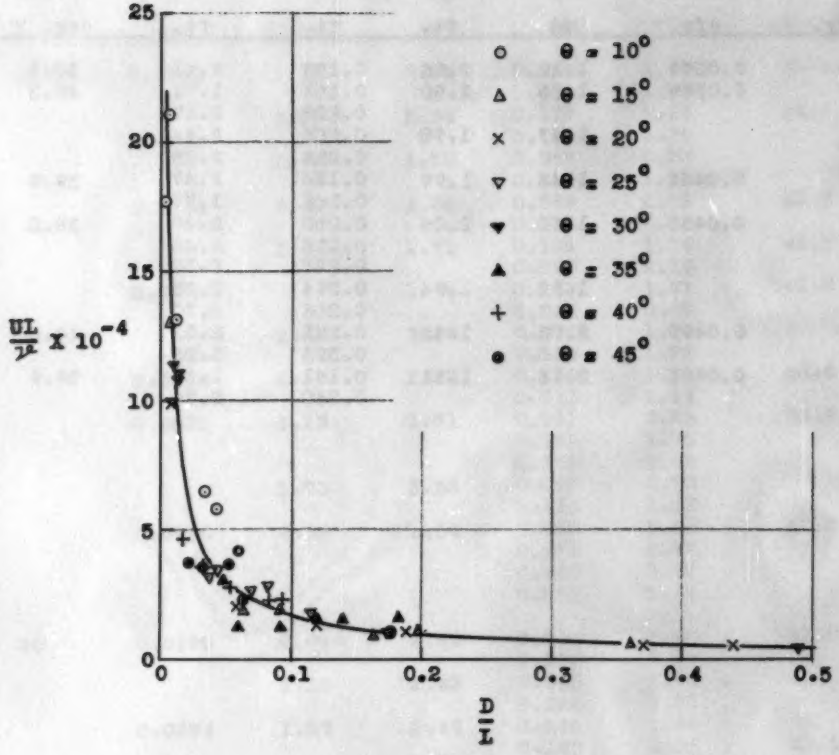

Fig. 1 -- Relation of parameters describing conditions just sufficient for initiation of the free-surface disturbance at the channel wall

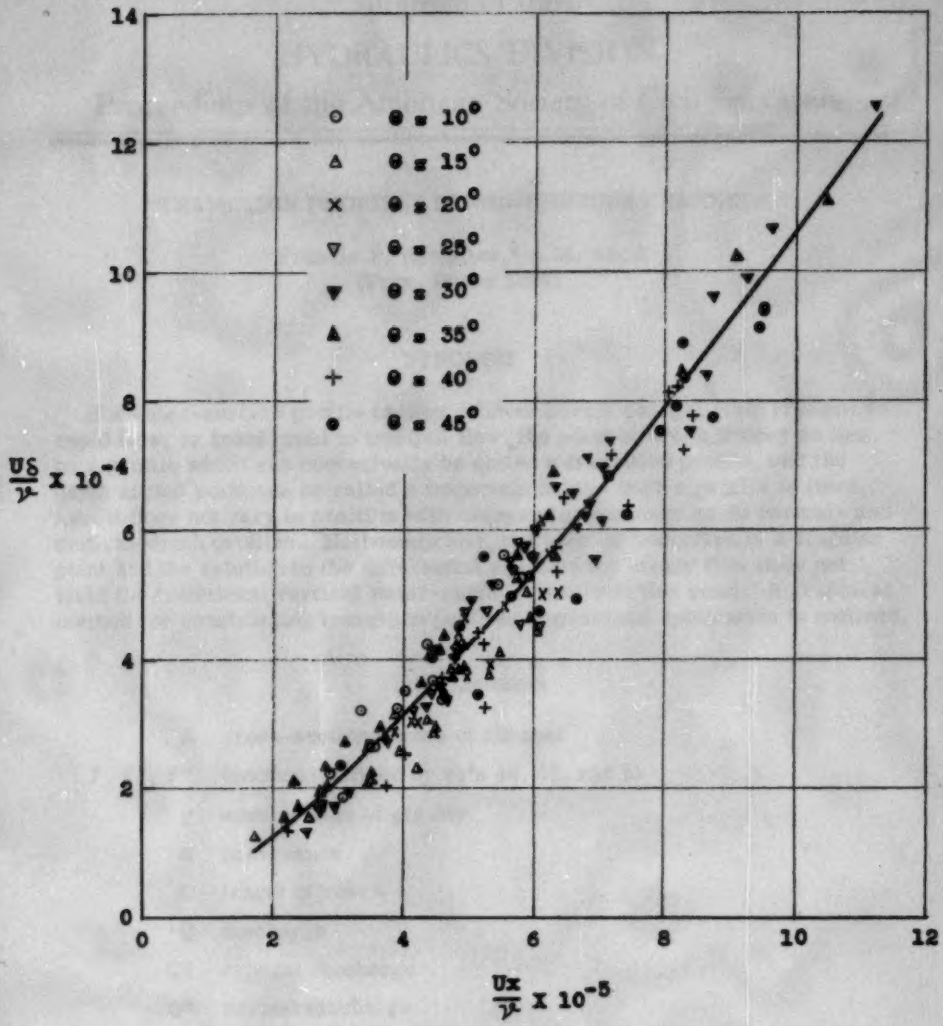

Fig. 2 -- Relation of parameters describing development of the free-surface disturbance along the channel wall

Journal of the
HYDRAULICS DIVISION
Proceedings of the American Society of Civil Engineers

TRANSITION PROFILES IN NON-UNIFORM CHANNELS

Francis F. Escoffier,[1] A.M. ASCE
(Proc. Paper 1006)

SYNOPSIS

If a water-surface profile passes, without abrupt change, from tranquil to rapid flow, or from rapid to tranquil flow, the point at which it does so lies on a profile which can conveniently be called a transition profile, and the depth at that point can be called a transition depth. Such a profile is fixed, i.e., it does not vary in position with changes in discharge as do normal- and critical-depth profiles. Mathematically, the point of transition is a singular point and the solution to the differential equation for steady flow does not yield the traditional vertical water-surface profile at that point. A graphical method for constructing transition profiles in practical application is outlined.

List of Symbols

A	cross-sectional area of channel
F, F', F''	functions defined by eq's 49, 50, and 51
g	acceleration of gravity
K	conveyance
L	length of reach
Q	discharge
Q^c	critical discharge
Q^n	normal discharge
Q'^n	paranormal discharge, defined by eq. 9
r	a dimensionless number, defined by eq. 18
S	slope of water surface

Note: Discussion open until November 1, 1956. Paper 1006 is part of the copyrighted Journal of the Hydraulics Division of the American Society of Civil Engineers, Vol. 82, No. HY 3, June, 1956.

1. Hydr. Engr., Corps of Engrs., U. S. Dept. of the Army, Mobile Dist., Mobile, Ala.

S_A slope of profile along which A = const.

S^c slope of profile along which Q^c = const.

S^m slope defined by eq. 24

S^n slope of profile along which Q^n or Q'^n = const.

S^o slope of bottom of channel

v velocity

W width of channel at water surface

x distance along channel

y depth of water

z elevation of water surface

λ a dimensionless number defined by eq. 29

ρ a dimensionless number defined by eq. 30

σ a dimensionless number defined by eq. 31

The Transition Profile in Uniform Channels

If we consider the differential equation for water-surface profiles in uniform channels

$$\frac{dy}{dx} = S_o \frac{1 - \left(\frac{Q}{Q_n}\right)^2}{1 - \left(\frac{Q}{Q_c}\right)^2} \tag{1}$$

and assume that for some depth

$$Q_n = Q_c \neq Q \tag{2}$$

we see that the expression on the right side of eq. 1 becomes simply S^o. This means that the depth y increases in relation to the distance x at a rate equal to the bottom slope S_o and that therefore the water-surface profile at the point in question is horizontal. The profile defined by the eq. $Q^n = Q^c$ is conveniently termed a transition profile, and it is a general characteristic of such a profile that the water-surface profiles intersecting it are horizontal at the point of intersection as long as $Q \neq Q^c$, i.e., as long as the water-surface does not pass through critical depth as it intersects the transition profile.

If, however, a water-surface profile does pass through critical depth as it intersects the transition profile so that

$$Q_n = Q_c = Q \tag{3}$$

the right side of eq. 1 assumes the indeterminate form $\frac{0}{0}$. The point of

intersection is a singular point and it is possible to evaluate the expression in question by replacing the numerator and the denominator by their derivatives. The result is

$$\frac{dY}{dx} = S_o \frac{dQ_n}{dQ_c} \tag{4}$$

a formula that can be used to determine the slope of a water-surface profile, in a uniform channel, as it intersects the transition profile and simultaneously passes through critical depth. Two such intersections are shown in figs. 1 and 2. In fig. 1 we have

$$\frac{dQ_n}{dQ_c} > 1$$

and the profile is passing from tranquil to rapid flow, whereas in fig. 2

$$\frac{dQ_n}{dQ_c} < 1$$

and the opposite change is taking place.

An important property of the transition profile is that it forms a line of separation between two zones. In one zone we have $Q_n > Q_c$ and the water-surface profiles have the properties normally associated with a mild-slope channel; in the other we have $Q_n < Q_c$ and they have the properties normally associated with a steep-slope channel. We will refer to these two zones as mild and steep zones, respectively.

Transition depths in uniform channels were discussed by Lazard[1] who referred to them as "characteristic" depths. He gives credit to Mouret[2] for the development of the idea. The writer prefers the term "transition" to "characteristic" because the profiles in question represent the normal location of transitions from tranquil to rapid flow, a property that becomes of considerable importance in non-uniform channels.

Lazard points out that in rectangular channels and in closed conduits the number of transition profiles will be 2, 1, or 0, depending on whether the channel slope is greater than, equal to, or less than a value which he designates as the limiting slope. If there exist two transition profiles the zone below the lower profile and that above the upper profile are both mild zones, whereas that between the two profiles is a steep zone. As the slope of the channel is reduced the two transition profiles approach each other until they coincide, at which time the slope becomes equal to the limiting slope and the steep zone disappears. For that slope and for lesser slopes all water-surface profiles have the properties normally associated with mild-slope channels.

Lazard also introduces the concept of a characteristic discharge, or in the terminology of this paper, a transition discharge, which is equal to the common value assumed by both the normal and the critical discharges on the transiton profile.

The writer, in a discussion of a paper by Von Seggern,[3] pointed out that the functions developed in that paper could be used to show the existence of

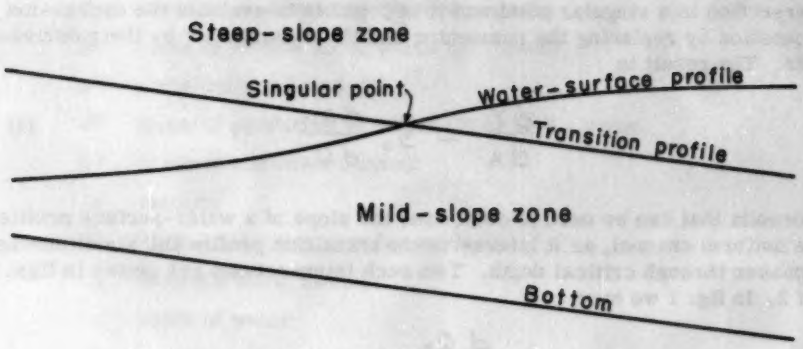

Fig. 1

Fig. 1. Transition profile in uniform channel $\left(\frac{dQn}{dQc} > 1\right)$

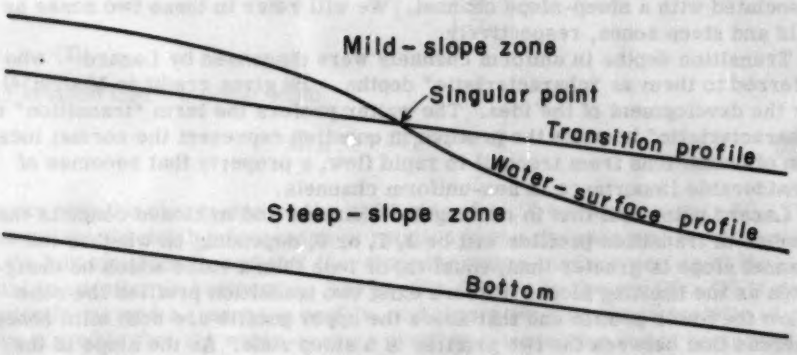

Fig. 2

Fig. 2. Transition profile in uniform channel $\left(\frac{dQn}{dQc} < 1\right)$

transition profiles. At the time of this discussion the writer was unaware of the existence of Lazard's paper.

Transition Profiles in Non-uniform Channels

To extend the concept of a transition depth to non-uniform channels it is necessary to derive an appropriate generalization of eq. 1. We start with the dynamic equation in the form

$$d\left(z + \frac{v^2}{2g}\right) = -\left(\frac{Q}{K}\right)^2 dx \tag{5}$$

Choosing x and z as independent variables we can write

$$\begin{aligned} d\left(\frac{v^2}{2g}\right) &= \frac{Q^2}{gA^3}\left(\frac{\partial A}{\partial x}dx + \frac{\partial A}{\partial z}dz\right) \\ &= -\left(\frac{Q}{Q_c}\right)^2\left(S_A\,dx + dz\right) \end{aligned} \tag{6}$$

where

$$S_A = -\left(\frac{dz}{dx}\right)_{A=\text{const.}} = \frac{\frac{\partial A}{\partial x}}{\frac{\partial A}{\partial z}} \tag{7}$$

The slope term S_A, which is analogous to the bottom slope S_o, is a function of both x and z.

Substituting from eq. 6 into eq. 5 we obtain

$$dz - \left(\frac{Q}{Q_c}\right)^2\left(S_A\,dx + dz\right) = -\left(\frac{Q}{K}\right)^2 dx$$

which can be rearranged in the form

$$\frac{dz}{dx} + S_A = \frac{S_A - \left(\frac{Q}{K}\right)^2}{1 - \left(\frac{Q}{Q_c}\right)^2} \tag{8}$$

We now make use of the concept of a paranormal discharge

$$Q_n' = K\sqrt{S_A} \tag{9}$$

a quantity introduced by Masse[4] in his study of channels having uniform

rectangular cross sections but variable bottom slopes. When this is substituted into eq. 8 there is obtained

$$\frac{1}{S_A}\frac{dz}{dx} + 1 = \frac{1 - \left(\frac{Q}{Q_n'}\right)^2}{1 - \left(\frac{Q}{Q_c}\right)^2} \qquad (10)$$

which is the desired generalized form of eq. 1.

The idea quite naturally suggests itself that the left side of eq. 10 can be replaced by the term $\frac{dy}{dx}$ as in eq. 1, but unfortunately the appropriate differential expression

$$dy = dz + S_A\,dx$$

is not an exact differential and consequently the supposed function y does not exist.

The transition profile can now be defined as the profile along which $Q'_n = Q_c$ and this profile again forms the boundary between a zone with mild-slope characteristics and one with steep-slope characteristics. The transition discharge for any cross section is equal to the common value assumed by the paranormal and the critical discharges on the transition profile in that cross section. If the water surface for a given discharge passes from subcritical to supercritical flow it will do so on the transition profile and in the cross section where that discharge is equal to the transition discharge. The cross section in question is the control for that particular discharge and if the discharge changes the control will move upstream or downstream (except in a uniform channel). A ready means for locating the controlling cross sections in a channel is obtained by plotting the transition discharge as a function of the variable x. As before, if we have

$$Q_n' = Q_c \neq Q \qquad (11)$$

the numerator and the denominator on the right side of the equation are equal and therefore $\frac{\partial z}{\partial x} = 0$ which implies that the water-surface profile is horizontal at the point of intersection with the transition profile. Also, as before, if the profile passes through critical depth as it crosses the transition profile, we have

$$Q_n' = Q_c = Q \qquad (12)$$

and the right side of eq. 10 takes on the indeterminate form $\frac{0}{0}$. The point of intersection is a singular point and we evaluate the expression in question by replacing the numerator and the denominator by their derivatives. The result is

$$\frac{1}{S_A}\frac{dz}{dx} + 1 = \frac{dQ_n'}{dQ_c} \tag{13}$$

However, this expression is not so simple to evaluate as that in eq. 4 because Qn' and Qc are now functions of the two variables x and z. In fact we have

$$dQ_n' = \frac{\partial Q_n'}{\partial x}dx + \frac{\partial Q_n'}{\partial z}dz \tag{14}$$

and

$$dQ_c = \frac{\partial Q_c}{\partial x}dx + \frac{\partial Q_c}{\partial z}dz \tag{15}$$

which are substituted into eq. 13 to give

$$\frac{1}{S_A}\frac{dz}{dx} + 1 = \frac{\frac{\partial Q_n'}{\partial x} + \frac{\partial Q_n'}{\partial z}\frac{dz}{dx}}{\frac{\partial Q_c}{\partial x} + \frac{\partial Q_c}{\partial z}\frac{dz}{dx}} \tag{16}$$

If we now let the water surface slope be S so that

$$S = -\frac{dz}{dx} \tag{17}$$

and let

$$r = \frac{\frac{\partial Q_n'}{\partial z}}{\frac{\partial Q_c}{\partial z}}, \tag{18}$$

$$S_n = -\left(\frac{dz}{dx}\right)_{Q_n' = \text{const.}} = \frac{\frac{\partial Q_n'}{\partial x}}{\frac{\partial Q_n'}{\partial z}} \tag{19}$$

and

$$S_c = -\left(\frac{dz}{dx}\right)_{Q_c = \text{const.}} = \frac{\frac{\partial Q_c}{\partial x}}{\frac{\partial Q_c}{\partial z}} \tag{20}$$

we can rewrite eq. 16 in the form

$$1 - \frac{S}{S_A} = r \frac{S_n - S}{S_c - S} \tag{21}$$

This can be rearranged in the somewhat more useful form

$$\frac{S}{S_A} = \frac{(S_c - r S_n) + S(r - 1)}{S_c - S} \tag{21'}$$

It is convenient at this point to introduce the slope of the transition profile S_T. Since along this profile we have $Q_n' = Q_c$ we also must have

$$\frac{d(Q_n' - Q_c)}{dx} = \frac{\partial Q_n'}{\partial x} + \frac{\partial Q_n'}{\partial z}\frac{dz}{dx} - \frac{\partial Q_c}{\partial x} - \frac{\partial Q_c}{\partial z}\frac{dz}{dx} = 0$$

and therefore

$$S_T = -\left(\frac{dz}{dx}\right)_{Q_n' = Q_c} = \frac{\frac{\partial Q_n'}{\partial x} - \frac{\partial Q_c}{\partial x}}{\frac{\partial Q_n'}{\partial z} - \frac{\partial Q_c}{\partial z}} \tag{22}$$

On substituting from eq's 18, 19, and 20, this is further reduced to

$$S_T = \frac{r S_n - S_c}{r - 1} \tag{23}$$

Substituting from eq. 23 into eq. 21' and introducing at the same time the slope

$$S_m = (1 - r) S_A \tag{24}$$

we obtain

$$S = S_m \frac{S_T - S}{S_c - S} \tag{25}$$

Eq. 25 reduces to the quadratic equation

$$S^2 - (S_c + S_m) S + S_m S_T = 0 \tag{26}$$

the solution to which is

$$S = \frac{S_c + S_m \pm \sqrt{(S_c + S_m)^2 - 4 S_m S_T}}{2} \qquad (27)$$

This last equation gives us the slope of a water-surface profile passing through a singular point on a transition profile.

In the mathematical theory of singular points, which was developed by H. Poincare,[5] it is shown that there can occur four types of singular points depending on the nature of the roots to the equation

$$\lambda^2 - (S_c - S_m)\lambda + S_m (S_T - S_c) = 0 \qquad (28)$$

which is known as the characteristic equation. This equation can be obtained from eq. 26 by means of the substitution

$$S = \lambda + S_m \qquad (29)$$

which also defines the variable λ.

If the two roots to eq. 28 are real but unlike in sign, the singular point is a saddleback. Such a singular point is shown in fig. 3. The profile AOB represents a transition from subcritical to supercritical flow and the point is therefore a control. The water-surface profile COD, however, represents a transition from supercritical to subcritical flow and the point O is not a control. The segment CO represents a type of flow that can occur only if a suitable control exists farther upstream. Similarly, the segment OD represents a type of flow that can exist only if a suitable control exists farther downstream. If these two suitable controls do not exist, the continuous transition is not possible and a hydraulic jump must form either upstream or downstream from the point O.

A number of water-surface profiles that do not pass through the singular point O are also shown in fig. 3. It should be noted that these profiles are always vertical where they intersect the critical-depth profile and are always horizontal where they intersect the transition profile.

If the two roots to eq. 28 are real but like in sign the singular point is a node. Such a singular point for which $S_c > S_m$ is shown in fig. 4. All of the water-surface profiles shown in this diagram are transitions from supercritical to subcritical flow and therefore the point O is never a control. A continuous profile is possible only if suitable controls exist upstream and downstream from the point O. All of the water-surface profiles except EOF pass through the point O with the same slope, this slope being one of the roots to eq. 27. The other root is the slope with which the one profile EOF passes through O.

If the relative magnitude of S^c and S^m are reversed so that $S_c < S_m$ a node will occur again, but in this case the water-surface profiles will all pass from subcritical to supercritical flow and the singular point becomes a control.

If the two roots to eq. 28 are not real they become conjugate complex numbers of the form $\alpha + i\beta$ and $\alpha - i\beta$ where $\beta \neq 0$. If $\alpha \neq 0$ the singular point is a focus but if $\alpha = 0$ it is a center. These two singular points are shown in figs. 5 and 6. In neither case is a transition from subcritical to supercritical

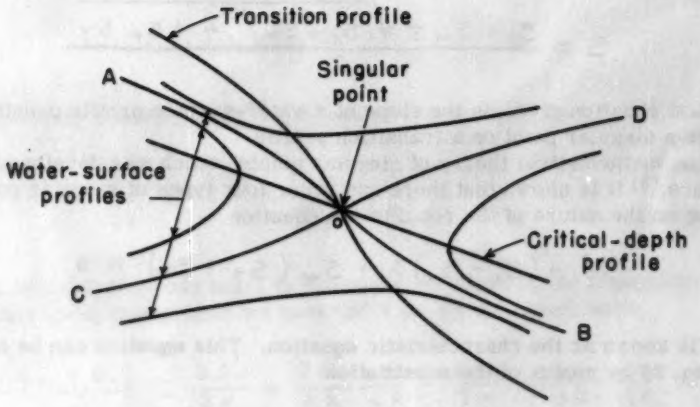

Fig. 3. Saddleback

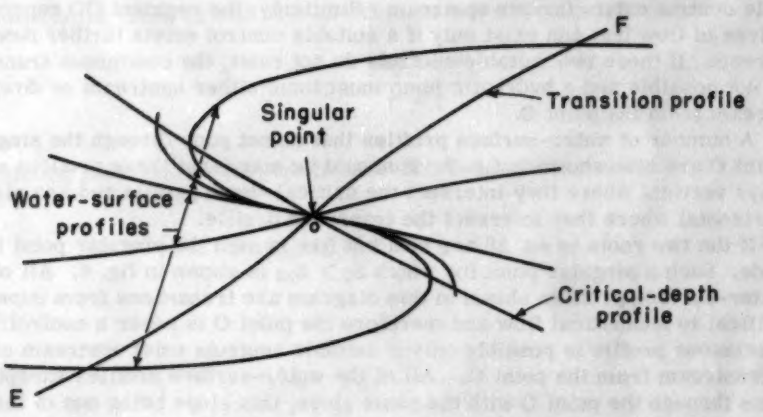

Fig. 4. Node

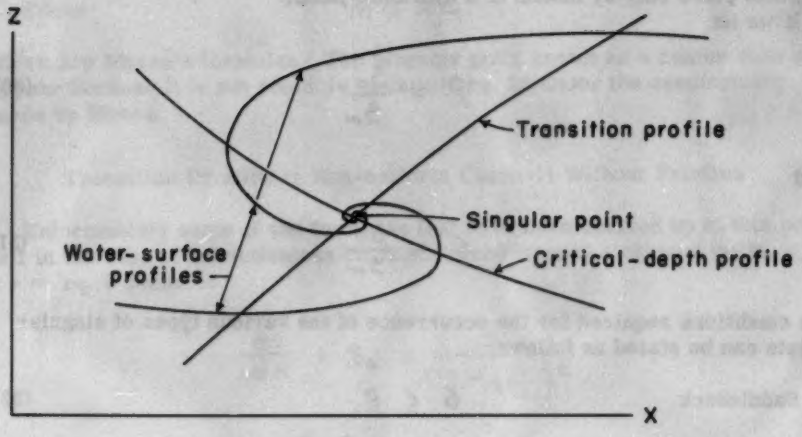

Fig. 5. Focus

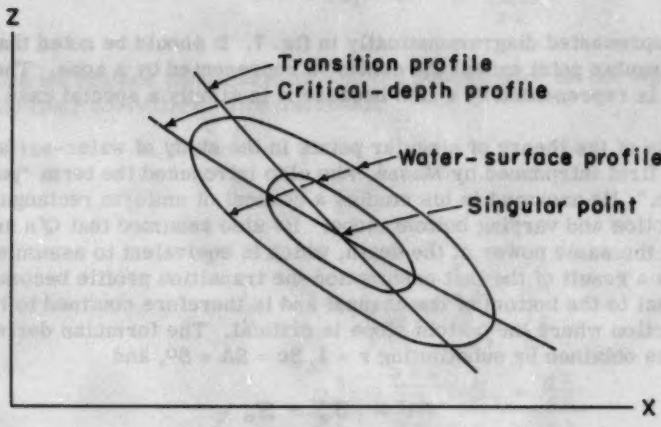

Fig. 6. Center

flow possible, and the reverse change from supercritical to subcritical flow can take place only by means of a hydraulic jump.

If we let

$$\rho = \frac{S_c}{S_m} \tag{30}$$

and

$$\sigma = \frac{S_T}{S_m} \tag{31}$$

the conditions required for the occurrence of the various types of singular points can be stated as follows:

Saddleback $$\sigma < \rho \tag{32}$$

Node $$\rho < \sigma < \left(\frac{1+\rho}{2}\right)^2 \tag{33}$$

Focus $$\sigma > \left(\frac{1+\rho}{2}\right)^2 \quad \text{and} \quad \rho \neq 1 \tag{34}$$

Center $$\sigma > 1 \quad \text{and} \quad \rho = 1 \tag{35}$$

This is represented diagrammatically in fig. 7. It should be noted that each type of singular point except the center is represented by a zone. The center, however, is represented by a line because it is simply a special case among foci.

The use of the theory of singular points in the study of water-surface profiles was first introduced by Massé, who also introduced the term "paranormal depth." He assumed in his studies a channel of uniform rectangular cross-section and varying bottom slope. He also assumed that Q'n and Qc varied as the same power of the depth, which is equivalent to assuming that r = 1. As a result of the last assumption the transition profile becomes a line normal to the bottom of the channel and is therefore confined to the one cross-section where the bottom slope is critical. The formulas derived by him can be obtained by substituting r = 1, Sc = SA = S^o, and

$$m = S_o - S_n \tag{36}$$

into eq's 24, 25, and 26 with the result

Saddleback $$m < o \tag{37}$$

Node $$o < m < \frac{S_o}{4} \tag{38}$$

Focus $$m > \frac{S_o}{4} \qquad (39)$$

which are Massé's formulas. The singular point known as a center does not appear because it is not possible to satisfy eq. 28 under the assumptions made by Massé.

Transition Profiles in Non-uniform Channels Without Friction

Unfortunately some of the formulas that have been derived up to this point fail in the case of a frictionless channel. Since in such a channel we have $k = \infty$ eq. 8 becomes

$$\frac{dz}{dx} + S_A = \frac{S_A}{1 - \left(\frac{Q}{Q_c}\right)^2} \qquad (40)$$

If we now consider the profile along which SA = O we see that any water-surface profile intersecting this profile will have a horizontal slope at the point of intersection unless Q = Qc in which case the right side of eq. 40 becomes indeterminate and the point of intersection becomes a singular point. The profile along which SA = O is therefore a transition profile and we have

$$S_T = -\left(\frac{dz}{dx}\right)_{S_A = o} = \frac{\frac{\partial S_A}{\partial x}}{\frac{\partial S_A}{\partial z}} \qquad (41)$$

As before we replace the numerator and the denominator on the right side of eq. 40 by their derivatives with the result

$$\frac{dz}{dx} = \frac{1}{2} \frac{Q_c^3}{Q^2} \frac{dS_A}{dQ_c}$$

$$= \frac{1}{2} \frac{Q_c^3}{Q^2} \frac{\frac{\partial S_A}{\partial x} + \frac{\partial S_A}{\partial z}\frac{dz}{dx}}{\frac{\partial Q_c}{\partial x} + \frac{\partial Q_c}{\partial z}\frac{dz}{dx}}$$

$$= \frac{1}{2} \frac{Q_c^3}{Q^2} \frac{\frac{\partial S_A}{\partial z}}{\frac{\partial Q_c}{\partial z}} \frac{S_T + \frac{dz}{dx}}{S_c + \frac{dz}{dx}}$$

On substituting -S for its equal $\frac{dz}{dx}$ and taking note of the fact that on a singular point we have Q = Qc we obtain

$$S = -\frac{Q_c}{2}\,\frac{\frac{\partial S_A}{\partial z}}{\frac{\partial Q_c}{\partial z}}\,\frac{S_T - S}{S_c - S} \tag{42}$$

To further transform this equation we will now show that

$$\frac{\partial Q_c}{\partial x} = -\frac{Q_c}{2}\,\frac{\partial S_A}{\partial z} \tag{43}$$

Applying the operator $\frac{\partial}{\partial z}$ to eq. 7 we obtain

$$\frac{\partial S_A}{\partial z} = \frac{\frac{\partial A}{\partial z}\,\frac{\partial^2 A}{\partial x\,\partial z} - \frac{\partial A}{\partial x}\,\frac{\partial^2 A}{\partial z^2}}{\left(\frac{\partial A}{\partial z}\right)^2}$$

but $\frac{\partial A}{\partial x} = 0$ on a transition profile and therefore

$$\frac{\partial S_A}{\partial z} = \frac{\frac{\partial^2 A}{\partial x\,\partial z}}{\frac{\partial A}{\partial z}} \tag{44}$$

The critical discharge Qc is given by the equation

$$Q_c = A\sqrt{\frac{gA}{w}} \tag{45}$$

which in view of the relationship

$$w = \frac{\partial A}{\partial z} \tag{46}$$

becomes

$$Q_c = A\sqrt{\frac{gA}{\frac{\partial A}{\partial z}}} \tag{47}$$

Applying the operator $\frac{\partial}{\partial x}$ to eq. 47 we obtain

$$\frac{\partial Q_c}{\partial x} = \frac{1}{2}\left(\frac{gA^3}{\frac{\partial A}{\partial z}}\right)^{-\frac{1}{2}}\,\frac{3gA^2\,\frac{\partial A}{\partial x}\,\frac{\partial A}{\partial z} - gA^3\,\frac{\partial^2 A}{\partial x\,\partial z}}{\left(\frac{\partial A}{\partial z}\right)^2}$$

Since $\frac{\partial A}{\partial x} = o$ on the transition profile this becomes

$$\frac{\partial Q_c}{\partial x} = -\frac{1}{2} Q_c \frac{\partial S_A}{\partial z}$$

which is eq. 43. On making the appropriate substitution from eq. 43 into eq. 42 we obtain

$$S = S_c \frac{S_T - S}{S_c - S} \tag{48}$$

which is the desired equation.

On comparing eq. 48 with eq. 25 we see that a singular point in a frictionless channel is a special case among singular points for which $S^m = S^c$. This implies $\rho = 1$ and from fig. 7 we see the singular points for a frictionless channel are all either saddlebacks or centers.

Graphical Construction of Transition Profiles

The mathematical methods used up to this point have permitted us to show some of the more important properties of transition profiles. However, they have not provided us with a practical way of plotting these profiles. A practical approach is provided by a graphical method in which use is made of the three functions

$$F = \frac{1}{2gA^2} \tag{49}$$

$$F' = \frac{1}{2gA^2} + \frac{L}{2K^2} \tag{50}$$

$$F'' = \frac{1}{2gA^2} - \frac{L}{2K^2} \tag{51}$$

These functions are plotted horizontally in rectangular coordinates against the water-surface elevation z which is plotted vertically. The use of these functions in the graphical determination of water-surface profiles has been discussed elsewhere[6,7,8] and will not be touched upon here except insofar as it relates to frictionless channels. It will suffice to point out that if we plot the function F' for the cross section at the downstream end of a reach and the function F" for the cross section at the upstream end then the intersection of the two curves will provide us with an approximate elevation for the transition profile at the mid point of the reach. The accuracy of the estimate can be improved to any degree desired by suitably shortening the reach. The construction of a transition profile in this way is illustrated in fig. 8.

The same construction can be used for a frictionless channel except that the functions F' and F" are replaced with the function F. Here again, the

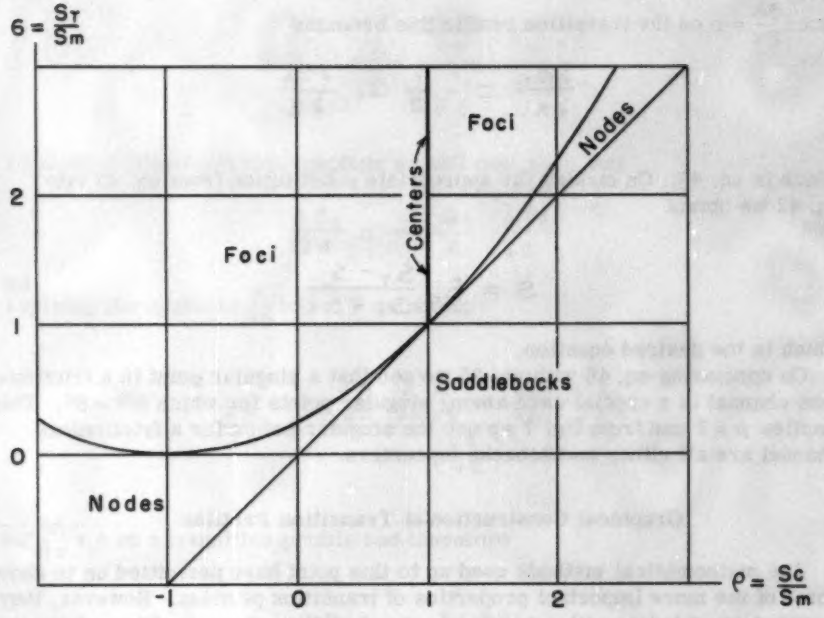

Fig. 7.

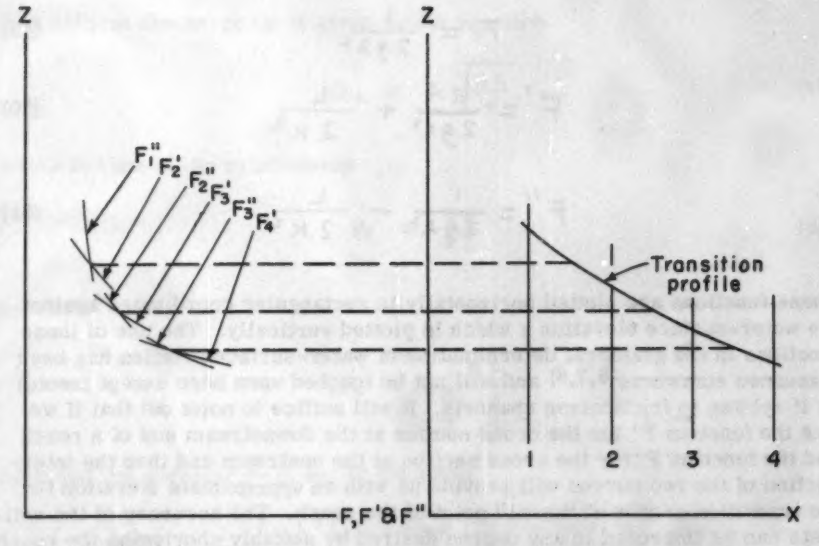

Fig. 8. Constructing transition profile

transition profile so obtained is approximate only but in this case a precise solution can be obtained by drawing an envelope to the F. curves. This is shown in fig. 9.

The construction of a water-surface profile for flow in a frictionless channel is readily carried out with the help of the F curves. A straight line having a slope equal to $-Q^2$ and drawn so as to intersect the F curves will determine by these intersections a water-surface profile, and the elevation of that profile in any cross section will be the same as the elevation of the intersection on the corresponding F curve. The intersection of the same straight line with the z-axis will also determine the energy head for the water-surface profile in question. An important characteristic of the foregoing construction is that if flow at critical depth occurs in any of the cross sections represented in the diagram the straight line in question will be tangent to the corresponding F curve. Figs. 10 and 11 which illustrate a saddleback and a center, respectively, show how the construction is carried out. In fig. 10 the line ab determines the two hyperbola-like profiles; the line cd, the two profiles that pass through the singular point; and the line ef, the two profiles that pass above and below the singular point. Since flow at critical depth occurs at the points o, m, and n, the line cd is tangent to the curve F_3 and the line ab, to the curves 2 and 4. In fig. 11 the line ij determines the oval-shaped profile. Flow at critical depth occurs in cross sections 1 and 5 and, accordingly, the line ij is tangent to the curves F_1 and F_5. The tangency of the line gh to the curve F_3 implies flow at critical depth at the singular point. However, since this line does not intersect any other F curve, no water-surface profile passes through the singular point.

REFERENCES

1. Coutribution a l'étude theorique du mouvement graduellement varié en hydraulique, A. Lazard, Annales des Ponts et Chaussées, Mars - Avril 1947.
2. L'Hydraulique générale et appliquée, Mouret.
3. Integrating the equation of non-uniform flow, M. E. Von Seggern, Trans., ASCE, Vol. 115, 1950, p. 71.
4. Ressaut et ligne d'eau dans les cours d'eau a pente variable, Pierre Massé, Revue Générale de l'Hydraulique, Nos. 19 et 20, Jan - Apr. 1938.
5. See Goursat's Mathematical Analysis, Vol. II, Part II, Differential Equations, translated by Hedrick and Dunkel. Also see Mathematical Methods in Engineering, Kármán and Biot, where the four singular points are called saddle point, nodal point, spiral point, and vortex point instead of saddleback, node, focus, and center.
6. Determination graphique de la ligne d'eau et calcul des remous, N. Raytchine and P. Chatelain, La Houille Blanche, No. 3, May-June 1950.
7. Engineering Manual, Civil Works Construction, Part CXVI, Chap. 9, Corps of Engineers.
8. Backwater profiles solved by Escoffier-Raytchine-Chatelain method, John R. Stipp, Civil Engineering, August 1953.

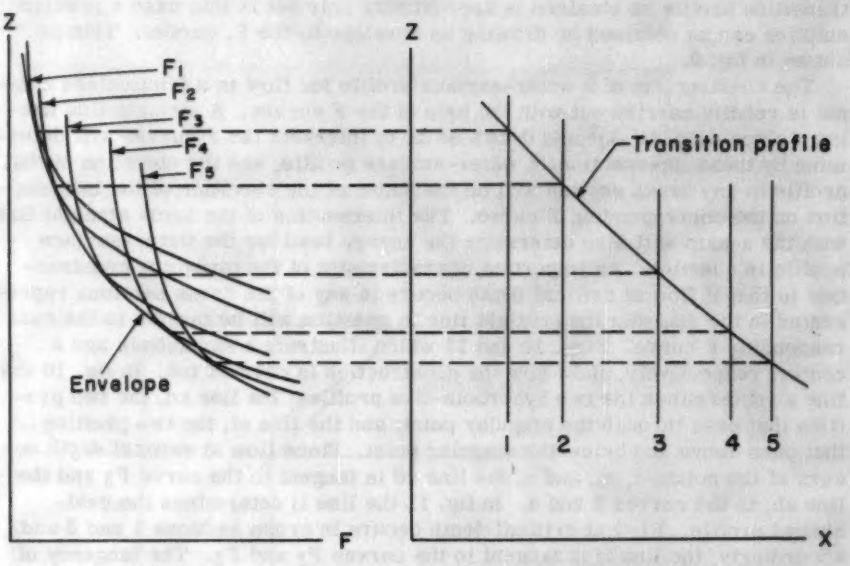

Fig. 9. Transition profile in frictionless channel

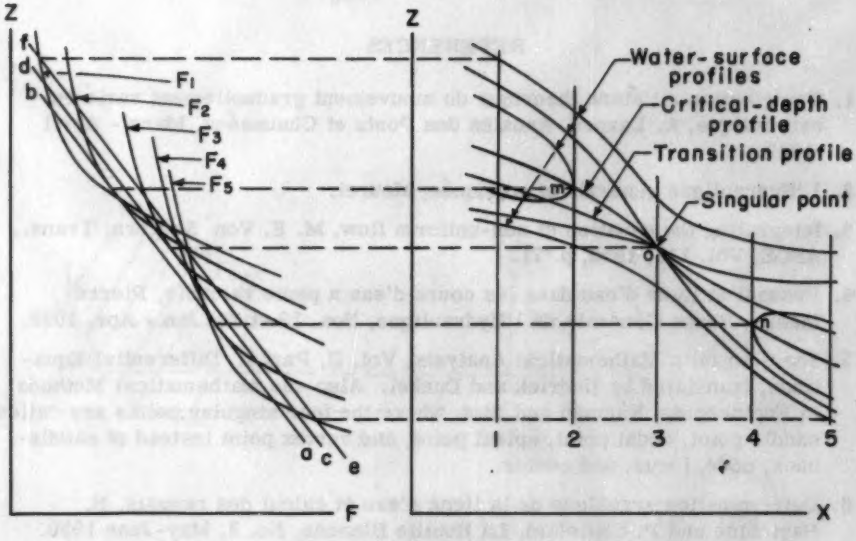

Fig. 10. Saddleback in frictionless channel. To avoid excessive complexity five only of the connecting lines have been drawn.

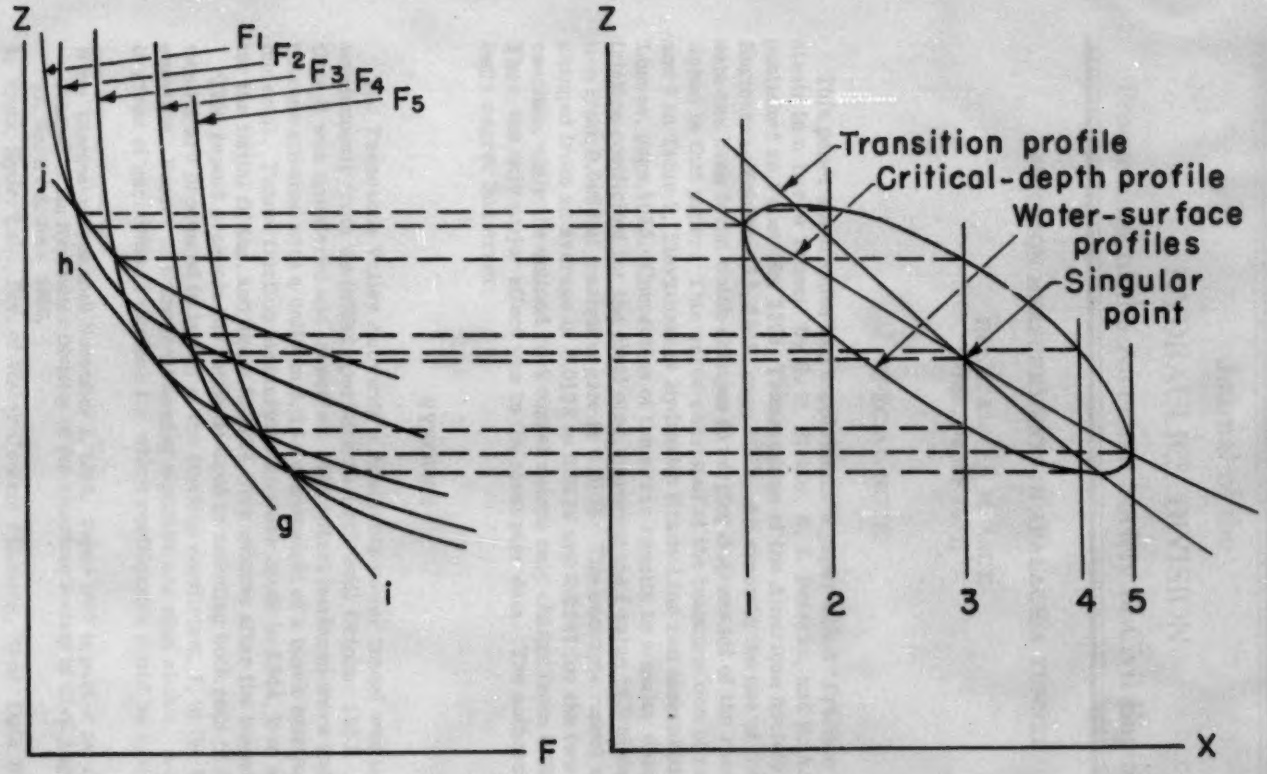

Fig. 11. Center in frictionless channel

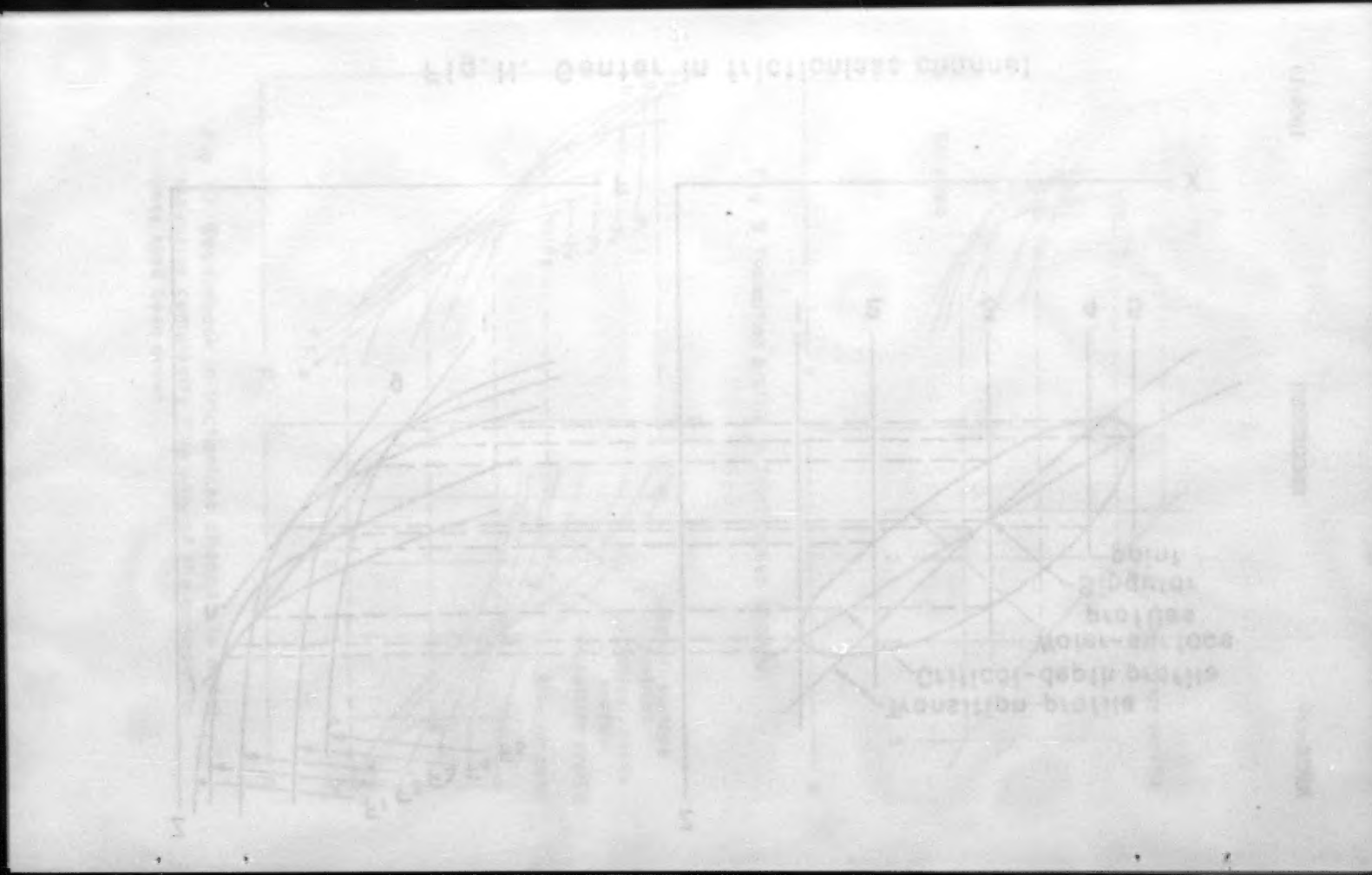

Journal of the
HYDRAULICS DIVISION
Proceedings of the American Society of Civil Engineers

FRICTION MEASUREMENTS IN APALACHIA TUNNEL

Rex A. Elder,[1] M. ASCE
(Proc. Paper 1007)

SPECIAL NOTE

This paper supersedes and supplements a paper titled "Friction Coefficients in a Large Tunnel" by G. H. Hickox, A. J. Peterka, and R. A. Elder, published as Paper No. 2353, Transactions of the American Society of Civil Engineers, Volume 113, 1948, page 1027. An error in the use of the basic data has been found which changes to varying degrees all of the results published in that paper. This error consisted of the transposition of columns 7 and 8 in Table 2, Elevations of Hydraulic Grade Line and Measured Head Losses, page 1035. Correction of the error results in a major change in the friction coefficient for the steel pipe, changing the f value in Weisbach's equation from 0.0085 at maximum gate to 0.0138. The concrete tunnel values changed from an average of 0.0133 to 0.0138 and 0.0127 for the two test reaches, while the unlined rock tunnel values only change from 0.094 to 0.096. Thus, the only major effect was in the steel pipe data. The authors exceedingly regret this error.

SYNOPSIS

The Tennessee Valley Authority's Apalachia power tunnel was in operation continuously from its initial operation in 1943 until October 1953. At that time it was unwatered and inspected. The tunnel surfaces were found to have become covered with a uniform 5/16-inch deposit of a black mucilaginous material. Tunnel friction measurements were made in 1944, five months after the initial filling, and again in 1954, five months after the inspection.

This report presents the methods used in reducing both sets of data. The results are presented in terms of the friction coefficient, f, in the Weisbach equation. Values of n for the Manning equation are also shown. A description is given of each type of surface for which coefficients could be calculated.

Note: Discussion open until November 1, 1956. Paper 1007 is part of the copyrighted Journal of the Hydraulics Division of the American Society of Civil Engineers, Vol. 82, No. HY 3, June, 1956.

1. Head, Hydr. Lab., Div. of Water Control Planning, Hydr. Data Branch, Tennessee Valley Authority, Norris, Tenn.

Description of Tunnel

The Apalachia Project of the Tennessee Valley Authority was built primarily as a power project and has been described by H. W. Goodhue, R. L. Smart, and A. A. Meyer.(1) The main structures are a comparatively low ponding and diversion dam, a pressure conduit approximately 8.3 miles long, a surge tank, and a powerhouse containing two turbines.

Although the pressure conduit consists mainly of a concrete-lined tunnel 18 feet in diameter, it does have two fairly long reaches of unlined rock which have nominal diameters of 20 feet and 22 feet. Just below the dam there is a comparatively short length of steel pipe 18 feet in diameter. At several other places where sufficient cover for the pressure tunnel is lacking, short lengths of steel pipe of 16-foot and 18-foot diameters are used. The alignment is nearly straight, but topographical considerations necessitated several bends. In general, the grade is quite flat, sloping toward the powerhouse. Figure 1 shows a plan of the test reach, which is approximately the upper two-thirds of the conduit length. All significant features, such as lengths, diameters, types of linings, and alignment are shown.

Piezometers

During the construction of the conduit seven sets of piezometers were installed at the locations shown in Figure 1 so that tests could be made to determine the various hydraulic losses.

The installations at piezometers A, B, C, D, and E consisted of a ring of four piezometers spaced at 90° intervals around the conduit and manifolded together so that an average pressure could be obtained. In 1954 two of the four piezometer openings at A were unusable. Piezometers F and G consisted of a single opening at the horizontal centerline.

Figure 1 shows that the piezometers are so placed that friction loss measurements could be obtained on sections containing three types of conduit: 18-foot steel pipe, 18-foot concrete-lined tunnel, and unlined rock tunnel. It was also possible to measure the loss in one of the bends.

Conduit Surfaces at Completion of Construction

At the completion of construction several very different and distinctive tunnel surfaces were present. These are described in some detail in the following section since a clear understanding of the surface characteristics is necessary for an intelligent interpretation of the data.

Steel Pipe

The various steel pipe sections were formed of plates rolled to the proper curvature and butt-welded. After the pipes were completed, the inner surfaces were covered with bituminous paint, applied hot with swabs. Each application of the swab covered an area approximately 6 inches wide and 2 feet long and deposited a layer of bituminous material approximately 1/16 inch deep. The cold steel cooled the paint so rapidly that the resulting surface was quite irregular and included ridges and bumps up to 1/8 inch high. However, the surface of the paint itself was almost glossy. Figure 2 shows the interior of one of the steel pipes treated in this manner.

Between Stations 255+97.50 and 259+17.67 the steel liner was not painted hot because of the lack of ventilation in this section at the time of painting. Instead, the bituminous paint was applied cold in a slightly diluted condition. This produced a smoother surface than that in the other pipe sections.

Concrete Tunnel

The 18-foot concrete tunnel lining was poured in two stages. An 80° invert section was poured first. The surface of the invert, which was formed by a screed traveling along the top of the longitudinal invert forms, was floated with steel floats immediately after the screed had passed. The quality of the concrete was controlled very carefully so that the best possible surface would result. In addition, concreting was carried on continuously so that no joint irregularities would occur in the invert section.

The arch section was poured against a three-piece steel form, of which the top piece covered a 90° arc and the two side pieces 95° each. Hinged at each joint, these form sections, each 5 feet long, could be collapsed and moved ahead through the other sections. Thus, irregularities due to transverse form joints occurred every 5 feet on the final surface. For convenience in erection, four form sections were kept bolted together as a unit during each change. There is no reason to believe that irregularities at the unit joints are larger than any of the others, because the units were aligned by drift pins in the same manner as were the sections composing the units. Each piece of each section was equipped with an 18-inch by 24-inch inspection door and two or three 2-inch grout pipe holes. Each of these left a slight irregularity on the surface, averaging probably not more than 1/32 inch high. Some 400 feet of forms were used so that concrete could be placed continuously without resorting to transverse bulkheads.

After the forms were removed, the surface was given a coat of curing compound. This compound disintegrates with time and was probably completely washed off by the time the tests were made. Figure 3 shows the concrete tunnel lining after the forms were removed and before the curing compound was applied.

The concrete for the tunnels was obtained from two mixing plants with aggregate for both plants from the same source. All concrete upstream from the Turtletown Creek Adit was obtained from the mixer at the dam site. All concrete downstream from Turtletown Creek was from the McFarland mixing plant. The concrete upstream from Turtletown Creek was placed after that downstream from that point.

Unlined Rock Tunnel

The unlined rock tunnel sections are of two nominal diameters, but are otherwise similar. Headings were advanced by shooting drifts 11 feet long; and, although the nominal diameter was approximated at the beginning of each drift, the actual diameter gradually increased away from the heading. In addition, the unusually hard rock broke quite irregularly, as shown in Figure 4. Maximum, minimum, and typical sections for both the 20-foot-diameter and the 22-foot-diameter unlined sections are given in Figure 5. The bottom of the tunnel had not been cleaned out when the cross sections were measured so that the exact shape of the bottom 80° to 90° arc is unknown. Areas and perimeters have been determined by measuring the known part and assuming the remainder of the cross section to be similar. Characteristics of the unlined sections are summarized in Table 1.

TABLE 1

CHARACTERISTICS OF UNLINED ROCK TUNNEL SECTIONS

Nominal Diameter (ft)	Area, in Square Feet			Diameter, Equivalent Circle (ft)	Hydraulic Radius, in Feet		Average Overbreak (ft)
	Maximum	Minimum	Average		Equivalent	Measured	
(1)	(2)	(3)	(4)	(5)	(6)	(7)	(8)
20...	419	335	375.3	21.86	5.465	5.36	0.93
22...	504	368	430.8	23.42	5.855	5.68	0.71

Conduit Surfaces after 10 Years of Service

The initial filling of the Apalachia tunnel was made on August 6, 1943. It remained filled from that time until October 16, 1953, when the tunnel was unwatered for inspection purposes. The October 1953 inspection found the tunnel to be in the following condition.

General

All tunnel surfaces were found to be coated with a 5/16-inch layer of black mucilaginous material. This deposit was exceedingly uniform both in depth and in surface roughness characteristics. It covered and eliminated all small original surface roughnesses but it reproduced all major surface shapes such as joint misalignments. This material so effectively eliminated the original surface roughness characteristics that the steel and concrete sections were indistinguishable.

X-ray spectrographic analyses showed the coating material to be primarily manganese in the forms MnO and Mn_2O_3. It is assumed that deposition was due to the adsorption of the manganese by algal polysaccharides through the process determined by the University of Tennessee and the Aluminum Company of America(2) after a similar deposition was found in one of Alcoa's tunnels located 35 miles north of the Apalachia project.

Downstream from the unlined rock section a strip approximately 1-1/2 feet wide along the bottom was free of the deposited material. The cause of this was felt to be the continual movement of small amounts of sand and gravel picked up in the unlined section.

Throughout the tunnel, areas were found where sometime previous to the inspection the material had peeled off. New deposition had started but the edges at the break remained well defined. These areas varied in size from less than one square foot to 15 or 20 square feet. No particular surface seemed to peel more than the others and probably not more than 2 to 3 percent of the total tunnel surface was affected. Figure 6 shows the general surface texture of the coating and illustrates the reproduction of major surface shapes and the sharp edges at a point where peeling had occurred.

Steel Pipe

The irregularities created by the bitumastic paint were eliminated by the manganese coating.

The tunnel was unwatered 2-1/2 days for the 1953 inspection. At the end of that time it was noted that considerable flaking of the deposited coating occurred along the overhead portions of the exposed steel pipes, due to the drying out of the material. Probably 20 to 30 percent of the total surface was affected. Thus, the exposed pipe surfaces at the dam and at Turtletown Creek Adit became considerably roughened from a hydraulic standpoint. These exposed lengths extended between Stations 1+28 and 9+15 and between Stations 218+66 and 221+01. The liners at Apalachia Adit, McFarland, and the one between Turtletown Creek and McFarland are all buried and were not exposed to the sun. They did not, therefore, become roughened.

Concrete Tunnel

The coating on the concrete surfaces was of uniform texture. All irregularities due to the form joints and inspection doors were completely obliterated by the deposited coating.

Unlined Rock Tunnel

The 5/16-inch coating could not materially change the shape of the unlined rock surfaces. It did tend to round over the edges of the protruding rock. The bottom in this section may have changed slightly from a hydraulic roughness standpoint. Originally some of the holes were filled with some sand and gravel. Ten years of use has washed the fine material out of the unlined sections and has worked the larger particles downstream. Most of these larger stones have become worn until they look like river gravel. In many places, especially in the 22-foot-diameter reach, these large stones have started pot holes. Some of these pot holes are 6 inches deep and 8 to 10 inches in diameter. There are not sufficient pot holes, however, to have any appreciable roughness effect.

1944 Field Tests

The 1944 field observations were made at the same time as the turbine index tests. This procedure was possible because both types of tests required that the turbines be operated over a large range of gate openings with each gate position held constant for a sufficient length of time to allow the flow to become steady.

On January 25, 1944, unit 1 was operated alone. The day started clear but became partly cloudy by late afternoon. On January 26, both units were operated identically. This day was dark and rainy.

Manometer Installations

At Apalachia Dam Adit, two water-air differential manometers and one open U-tube mercury manometer were used, the latter being attached to piezometer C and the others to piezometers A and B, and B and C, respectively.

At Apalachia Adit, one water-air differential manometer and one open U-tube mercury manometer were used. In this location the open mercury manometer was connected to piezometer E and the water-air differential manometer to piezometers D and E.

At both Turtletown Creek Adit and McFarland Adit, single-column 10-foot mercury manometers were used. These manometers were made in two sections to facilitate carrying and were carefully calibrated in the Hydraulic Laboratory of the Tennessee Valley Authority.

At the Apalachia Dam Adit, the pressures were low enough so that the gages could be installed nearly at tunnel level. Each manometer was equipped with a blowoff cock so that the piezometer lines could be flushed frequently.

Maximum and minimum pressures at the other three locations were too great to allow the manometers to be installed at tunnel level. Therefore, it was necessary to place them on the hillsides above the tunnel. Considerable difficulty was encountered in finding suitable manometer sites at the proper elevations because of the steepness of the terrain. Data from all manometers were tied together through the level system established for the tunnel construction.

Connection of the manometers to the piezometer lines was by 3/4-inch pipe. The long lines used for most of these connections could have been a source of considerable trouble due to differential temperature effects. Fortunately, however, the tests were conducted on days when the air temperatures were within a few degrees of the water temperature and did not vary materially.

On January 25, solar heating may have slightly affected some of the pressure data, but this effect should have been negligible since at Apalachia where the small differentials were measured the vertical length subjected to differential heating was not more than 3 feet. It being January and a partly cloudy day, the available solar energy was not sufficient to appreciably affect the larger differentials between the other piezometers.

Observations

Because each of the four locations was entirely isolated from the others and from the powerhouse, it was necessary to take readings at 1-minute intervals continuously throughout the test period to ensure a complete record. All observers' watches were carefully compared at the beginning and end of each day's observations and all time readings were corrected to correspond with a master electric clock at the powerhouse. At each location the manometers were operated and read by an experienced member of the Hydraulic Laboratory's engineering staff.

Although every effort was made to obtain continuous records at each location, a number of breaks did occur. For example, on January 26 rain interfered several times with the recording of the measurements, as the data paper became so wet that a legible record could not be kept. At one gate opening on January 26, the top of the mercury column at Turtletown Creek was behind a rubber connector which united the two 5-foot gage sections.

1954 Field Tests

The 1954 field tests were made on March 27 and 28, the single-unit test being performed on unit 1 on the 28th and the double-unit tests on the 27th. The 27th was a dark rainy day and the 28th was clear. The gates for the units are presently blocked at approximately a 90 percent scale reading. A test was made at this point on the 27th but time did not permit a reading at this point on the 28th.

Piezometer Cleaning

At the time of the October 1953 inspection, an area at least 3 feet in diameter was cleaned around all piezometer openings.

Manometer Installations

At Apalachia Dam three single-column, 5-foot water gages were mounted on the hillside at such an elevation that all readings would be within the 5-foot range.

At Apalachia Adit the same equipment was used as in the 1944 tests.

At Turtletown Creek Adit a 5-foot U-tube mercury manometer was mounted while at McFarland a 5-foot single-column water gage was used at multiple locations. A series of temporary benchmarks was set on the steep hillside at the McFarland site and as the hydraulic grade line varied the water column gage was moved to keep the reading within the range of the gage.

All gages were connected to the piezometer outlets by means of 1/2-inch translucent polyethylene plastic tubing. Solar radiation probably caused an appreciable effect on the piezometer A to B differentials on March 28; otherwise no effect should have occurred.

Observations

Portable two-way radio equipment was available for use at each adit and at the powerhouse. A 1-minute time signal was broadcast from the powerhouse to initiate a reading at each gage site. Time signal checks were broadcast about every 20 minutes and at the beginning of each steady test period. The use of the radio made it possible to get complete data at every station for every gate position. As in the 1944 tests, experienced Hydraulic Laboratory personnel were used at all gage sites.

Tunnel Discharges

Tunnel discharges for both test periods were based on records obtained at a gaging station immediately below the powerhouse. Since steady river flow did not occur during the actual testing period because of the short period of time each gate position was held, the actual discharges were calculated on the basis of differential pressure measurements obtained from turbine scroll case piezometers. These pressures were correlated to the river discharges by measurements obtained at periods when the gate openings were held constant for a sufficient period for the river flow to stabilize and thus to allow the determination of the discharge from the gage rating curves. Discharge measurements made at the station by the United States Geological Survey were carefully examined and plotted to give the best rating curve for the time of the friction measurements.

1944 Tests

The actual gate opening depends on the movement of the servomotor piston. In turn, the discharge varies with the gate opening, and the differential pressure with the discharge. Thus, the differential pressure should vary smoothly with the observed movement of the servomotor piston.

It is probable that in 1944 the measurement of piston travel was more

accurate than the measurement of differential pressure. Accordingly, the turbine gate openings were recorded in terms of the movement of the servomotor piston that opens the gates and the differential pressure for each gate opening was taken from smooth curves drawn through the points determined by the observed relationship between piston movement and differential pressure. Table 2 summarizes, for each gate opening on January 25 and 26, the piston movement, the observed differential pressure, and the adjusted value taken from the smooth curve.

River stages existing at the gaging station during the 25 percent and 100 percent gate openings were found to indicate river discharges of 1150 cubic feet per second and 3290 cubic feet per second, respectively. These discharges included both the flow through the tunnel and the flow in the river above the powerhouse. The latter discharge was measured during the tests and was found to be 84 cubic feet per second; but, as the river discharge can be determined only to the nearest 10 cubic feet per second, the net discharges through the turbines may be considered as 1070 cubic feet per second and 3210 cubic feet per second.

The known discharge of 3210 cubic feet per second for both units at 100 percent gate opening on January 26 was divided between the two units in proportion to their power outputs, which index test data showed to be 39,790 kw and 40,000 kw for units 1 and 2, respectively. Assuming that both units were operating at the same head and efficiency, the corresponding discharges were 1600 cubic feet per second and 1610 cubic feet per second. Discharges for each unit at other gate openings were then calculated by assuming the discharge to be proportional to the square root of the differential pressure. These values for units 1 and 2 on January 26 are also given in Table 2, which shows the calculated discharge for 25 percent gate opening to be 1060 cubic feet per second. This compares favorably with the value of 1070 cubic feet per second obtained from the rating curve. Discharges for unit 1 on January 25 were calculated from the same relationship and are also given in Table 2.

1954 Tests

The method used in measuring the scroll case differentials for the 1954 tests was more accurate than that used in 1944. Therefore, it was not necessary to adjust these values on the basis of the servo piston movement measurements. Table 3 gives the measured scroll case differential pressures.

Steady river stages were not obtainable on the days of the tests but arrangements were made to get discharge tests shortly after the friction measurement tests. Single-unit tests were possible and were made at gate openings of 60 percent on unit 1 and 58 percent for unit 2. The rating curve gave a discharge of 1300 cubic feet per second for both units. These discharges include the flow in the river above the powerhouse and the leakage through the shutdown unit. Subsequent field measurements gave a value of 50 cubic feet per second to these flows. The net turbine flows were thus 1250 cubic feet per second. The scroll case differentials were measured as 94.92 and 90.52 inches of water for units 1 and 2, respectively. By using these discharges and differential pressures, the coefficients K in the equation:

$$Q = K\sqrt{\Delta P} \qquad (1)$$

TABLE 2

1944 TURBINE DIFFERENTIAL PRESSURES AND DISCHARGES

Gate Opening (%)	(a) January 25				(b) January 26								
	Unit 1				Unit 1			Unit 2			Discharge (cfs)		
	Piston Movement (in.)	Differential Pressure (In. of mercury)		Discharge (cfs)	Piston Movement (in.)	Differential Pressure (in. of mercury)		Piston Movement (in.)	Differential Pressure (in. of mercury)		Unit 1	Unit 2	Total
		Observed	Adjusted			Observed	Adjusted		Observed	Adjusted			
	(1)	(2)	(3)	(4)	(5)	(6)	(7)	(8)	(9)	(10)	(11)	(12)	(13)
25...	4.22	1.32	1.32	525	4.25	1.345	1.35	3.19	1.360	1.36	530	530	1,060
30...	4.69	1.99	1.97	640	4.75	1.926	1.90	3.72	1.964	1.99	628	640	1,270
35...	5.19	2.76	2.74	755	5.25	2.545	2.57	4.25	2.726	2.70	730	745	1,475
40...	5.69	3.56	3.56	860	5.72	3.405	3.35	4.78	3.516	3.50	833	850	1,685
45...	6.25	4.60	4.59	975	6.25	4.255	4.25	5.28	4.313	4.31	939	943	1,880
50...	6.75	5.56	5.58	1,075	6.75	5.112	5.12	5.78	5.188	5.19	1,030	1,033	2,060
55...	7.28	6.67	6.72	1,180	7.22	5.938	5.90	6.31	6.163	6.14	1,106	1,124	2,230
60...	7.75	7.77	7.73	1,265	7.72	6.819	6.75	6.81	6.978	6.98	1,182	1,198	2,380
65...	8.25	8.84	8.80	1,350	8.22	7.455	7.58	7.31	7.883	7.83	1,252	1,269	2,520
70...	8.75	9.85	9.87	1,430	8.75	8.500	8.45	7.81	8.528	8.62	1,322	1,331	2,650
75...	9.25	10.93	10.93	1,500	9.25	9.330	9.26	8.28	9.598	9.36	1,383	1,387	2,770
80...	9.75	12.00	11.98	1,575	9.75	10.020	10.03	8.81	9.971	10.15	1,440	1,443	2,880
85...	10.22	13.09	12.95	1,640	10.25	10.620	10.73	9.31	10.905	10.86	1,490	1,495	2,980
90...	10.72	13.82	13.97	1,700	10.72	11.305	11.33	9.81	11.700	11.53	1,530	1,540	3,070
95...	....	....	....	....	11.25	12.110	11.92	10.37	12.253	12.18	1,570	1,582	3,150
100...	....	....	....	....	11.73	12.195	12.36	10.81	12.425	12.61	1,600	1,610	3,210

TABLE 3

1954 TURBINE DIFFERENTIAL PRESSURES AND DISCHARGES

Gate Opening (%)	March 28 Unit 1 Piston Movement (in.)	March 28 Unit 1 Observed Differential Pressure (in. water)	March 28 Unit 1 Discharge (cfs)	March 27 Unit 1 Piston Movement (in.)	March 27 Unit 1 Observed Differential Pressure (in. water)	March 27 Unit 2 Piston Movement (in.)	March 27 Unit 2 Observed Differential Pressure (in. water)	Discharges (cfs) Unit 1	Unit 2	Total
25	...	...	...	4.25	14.08	3.50	18.41	481	564	1045
35	...	...	...	5.22	29.65	4.34	32.68	699	751	1450
40	5.72	40.46	826	5.75	38.88	4.75	39.56	800	826	1626
45	6.25	51.95	935	6.44	52.59	5.38	52.80	930	955	1885
50	6.75	64.50	1040	6.97	63.67	5.91	63.65	1024	1048	2072
55	7.25	77.62	1140	7.50	74.97	6.44	75.07	1111	1138	2249
60	7.75	92.35	1243	7.97	85.31	6.94	86.54	1185	1222	2407
65	8.25	104.68	1323	8.50	96.46	7.62	101.05	1260	1321	2581
70	8.75	119.00	1410	9.00	107.10	7.97	107.88	1328	1365	2693
75	9.25	131.93	1484	9.47	116.71	8.44	117.89	1386	1427	2813
80	9.72	144.56	1553	10.00	125.78	8.97	126.64	1439	1479	2918
85	10.25	159.36	1630	10.44	135.05	9.44	135.65	1491	1530	3021
Open	...	...	...	11.12	144.88	10.31	149.73	1544	1608	3152

were calculated and found to be 128.3 for unit 1 and 131.4 for unit 2. These compare with a coefficient of 128.3 determined for unit 1 in 1944 and 127.9 for unit 2. One of the unit 2 scroll case piezometers was modified when the unit was shut down in 1953 so this change in coefficient is reasonable. Table 3 gives the discharges calculated on the basis of the 1954 coefficients.

Reduction of Test Data

Manometer readings were reduced to elevations of pressure grade line. These elevations, as well as the differential pressures between piezometers A and B, B and C, and D and E, are shown in Table 4 for the 1944 data and in Table 5 for the 1954 data. Reservoir elevations for the test periods were taken from the chart of the headwater recording gage at the dam and are also shown in Tables 4 and 5.

The hydraulic grade line elevations and differential pressures given in Tables 4 and 5, together with the discharge rates in Tables 2 and 3 and the general data shown in Figure 1, were sufficient for computation of the various losses in the test sections of the tunnel.

The tunnel conditions in 1944 were such that the data in Table 4 could be reduced to give friction loss coefficients for three general tunnel surface roughnesses: bitumastic painted steel, concrete, and unlined rock. The data also allowed calculation of the bend loss coefficient for bend 1.

The tunnel conditions in 1954 also resulted in three general tunnel surface roughnesses for which friction loss coefficients could be calculated from the data of Table 5. Two of the three 1944 surface roughness types were materially changed by the 5/16-inch manganese coating and only the rock was essentially similar in 1954 and 1944. The bend 1 loss coefficient could also be calculated from the 1954 data.

The section between piezometers D and E contained one contraction and one expansion from 18 feet to 16 feet. The losses due to these proved to be so small for both sets of test data that they could not be separated.

Friction losses for each type of surface were expressed in terms of the friction coefficient f in the Weisbach equation:

$$h_f = f \frac{L}{D} \frac{V^2}{2g} \qquad (2)$$

and the results are plotted as a function of Reynolds' number Re in which

$$\text{Re} = \qquad \text{Re} = \frac{VD}{\nu} \qquad (3)$$

In these equations, L in the length of any test reach; D is the diameter of the pipe; V is the average flow velocity; h_f is the energy loss, over the length L; and ν is the kinematic viscosity of the flowing water.

The water temperature on January 25, 1944, and on March 27 and 28, 1954, was 8° C, while the temperature on January 26, 1944, was 7° C. A value of ν of 1.498×10^{-5} was used at 8° C and a value of 1.542×10^{-5} at 7° C.

The values of the roughness coefficient n in the Manning equation:

TABLE 4

ELEVATIONS OF HYDRAULIC GRADE LINE AND MEASURED HEAD LOSSES--1944 TESTS

Gate Opening (%)	Grade Line Elevation (ft. above el. 1200) at Piezometer					Measured Loss, in Feet, in Sections		
	...	C	E	F	G	A-B	B-C	D-E
(1)	(2)	(3)	(4)	(5)	(6)	(7)	(8)	(9)
	Reservoir	Apalachia Dam	Apalachia	Turtletown Creek	McFarland	18-foot Steel Pipe	Bend 1	Apalachia Transition
				January 25--One Unit				
45	77.65	76.96	75.85	.....	.....	0.076	0.047	0.120
50	77.75	76.98	75.59	70.75	69.50	0.096	0.064	0.148
55	77.82	76.99	75.23	69.39	67.91	0.110	0.073	0.177
60	77.84	76.80	74.77	68.07	66.17	0.128	0.089	0.211
65	77.91	76.83	74.48	66.80	64.64	0.145	0.098	0.232
70	77.93	76.79	74.07	65.44	63.04	0.166	0.110	0.260
75	78.00	76.74	73.75	64.15	61.64	0.183	0.123	0.287
80	78.01	76.61	73.34	62.92	60.13	.....	.....	0.312
				January 26--Two Units				
25	78.38	77.64	76.29	71.46	70.51	0.088	0.051	0.145
30	78.47	77.50	76.48	68.76	67.23	0.131	0.075	0.199
35	78.55	77.31	.....	65.13	62.62	0.188	0.108	.....
40	78.58	77.02	73.15	61.10	57.54	0.241	0.144	0.368
45	78.62	76.72	71.93	57.13	52.98	0.297	0.177	0.450
50	78.61	76.40	70.62	52.78	47.65	0.357	0.210	0.546
55	78.66	76.08	69.32	48.61	42.59	0.411	0.251	0.634
60	78.68	75.78	67.96	.....	37.24	0.475	0.290	0.724
65	78.69	75.48	66.63	39.96	31.94	0.535	0.325	0.820
70	78.70	75.11	65.33	35.86	27.02	0.592	0.363	0.899
75	78.70	74.78	64.12	31.81	22.04	0.645	0.396	0.994
80	78.69	74.46	62.84	27.91	17.28	0.699	0.432	1.066
85	78.70	74.18	61.75	24.43	13.10	0.747	0.458	1.147
90	78.69	73.92	60.76	21.28	9.14	0.788	0.489	.....
95	78.67	73.71	.....	18.45	5.70	0.834	0.521	.....
100	78.66	73.51	.....	16.72	3.68	0.862	0.536	.....
100	78.65	.....	59.28	16.69	3.67	.....	.....	1.315

TABLE 5

ELEVATIONS OF HYDRAULIC GRADE LINE AND MEASURED HEAD LOSSES--1954 TESTS

Gate Opening (%)	Grade Line Elevation (ft. above el. 1200) at Piezometer					Measured Loss, in Feet, in Sections		
	...	C	E	F	G	A-B	B-C	D-E
(1)	(2)	(3)	(4)	(5)	(6)	(7)	(8)	(9)
	Reservoir	Apalachia Dam	Apalachia	Turtletown Creek	McFarland	18-foot Steel Pipe	Bend 1	Apalachia Transition
				March 28--One Unit				
40	78.06	77.789	77.059	74.156	73.538	0.070	0.026	0.070
45	78.08	77.773	76.792	73.158	72.316	0.089	0.040	0.095
50	78.12	77.698	76.408	71.993	70.896	0.107	0.048	0.124
55	78.14	77.618	76.066	70.744	69.248	0.135	0.059	0.149
60	78.20	77.510	75.654	69.454	67.616	0.161	0.075	0.173
65	78.22	77.359	75.164	68.103	65.925	0.166	0.083	0.198
70	78.16	77.125	74.595	66.623	64.096	0.178	0.092	0.225
75	78.07	76.892	74.057	65.200	62.352	0.195	0.099	0.250
80	77.92	76.652	73.564	63.829	60.725	0.219	0.108	0.274
85	77.84	76.419	73.050	62.301	58.932	0.242	0.117	0.299
				March 27--Two Units				
25	78.21	77.656	76.328	71.920	70.546	0.095	0.047	0.115
30	.....	.....	.....	.....	.....	.....	.....	.....
35	78.23	77.222	74.606	66.227	63.629	0.186	0.095	0.228
40	78.17	76.994	73.702	63.062	59.804	0.234	0.116	0.289
45	78.01	76.433	72.030	57.707	53.339	0.321	0.162	0.396
50	78.00	75.996	70.655	53.412	48.174	0.386	0.195	0.478
55	77.90	75.563	69.258	49.019	42.819	0.455	0.231	0.565
60	77.80	75.104	67.867	44.589	37.498	0.521	0.261	0.650
65	77.70	74.546	66.226	39.616	31.472	0.588	0.306	0.741
70	77.66	74.180	65.131	36.145	27.288	0.644	0.330	0.809
75	77.67	73.790	63.931	32.384	22.755	0.699	0.359	0.886
80	77.63	73.453	62.788	28.665	18.220	0.757	0.391	0.959
85	77.59	73.164	61.786	25.246	14.138	0.812	0.412	1.024
Open	77.64	72.708	60.335	20.641	8.589	0.880	0.449	1.115

$$V = \frac{1.486}{n} R^{2/3} S^{1/2} \quad (4)$$

can be directly related to f in equation 2 and are also shown on the plotted data for the benefit of those engineers who are more familiar with the use of n than f.

The bend losses were expressed in terms of the velocity head by the equation:

$$H_B = C_B \frac{V^2}{2g} \quad (5)$$

in which H_B is the head loss due to the bend and C_B is the loss coefficient.

1944 Friction Loss in 18-foot Steel Pipe

The friction coefficients for the 18-foot steel pipe were computed by equation 2 from the discharges given in Table 2, the observed pressure drops given in column 7, Table 4, and the dimensions of the test section taken from Figure 1. These values are given in Table 6 and are plotted in Figure 7 (a).

1954 Friction Loss for Flakes-coated Surface

In 1954 the manganese coating in the steel pipe which contains piezometer reach A-B was roughened by the flaking of the coating during the inspection unwatering period. Friction coefficients for this type of surface were computed by equation 2 from the discharges of Table 3, the observed pressure drops given in column 7, Table 5, and the dimensions of the section. These values are given in Table 7 and are plotted in Figure 7 (b).

Bend Losses

The pressure drop measured between piezometers B and C was composed in 1944 of the loss due to bend 1 and the friction loss in 198 feet of tunnel, of which 120 feet was 18-foot steel pipe and 78 feet was 18-foot concrete-lined tunnel. In 1954 the 198 feet was of the normal-coated type. As both test sections of the 18-foot concrete-lined tunnel contain bends, it was necessary to determine the bend loss coefficients and the friction coefficients for the concrete tunnel by the method of successive approximations.

In reducing the 1944 data the tunnel between piezometers B and C was first assumed to be composed entirely of 18-foot steel pipe for which the friction coefficient was known. The friction loss in this reach was then approximated by assuming it to be proportional to the measured loss between piezometers A and B. Subtracting this calculated friction loss from the total measured loss gave the loss for bend 1, from which the preliminary bend loss coefficient C_B was computed by equation 5. The value of C_B thus determined was applied to bends 2 and 3 between piezometers C and D for determination of an approximate f value for the concrete tunnel. The bend loss coefficient C_B for bend 1 was then recalculated by using the f values for the steel pipe and concrete tunnel.

TABLE 6

1944 FRICTION LOSS COMPUTATIONS

Gate Opening (%)	Velocity (ft/sec)	Reynolds' Re	18-foot Steel Pipe Weisbach's f	Bend 1 Loss Net Loss (ft)	Bend 1 Loss Coefficient C_B	18-foot Concrete-lined Tunnel[a] Computed Loss (ft) Bend	18-foot Concrete-lined Tunnel[a] Computed Loss (ft) Friction	18-foot Concrete-lined Tunnel[a] Weisbach's f
(1)	(2)	(3)	(4)	(5)	(6)	(7)	(8)	(9)
			January 25--One Unit					
45	3.83	4.6×10^6	0.0130	0.017	0.0746	0.07	0.92	0.0110
50	4.22	5.1×10^6	0.0136	0.026	0.0939	0.08	1.16	0.0114
55	4.63	5.6×10^6	0.0129	0.026	0.0781	0.10	1.48	0.0121
60	4.97	6.0×10^6	0.0130	0.034	0.0850	0.11	1.71	0.0121
65	5.30	6.4×10^6	0.0130	0.035	0.0800	0.13	1.99	0.0124
70	5.61	6.7×10^6	0.0133	0.038	0.0778	0.14	2.32	0.0130
75	5.89	7.1×10^6	0.0133	0.044	0.0816	0.16	2.54	0.0128
80	6.19					0.17	2.79	0.0127
			January 26--Two Units					
25	4.16	4.8×10^6	0.0128	0.014	0.0520	0.08	1.13	0.0114
30	4.99	5.8×10^6	0.0132	0.020	0.0517	0.11	1.71	0.0120
35	5.79	6.7×10^6	0.0141	0.031	0.0595	....	....	.....
40	6.61	7.7×10^6	0.0139	0.042	0.0619	0.20	3.30	0.0132
45	7.38	8.6×10^6	0.0137	0.050	0.0590	0.25	4.09	0.0131
50	8.09	9.4×10^6	0.0137	0.058	0.0570	0.30	4.93	0.0132
55	8.75	10.2×10^6	0.0135	0.071	0.0597	0.34	5.79	0.0137
60	9.35	10.9×10^6	0.0137	0.084	0.0618	0.40	6.70	0.0134
65	9.89	11.5×10^6	0.0138	0.094	0.0618	0.44	7.59	0.0136
70	10.40	12.1×10^6	0.0138	0.107	0.0636	0.49	8.39	0.0136
75	10.88	12.7×10^6	0.0137	0.116	0.0630	0.53	9.14	0.0135
80	11.31	13.2×10^6	0.0137	0.129	0.0648	0.58	9.97	0.0136
85	11.70	13.6×10^6	0.0137	0.135	0.0634	0.62	10.66	0.0136
90	12.07	14.0×10^6	0.0136	0.145	0.0640	....	....	.....
95	12.38	14.4×10^6	0.0137	0.159	0.0667	....	....	.....
100	12.61	14.7×10^6	0.0136	0.160	0.0647	0.72	12.19	0.0134

a. From Dam Adit to Apalachia Adit.

TABLE 7

1954 FRICTION LOSS COMPUTATIONS

Gate Opening (%)	Velocity (ft/sec)	Reynolds' Re	18-foot Flaked Coating Weisbach's f	Bend 1 Loss Net Loss (ft)	Bend 1 Loss Coefficient C_B	18-foot Normal Coating[a] Computed Loss (ft) Bend	Friction	Weisbach's f
(1)	(2)	(3)	(4)	(5)	(6)	(7)	(8)	(9)
			March 28--One Unit					
20	1.56	1.9×10^6	0.0197	-	-	0.01	0.16	0.0115
30	2.44	2.9×10^6	0.0190	-	-	0.02	0.41	0.0121
40	3.25	3.9×10^6	0.0167	0.003	0.0207	0.04	0.62	0.0102
45	3.67	4.4×10^6	0.0166	0.011	0.0523	0.05	0.84	0.0108
50	4.09	4.9×10^6	0.0162	0.012	0.0463	0.06	1.10	0.0116
55	4.48	5.4×10^6	0.0169	0.016	0.0513	0.08	1.33	0.0116
60	4.88	5.9×10^6	0.0170	0.024	0.0649	0.09	1.59	0.0117
65	5.20	6.2×10^6	0.0155	0.025	0.0595	0.10	1.90	0.0123
70	5.54	6.6×10^6	0.0146	0.026	0.0545	0.12	2.19	0.0125
75	5.83	7.0×10^6	0.0144	0.026	0.0493	0.13	2.46	0.0127
80	6.10	7.3×10^6	0.0148	0.029	0.0502	0.14	2.68	0.0126
85	6.40	7.7×10^6	0.0149	0.029	0.0455	0.15	2.92	0.0125
			March 27--Two Units					
25	4.11	4.9×10^6	0.0142	0.011	0.0420	0.06	1.15	
35	5.70	6.8×10^6	0.0144	0.026	0.0515	0.12	2.27	0.0119
40	6.39	7.7×10^6	0.0144	0.029	0.0458	0.15	2.85	0.0122
45	7.41	8.9×10^6	0.0147	0.045	0.0528	0.20	3.80	0.0122
50	8.14	9.8×10^6	0.0147	0.053	0.0514	0.25	4.62	0.0121
55	8.84	10.6×10^6	0.0147	0.064	0.0526	0.29	5.45	0.0122
60	9.46	11.4×10^6	0.0147	0.070	0.0503	0.33	6.25	0.0122
65	10.14	12.2×10^6	0.0144	0.086	0.0538	0.38	7.20	0.0122
70	10.58	12.7×10^6	0.0145	0.090	0.0517	0.42	7.82	0.0122
75	11.05	13.3×10^6	0.0144	0.098	0.0516	0.46	8.52	0.0122
80	11.46	13.8×10^6	0.0145	0.110	0.0538	0.49	9.22	0.0122
85	11.87	14.2×10^6	0.0145	0.110	0.0502	0.53	9.83	0.0122
Open	12.38	14.9×10^6	0.0144	0.121	0.0507	0.57	10.69	0.0122

a. From Dam Adit to Apalachia Adit.

The preliminary 1954 bend loss calculations were made by estimating the B-C reach to have an f value of 0.0125. This bend loss factor was then used for bends 2 and 3 to compute the f value for the normal-coated type of surface. The f value for the normal-coated surface was then used to recalculate the bend loss coefficient for bend 1.

It has been proven that anywhere up to 50 diameters of straight pipe are required to re-establish the friction loss gradient downstream from a bend.(3,4) Yarnell and Nagler(3) further established that non-uniform velocity distribution had an appreciable effect on the length of straight pipe required to re-establish the friction gradient. Since piezometer C is located only 112 feet, or 6.2 diameters, downstream from the end of bend 1, it would appear that only a portion of the total loss due to the bend can be measured. On the basis of the Yarnell and Nagler data it was estimated that probably only 50 percent is measured by the B-C piezometer differentials and that the remainder is measured as part of the C-D losses. Bend 3 ends 141 diameters upstream from piezometer D. The loss from bends 2 and 3 should therefore be entirely contained in the C-D measurements. Bend 4 ends 10 diameters upstream from piezometer E. It was estimated that 80 percent of the bend loss was measured between piezometers D and E and 20 percent remained in the E-F section. Bend 5 ends 231 diameters upstream from F. The loss therefore should be entirely contained in the E-F section. Similarly, the loss for bend 6 should be entirely contained in the F-G section since it ends 208 diameters upstream from piezometer G.

By using the above assumed distribution of measured bend loss and the measured loss for bend 1 as the base value, bend loss coefficients were calculated for the remaining five bends. Table 8 lists the six bends included in the test sections, together with the deflection angle, the radius, and the pipe

TABLE 8

BEND LOSS COEFFICIENTS

Bend No.	Deflection Angle	Radius (ft) r	Pipe Diameter (ft) D	Deflection Factor[a] K	Ratio $\frac{r}{D}$	90° Bend Loss Coefficient[a] F	Coefficient C_B 1944	Coefficient C_B 1954
(1)	(2)	(3)	(4)	(5)	(6)	(7)	(8)	(9)
1	34° 15' 34"	90	18	0.571	5.00	0.28	0.12	0.10
2	15° 43' 05"	250	18	0.311	13.9	0.45	0.11	0.09
3	18° 18' 53"	250	18	0.359	13.9	0.45	0.12	0.10
4	12° 40' 35"	90	16	0.257	5.63	0.30	0.05	0.05
5	4° 41' 51"	250	18	0.100	13.9	0.45	0.03	0.03
6	8° 43' 25"	250	18	0.179	13.9	0.45	0.06	0.05

[a]As reported by Creager and Justin[5].

diameter of each. Available information concerning bend losses indicates that C_B varies with the deflection angle and the ratio of bend radius to pipe diameter. Relative values of the coefficient in terms of these variables are given by Creager and Justin(5) whose values of K, reflecting the effect of deflection angle, are given in column 5. Column 6 gives values of $\frac{r}{D}$ for each bend and column 7 gives the corresponding values of the bend loss coefficient for a 90-degree bend as recommended by Creager and Justin. The values of

C_B for bends 1 through 6 are given in columns 8 and 9. For bend 1 this value was found by doubling the value found from the second set of bend loss calculations. For bends 2 through 6, the value of C_B is the value for bend 1 multiplied by the ratios of appropriate factors in columns 5 and 7. For example, in 1944:

$$C_{B2} = C_{B1} \times \frac{K_2}{K_1} \times \frac{F_2}{F_1} = 0.12 \times \frac{0.311}{0.571} \times \frac{0.45}{0.28} = 0.11$$

The values for bends 2 and 3 given in Table 8 were used to recalculate the f values for reach C-D, and these f values were then used to recalculate the bend 1 loss. These final C_B values are shown in column 6, Tables 6 and 7, and on Figure 8. The change from the average values used in Table 8 was not sufficient to warrant any further refinement of f or C_B.

1944 Friction Loss in 18-foot Concrete-lined Tunnel, Apalachia Dam Adit to Apalachia Adit

Hydraulically between piezometers C and D the test section contained 6617 feet of concrete-lined, 18-foot-diameter tunnel, bends 2 and 3, and one-half of bend 1. Elevations of the hydraulic grade line at piezometers C and E and the differential pressures between piezometers D and E are given in Table 4. Addition of the differentials between piezometers D and E to the hydraulic grade line elevations for E gave the grade line elevations at D; subtraction of these elevations from those at C gave the hydraulic losses between piezometers C and D.

Losses for bends 1, 2, and 3 were calculated by equation 5 from the values of C_B given in Table 8, and values of f were calculated from equation 2. The results of these calculations are summarized in Table 6 and plotted on Figure 7 (c).

1954 Friction Loss for Normal-coated Surface, Apalachia Dam Adit to Apalachia Adit

In 1954 the surface in this section was of the normal-coated type. Identical reduction procedures were used for the 1954 data as for the 1944 data. Table 7 summarizes the calculations. Figure 7 (d) shows the plotted f values.

1944 Friction Loss in 18-foot Concrete-lined Tunnel, Turtletown Creek Adit to McFarland Adit

Between Turtletown Creek Adit and McFarland Adit, the tunnel was largely a concrete-lined tunnel 18 feet in diameter similar to that between Apalachia Dam Adit and Apalachia Adit. It should, therefore, have the same friction and roughness coefficients. The computations are somewhat more difficult because the test section included not only 6944 feet of the 18-foot concrete lining but also 118 feet of steel pipe 18 feet in diameter, 598 feet of steel pipe 16 feet in diameter, 60 feet of concrete transitions having an average diameter of 17 feet, one contraction, two expansions, and bend 6. In addition, the tunnel did not have the same diameter at the two adits so that the measured drop in the hydraulic grade line is not equal to the drop in the energy grade line.

The drop in the energy grade line can be calculated by adding the velocity

head at each piezometer to the elevation of the hydraulic grade line at that piezometer and taking the difference of these sums. Thus, if the energy grade line is represented by E and the hydraulic grade line by H, and the Turtletown Creek and McFarland Adits by subscripts T and M, respectively, the drop in the energy grade line is:

$$\Delta E = \left(H_T + \frac{V^2_T}{2g}\right) - \left(H_M + \frac{V^2_M}{2g}\right)$$

This can be rewritten as:

$$\Delta E = (H_T - H_M) + \left(\frac{V^2_T}{2g} - \frac{V^2_M}{2g}\right) = (H_T - H_M) + \frac{\Delta V^2}{2g} \quad (6)$$

The friction loss in the 18-foot concrete-lined section of the tunnel is this value of ΔE less the other losses listed.

Losses in the steel pipe sections were calculated from equation 2 by using f values from Figure 7 (a), with the assumption that f did not vary with the change in diameter. Losses in the transition sections were ignored since reduction of the data for piezometer section D to E indicated no measurable loss due to the transitions. The bend loss was based on C_B values taken from Table 8 for bend 6. Values of f were calculated for the combined concrete surface sections on the basis of the remaining loss. The computations are summarized in Table 9 and the results are plotted on Figure 7 (c).

1954 Friction Loss for Normal-coated Surface, Turtletown Creek Adit to McFarland Adit

The tunnel surfaces in this reach were all of the normal-coated type. The only loss other than friction loss due to this surface roughness was that due to bend 6. The calculated f value is based on a tunnel section of which 91.5 percent is 18 feet in diameter, 7-3/4 percent is 16 feet in diameter, and 3/4 of one percent is 17 feet in diameter. On the basis of the Nikuradse[6,7,8] relative roughness concept, these f values should be slightly larger than those for the Apalachia Dam to Apalachia Adit section.

The total energy loss for this section was calculated in the same manner as for the 1944 data and the bend 6 losses were based on the Table 8 C_B value. The computations are summarized in Table 10 and the results are plotted on Figure 7 (d).

1944 Friction Loss in Unlined Rock Tunnel

Between the Apalachia and Turtletown Creek Adits the tunnel consisted of 3098 feet of unlined tunnel 20 feet in nominal diameter, 2902 feet of unlined rock tunnel 22 feet in nominal diameter, 7626 feet of 18-foot concrete-lined tunnel, 20 feet of concrete-lined transition averaging 17 feet in diameter, and 369 feet of 16-foot steel pipe. Losses were also caused by bend 5, the remaining 0.2 of the bend 4 loss, by the expansions from 18-foot concrete to 20-foot rock, by the contraction from 20-foot rock to 18-foot concrete, and by

TABLE 9

1944 FRICTION LOSS IN AN 18-FOOT CONCRETE-LINED TUNNEL,

TURTLETOWN CREEK ADIT TO McFARLAND ADIT

Gate Opening (%)	Computed Friction Losses (ft) Steel Pipe Sections	Computed Bend Loss (ft)	Net Loss Concrete Section (ft)	Weisbach's f	Reynolds' Re
(1)	(2)	(3)	(4)	(5)	(6)
		January 25--One Unit			
50	0.24	0.02	1.16	0.0107	5.1×10^6
55	0.29	0.02	1.37	0.0106	5.6×10^6
60	0.34	0.02	1.77	0.0118	6.0×10^6
65	0.39	0.03	2.00	0.0117	6.4×10^6
70	0.44	0.03	2.23	0.0117	6.7×10^6
75	0.48	0.03	2.33	0.0111	7.1×10^6
80	0.54	0.03	2.57	0.0110	7.4×10^6
		January 26--Two Units			
25	0.23	0.02	0.86	0.0082	4.8×10^6
30	0.34	0.02	1.40	0.0093	5.8×10^6
35	0.47	0.03	2.33	0.0115	6.7×10^6
40	0.61	0.04	3.32	0.0125	7.7×10^6
45	0.76	0.05	3.85	0.0117	8.6×10^6
50	0.92	0.06	4.77	0.0120	9.4×10^6
55	1.08	0.07	5.60	0.0121	10.2×10^6
60	1.23	0.08	-	-	10.9×10^6
65	1.38	0.09	7.74	0.0126	11.5×10^6
70	1.53	0.10	8.23	0.0126	12.1×10^6
75	1.67	0.11	9.10	0.0127	12.7×10^6
80	1.81	0.12	9.90	0.0128	13.2×10^6
85	1.93	0.13	10.56	0.0127	13.6×10^6
90	2.06	0.14	11.30	0.0128	14.0×10^6
95	2.16	0.14	11.88	0.0128	14.4×10^6
100	2.25	0.15	12.13	0.0126	14.7×10^6

TABLE 10

1954 FRICTION LOSS FOR NORMAL-COATED SURFACE,

TURTLETOWN CREEK ADIT TO McFARLAND ADIT

Gate Opening (%) (1)	Computed Bend Loss (ft) (2)	Net Loss (ft) (3)	Weisbach's f (4)	Reynolds' Re (5)
		March 28--One Unit		
20	0.00	0.31	0.0177	1.9×10^6
30	0.00	0.50	0.0118	2.9×10^6
40	0.01	0.71	0.0095	3.9×10^6
45	0.01	0.96	0.0100	4.4×10^6
50	0.01	1.24	0.0105	4.9×10^6
55	0.02	1.67	0.0117	5.4×10^6
60	0.02	2.04	0.0121	5.9×10^6
65	0.02	2.41	0.0126	6.2×10^6
70	0.02	2.79	0.0128	6.6×10^6
75	0.03	3.14	0.0130	7.0×10^6
80	0.03	3.42	0.0130	7.3×10^6
85	0.03	3.72	0.0128	7.7×10^6
		March 27--Two Units		
25	0.01	1.52	0.0127	4.9×10^6
35	0.02	2.88	0.0125	6.8×10^6
40	0.03	3.61	0.0124	7.7×10^6
45	0.04	4.84	0.0124	8.9×10^6
50	0.05	5.81	0.0124	9.8×10^6
55	0.06	6.87	0.0124	10.6×10^6
60	0.07	7.86	0.0124	11.4×10^6
65	0.08	9.03	0.0124	12.2×10^6
70	0.09	9.82	0.0124	12.7×10^6
75	0.10	10.68	0.0123	13.3×10^6
80	0.10	11.59	0.0124	13.8×10^6
85	0.11	12.32	0.0123	14.2×10^6
Open	0.12	13.37	0.0123	14.9×10^6

the contraction from 18-foot concrete to 16-foot steel pipe. The expansion from 20-foot rock to 22-foot rock and the contraction from 18-foot concrete to 16-foot steel are so gradual that losses due to them were neglected.

The energy loss in this section was not equal to the fall in the hydraulic grade line between the piezometers because of the smaller diameter, with correspondingly higher velocity, at piezometer F. The energy loss was determined by adding the difference between velocity heads at piezometers E and F to the elevation of the hydraulic grade line at piezometer F and subtracting the sum from the elevation of the hydraulic grade line at piezometer E. This process is similar to that employed in finding the energy loss between Turtletown Creek and McFarland Adits. The loss in the unlined rock tunnel was found by subtracting from the total energy loss not only the friction losses in the 18-foot and 17-foot concrete sections and in the 16-foot steel pipe, but also the losses due to bends 4 and 5 and the expansions and contractions.

The value of f to use in computing the losses due to the two concrete sections caused some concern since, as can be seen in Figure 7 (c), the f values for the section from Apalachia Dam Adit to Apalachia Adit differ materially from those for the section from Turtletown Creek to McFarland. A search of the construction records disclosed that two separate mixing plants were used for the tunnel concrete. A plant at the dam mixed all concrete placed upstream from Turtletown Creek Adit, while a plant at McFarland Adit was used for the sections below Turtletown Creek. The same source of aggregate was used at both plants and the same type of agitator cars was used to haul the concrete to the pour sites. The same equipment was used to place the concrete but different types of batching equipment and mixers were used at the mixing plants. It would not seem that these differences in equipment would have been responsible for the difference in f. However, the 1954 data for these two sections, as shown in Figure 7 (d), produced nearly identical values. Since essentially the same method of reduction was used for each set of data it would appear that a difference did exist in the surface characteristics of the original concrete surfaces. It was, therefore, concluded that a difference did exist and that the difference must be due to the source of concrete. Since the Apalachia Adit to Turtletown Creek Adit concrete all came from the dam mixer the f values for the concrete in the reach were taken from the Apalachia Dam to Apalachia Adit curve shown on Figure 7 (c).

The steel pipe f values were taken from the data shown on Figure 7 (a). This assumed that the change in diameter did not affect the f value. Hydraulic losses due to bends 4 and 5 were computed from the C_B values of Table 8 with 0.2 of the calculated bend 4 loss used.

The loss due to the enlargement from the 18-foot lined section to the 20-foot unlined was calculated from the equation given by Rouse:[9]

$$H_E = \left[1 - \left(\frac{D_{18}}{D_{20}}\right)^2\right]^2 \frac{V^2_{18}}{2g} \qquad (7)$$

which is

$$H_E = 0.104 \frac{V^2_{18}}{2g} \qquad (8)$$

At the entrance to the 18-foot lined tunnel, the concrete lining has a 9-inch chamfer, as shown in Figure 1, detail D. Tests on concrete box culverts with a similar beveled entrance[10] indicate that the loss at the entrance may be expressed in the form of equation 5 with a coefficient of 0.15.

It was not possible to determine roughness coefficients for the 20-foot and 22-foot unlined tunnels separately. However, values of f were computed from equation 2 by assuming that the same value applies equally to both diameters. In Figure 7 (e), f is plotted against a value of Re based on the average diameters and areas of the two sections. Values of n and v are also shown. Calculations of these factors are summarized in Table 11. Column 5, Table 11, includes the bend, contraction, and expansion losses.

In making the computations of f, the diameter was taken as that of a circle whose area was equivalent to the average area of the section. The hydraulic radius used was one-fourth of the equivalent diameter. This assumption is not quite correct because of the irregularity of the tunnel cross sections. For example, the average hydraulic radii of the 20-foot and 22-foot tunnels as measured from the cross sections are actually 5.36 feet and 5.60 feet instead of the equivalent diameter values of 5.465 feet and 5.855 feet, respectively. Use of the measured values in equation 2 produces values 2.3 percent smaller than those given in Table 11. The differences are small, however; and, in view of the uncertainty of actual tunnel shapes (which depend on the character of rock and the manner in which it breaks, as well as on the care taken in measuring the irregular sections), it is believed better to use the simpler assumption of an equivalent circular area and the corresponding hydraulic radius.

1954 Friction Loss in Unlined Rock Tunnel

The composition of the Turtletown Creek to McFarland test reach was essentially the same in 1954 as 1944 except that the steel pipe sections had to be split into two categories since 234 feet was exposed to the sun and became roughened similar to the piezometer A-B section while the remaining 135 feet was covered and therefore was of the normal-coated surface type.

The total energy loss in the section was obtained in the same manner as in 1944. There was no question as to the values of f to use since the two sections with normal-coated surfaces gave essentially identical results. Therefore, f was taken from the curves of Figure 7 (d) for the normal-coated surfaces and from Figure 7 (b) for the flaked coating in the 234 feet of exposed steel pipe. Hydraulic losses due to bends 4 and 5 were computed from the C_B values of Table 8. The expansion and contraction losses were calculated in the same manner as for the 1944 data and the same equivalent area dimensions were used in computing the f values. The calculations are summarized in Table 12 and the f values are plotted in Figure 7 (f).

SUMMARY

Tests on the Apalachia tunnel were made at discharges between 826 cubic feet per second and 3210 cubic feet per second. Friction coefficients were determined for five widely different types of surfaces, including steel coated with bituminous paint, concrete placed against steel forms, unlined rock, a fairly uniform deposited coating on the concrete and steel surfaces, and a roughened coating on a steel surface. Discharges were based on a rating

TABLE 11

1944 FRICTION LOSSES IN UNLINED ROCK TUNNEL

Gate Opening (%)	Computed Friction Losses: 18-foot Concrete Tunnel (ft)	17-foot Concrete Tunnel (ft)	16-foot Steel Pipe (ft)	Computed Miscellaneous Losses (ft)	Net Loss Unlined Tunnel (ft)	Weisbach's f	Reynolds' Re
(1)	(2)	(3)	(4)	(5)	(6)	(7)	(8)
			January 25--One Unit				
50	1.35	0.00	0.13	0.06	3.25	0.104	4.0×10^6
55	1.68	0.01	0.16	0.08	3.87	0.103	4.4×10^6
60	2.00	0.01	0.19	0.09	4.37	0.100	4.7×10^6
65	2.30	0.01	0.22	0.10	5.00	0.101	5.1×10^6
70	2.63	0.01	0.24	0.11	5.58	0.101	5.4×10^6
75	2.92	0.01	0.27	0.12	6.20	0.102	5.6×10^6
80	3.26	0.01	0.30	0.14	6.63	0.098	5.9×10^6
			January 26--Two Units				
25	1.31	0.00	0.13	0.06	3.17	0.109	3.8×10^6
30	2.02	0.01	0.19	0.09	4.18	0.100	4.6×10^6
35	-	-	-	-	-	-	-
40	3.74	0.01	0.34	0.16	7.39	0.100	6.1×10^6
45	4.74	0.02	0.42	0.20	8.91	0.097	6.8×10^6
50	5.74	0.02	0.51	0.24	10.71	0.097	7.5×10^6
55	6.76	0.02	0.60	0.27	12.33	0.096	8.1×10^6
60	-	-	-	-	-	-	-
65	8.70	0.03	0.77	0.35	15.90	0.097	9.1×10^6
70	9.69	0.03	0.85	0.38	17.50	0.096	9.6×10^6
75	10.60	0.04	0.93	0.43	19.20	0.096	10.0×10^6
80	11.55	0.04	1.00	0.46	20.68	0.096	10.4×10^6
85	12.35	0.04	1.08	0.49	22.07	0.096	10.8×10^6
90	13.15	0.05	1.14	0.52	22.36	0.095	11.1×10^6
95	-	-	-	-	-	-	-
100	14.35	0.05	1.25	0.57	24.88	0.093	11.6×10^6

TABLE 12

1954 FRICTION LOSSES FOR NORMAL-COATED UNLINED ROCK TUNNEL

Gate Opening (%)	Computed Friction Losses: Normal-coated Surface (ft)	Computed Friction Losses: Flaked-coated Surface (ft)	Computed Miscellaneous Losses (ft)	Net Loss Unlined Tunnel (ft)	Weisbach's f	Reynolds' Re
(1)	(2)	(3)	(4)	(5)	(6)	(7)
			March 28--One Unit			
20	0.17	0.01	0.01	0.40	0.098	1.5×10^6
30	0.39	0.03	0.02	1.00	0.100	2.3×10^6
40	0.71	0.06	0.04	1.99	0.112	3.1×10^6
45	0.99	0.07	0.05	2.39	0.105	3.5×10^6
50	1.28	0.09	0.06	2.83	0.101	3.9×10^6
55	1.62	0.11	0.07	3.33	0.099	4.3×10^6
60	1.98	0.13	0.09	3.78	0.094	4.7×10^6
65	2.30	0.14	0.10	4.27	0.094	5.0×10^6
70	2.62	0.16	0.11	4.79	0.093	5.3×10^6
75	2.92	0.18	0.12	5.32	0.093	5.6×10^6
80	3.17	0.20	0.13	5.89	0.094	5.8×10^6
85	3.47	0.22	0.15	6.53	0.095	6.1×10^6
			March 27--Two Units			
25	1.30	0.09	0.06	2.79	0.098	3.9×10^6
35	2.79	0.17	0.12	5.00	0.092	5.4×10^6
40	3.45	0.22	0.15	6.44	0.094	6.1×10^6
45	4.61	0.29	0.20	8.71	0.094	7.1×10^6
50	5.56	0.35	0.24	10.47	0.094	7.8×10^6
55	6.55	0.41	0.28	12.27	0.093	8.4×10^6
60	7.50	0.47	0.32	14.15	0.094	9.0×10^6
65	8.63	0.54	0.37	16.11	0.093	9.7×10^6
70	9.39	0.59	0.40	17.56	0.093	10.1×10^6
75	10.25	0.64	0.44	19.08	0.093	10.5×10^6
80	11.03	0.70	0.47	20.69	0.094	10.9×10^6
85	11.82	0.75	0.51	22.14	0.093	11.3×10^6
Open	12.87	0.81	0.55	24.02	0.093	11.8×10^6

curve established by current meter measurements supported and supplemented by observations of turbine scroll case differential pressures.

While some of the methods used for obtaining the 1954 test data differed in detail from those for the 1944 tests, it is the opinion of the Laboratory personnel who worked on both projects that the data are equally reliable. Both sets of data obtained with single-unit operation were taken on clear or partly cloudy days so that some slight inaccuracy may have resulted from solar heating of some of the long connecting lines. The effect should have been more pronounced in 1954 since it was clear all day and the gages were mounted so that considerable vertical line could be affected. The two-unit tests were performed on rainy days and should not be so affected. An inspection of Figure 7 indicates that the apparent spread in the single-unit test data appears to follow the above-stated reasoning. In 1944 the single-unit data spread more than the two-unit data but not so much as the single-unit 1954 data. The 1954 two-unit data had little spread as would be expected.

There cannot be, of course, any direct comparison of the two sets of data taken ten years apart since the surfaces were essentially different. It is interesting to note, however, from Figure 7 that the manganese coating resulted in a decrease in friction coefficient for all surfaces except the Turtletown Creek to McFarland concrete lining which remained about constant and the flaked-coated surfaces in the exposed steel pipes. It is also interesting to note that the shapes of the curves changed. The original concrete and the normal-coated surfaces produced curves somewhat comparable with those found in laboratory tests on artifically roughened pipes.(6,7,8,11) The original bitumastic enamel painted steel surface gave a curve with a shape somewhat between an artifically roughened pipe curve and an average commercial pipe curve,(12,13,14) while the 1954 flaked coating in the exposed pipe seemed to indicate a curve of the commercial surface type. The wide spread of the single-unit data for this surface must not be considered too seriously since errors of from 0.008 to 0.010 foot in the observed losses would account for the spread at Reynolds' numbers below 5×10^6. Density variations due to solar heating of the piezometer lines could have resulted in errors of this magnitude.

Bend losses were approximated to enable more accurate calculation of the friction losses in the tunnel. These losses were not recalculated after the final determination of friction loss had been made; but the change, if any, would have been very small. Since these losses are a relatively small part of the total loss, the effect of a small change in the roughness coefficient used in determining them would change them only slightly and the final effect on the friction coefficients for the tunnel surfaces would be insignificant. Figure 8 shows that the measured bend loss was essentially the same for both sets of data.

Some question may be raised as to the adequacy of the method used for the bend loss computations. To determine the significance of the bend loss factor the data were reduced by using the bend loss values given by Wasielewski.(15) These data give values of C_B for bends 1 through 6 of 0.064, 0.030, 0.036, 0.025, 0.009, and 0.018, respectively. By using these values it was found that the f values for the Apalachia Dam Adit to Apalachia Adit section were increased about 4 percent while those for the Turtletown Creek to McFarland Adit reach were increased only 1 percent. If the Wasielewski data are correct, then the 1944 concrete data will show an even greater spread between the two test sections and the 1954 data will have about the same spread but

the Apalachia Dam to Apalachia Adit f values will be greater. Because of the 16-foot diameter section in the Turtletown to McFarland reach, if either were to be greater the latter should be the one. It is concluded, therefore, that the method used is probably more nearly correct and in any case the error due to the bend loss calculation cannot be too appreciable.

The friction coefficient, pipe diameter, and the size of the surface roughness can be equated on the basis of the von Karman equation and the Nikuradse experiments. This equation is:

$$\frac{1}{\sqrt{f}} = 1.74 + 2 \log \frac{r}{k} \qquad (9)$$

in which f is the friction coefficient, r is the radius of the pipe, and k is the diameter of the sand grains composing the surface. The equation is applicable only to the region of complete turbulence in which f remains constant with increasing Re. Although this condition was not quite reached in the tests, the constant value of f may be estimated by inspection of Figure 7. Table 13 lists the estimated values of f and r for each type of tunnel surface, together with the calculated values of $\frac{r}{k}$ and k.

From inspections in 1944, the interior of the steel pipe was found to be almost glassy smooth except for the irregularities caused by the method of application. These irregularities were up to 1/8 inch in height. The concrete lining was slightly grainy. Visual estimates of the mean sand grain diameter varied from 0.03 inch to 0.06 inch. The value of 0.04 is within this range. No accurate estimate of average roughness for the unlined rock can be made, but the value of 24 inches does not seem out of line. No good visual determination of surface roughness height or grain diameters could be made on the coated surfaces, since this material was soft and deformed upon touch.

ACKNOWLEDGMENTS

The investigations of the friction loss in the Apalachia tunnel were performed under the general direction of Albert S. Fry, Chief, Hydraulic Data Branch, Tennessee Valley Authority and M. ASCE, and under the immediate direction of the Tennessee Valley Authority's Hydraulic Laboratory. Dr. G. H. Hickox, M. ASCE, was head of the Laboratory when the 1944 tests were performed. Rex A. Elder, M. ASCE, was a member of the Laboratory staff during the 1944 tests and assisted in conducting the 1944 tests. He was head of the Laboratory during the 1954 tests.

REFERENCES

1. H. W. Goodhue, R. L. Smart, and A. A. Meyer, "The Design of Recent TVA Projects: VIII. Apalachia and Ocoee No. 3," Civil Engineering, October, 1943, pp. 465-468.

2. Arthur L. Pollard and Peter Byrd Smith, "The Adsorption of Manganese by Algal Polysaccharides," Science, October 19, 1951, Vol. 114, No. 2964, pp. 413-414.

TABLE 13

COMPUTATION OF SURFACE ROUGHNESS

Tunnel Surface	Friction Coefficient f	Pipe Radius r (ft)	Ratio r/k	Grain Diameter k (in)
18-foot Steel	0.0138	9.0	2430	0.0445
18-foot Concrete				
Apalachia Dam Adit to Apalachia Adit	0.0137	9.0	2510	0.0430
Turtletown Creek Adit to McFarland Adit	0.0128	9.0	3550	0.0304
22.6-foot Rock	0.096	11.3	5.50	24.7
Normal-coated Surface	0.0123	8.974	4360	0.0247
Flaked-coated Surface	0.0145	8.974	1900	0.0565
Coated Rock	0.093	11.3	5.89	23.0

3. D. L. Yarnell and F. A. Nagler, "Flow of Water Around Bends in Pipes," Trans. ASCE, 1935.

4. A. Hofmann, "Loss in 90-Degree Pipe Bends of Constant Circular Cross-Section," Trans. of the Hydraulic Institute of the Munich Technical University, Bulletin 3 (1929), published in 1935 by the American Society of Mechanical Engineers.

5. William P. Creager and Joel D. Justin, Hydro-electric Handbook (New York: John Wiley & Sons, Inc., 1950), pp. 104-105.

6. "Widerstandsgesetz und Geschwindigkeitsverteilung von turbulenten Wasserströmung in glatten und rauhen Röhren," Proceedings, III International Cong. on Technical Mechanics, Stockholm, 1930.

7. J. Nikuradse, "Strömungsgesetz in rauhen Röhren," Forschungsheft, Verein deutscher Ingenieure, Heft 361, 1933.

8. J. Nikuradse, "Gesetzmässigkeiten der turbulenten Strömung in glatten Röhren," Zeitschrift, Verein deutscher Ingenieure, Band 77, 1933, p. 48.

9. Hunter Rouse, Elementary Mechanics of Fluids (New York: John Wiley & Sons, Inc., 1946), p. 265.

10. "The Flow of Water Through Culverts," Bulletin No. 1, Studies in Engineering, University of Iowa, Iowa City, 1926, p. 119.

11. C. F. Colebrook and C. M. White, "Experiments with Fluid-Friction in Roughened Pipes," Proceedings, Royal Soc. of London, Vol. 161, 1937.

12. Hunter Rouse, "Modern Conceptions of the Mechanics of Fluid Turbulence," Transactions, ASCE, Vol. 102, 1937, p. 463.

13. C. F. Colebrook, "Turbulent Flow in Pipes with Particular Reference to the Transition Region Between the Smooth and Rough Pipe Laws." Journal, Inst. C. E., London, Vol. 11, 1938-1939, p. 133.

14. Hunter Rouse, "Evaluation of Boundary Roughness," Proceedings, 2d Hydraulics Conference, Studies in Eng., Bulletin No. 27, Univ. of Iowa, Iowa City, 1943.

15. Rudolph Wasielewski, "Loss in Smooth Pipe Bends with Bend Angles Less Than 90 Degrees" (in German), Proceedings of the Hydraulic Institute of the Technical College of Munich, Issue 5 (1032), pp. 53-67.

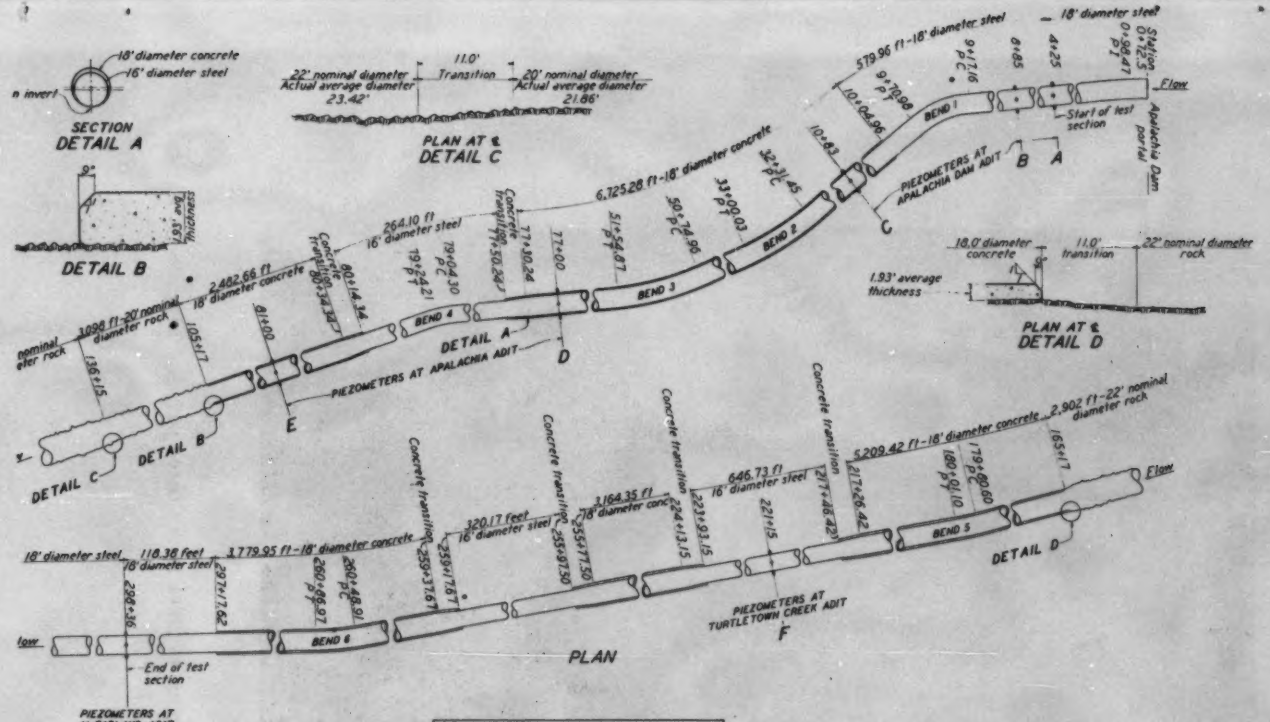

BEND DATA

BEND NO.	RADIUS FEET	ΔI	STA. P.C.	STA. P.T.
1	900.0	34°15'34"	9+17.16	9+70.98
2	250.0	15°43'05"	32+31.45	33+00.03
3	250.0	18°18'53"	50+74.96	51+54.87
4	900.0	12°40'35"	79+04.30	79+24.21
5	250.0	4°41'51"	179+80.60	180+01.10
6	250.0	8°43'25"	260+48.91	260+86.97

PLAN OF TUNNEL LAYOUT
APALACHIA DAM TO McFARLAND ADIT

Fig. 1. Plan of Tunnel Layout Apalachia Dam to McFarland Adit.

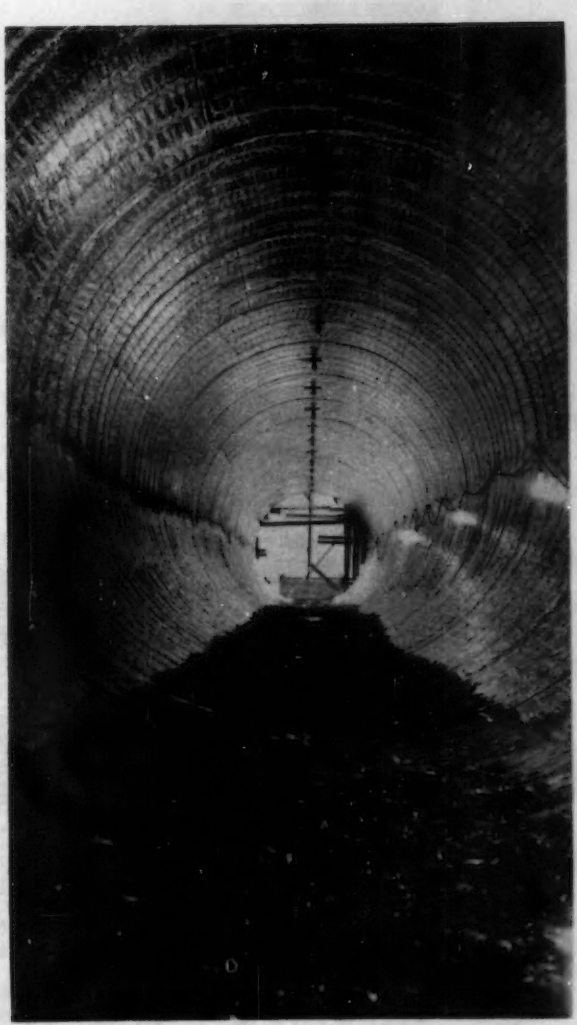

Fig. 2. Interior of Steel Pipe Coated with Hot Bituminous Paint.

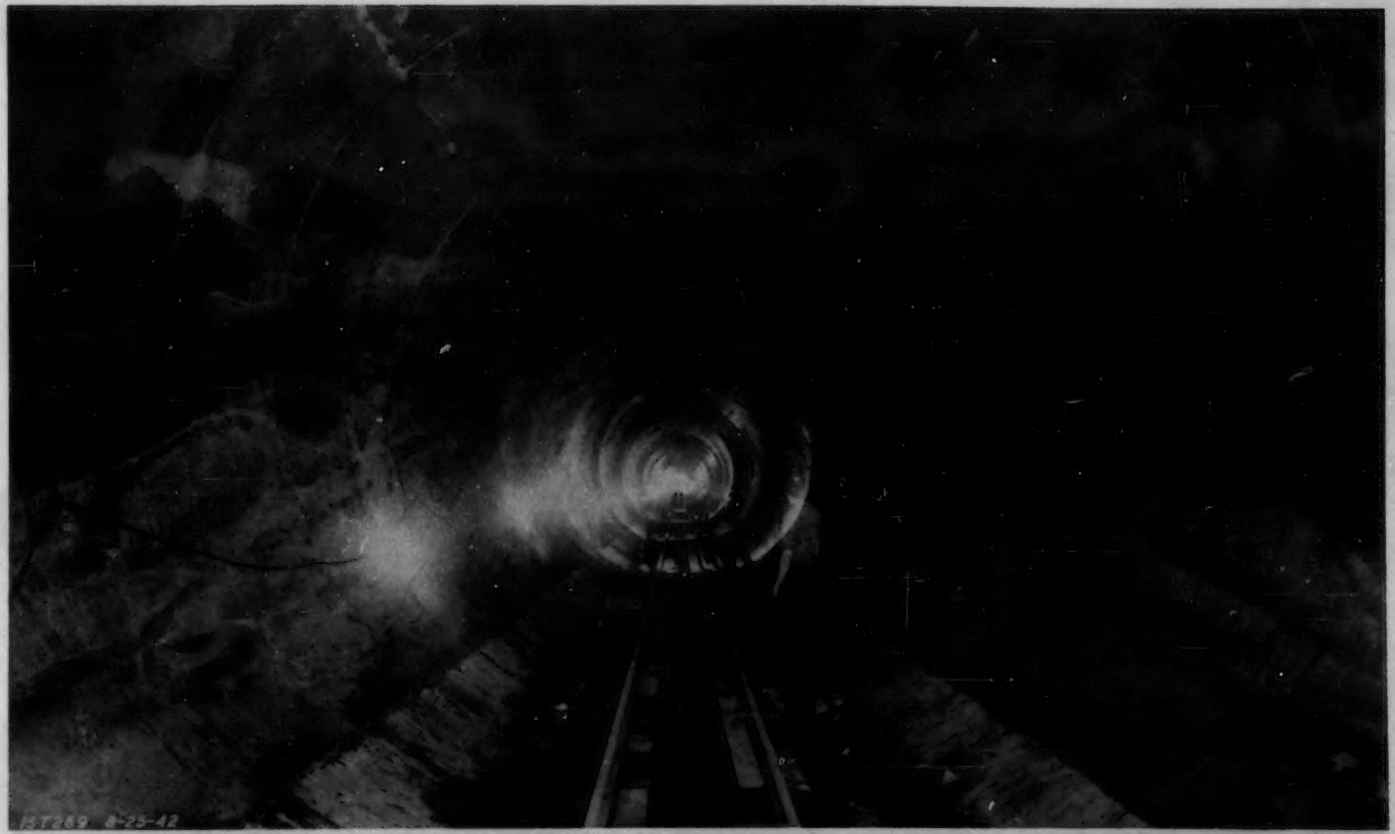

Fig. 3. Concrete-Lined Tunnel Section

Fig. 4. Completed Unlined Tunnel Section

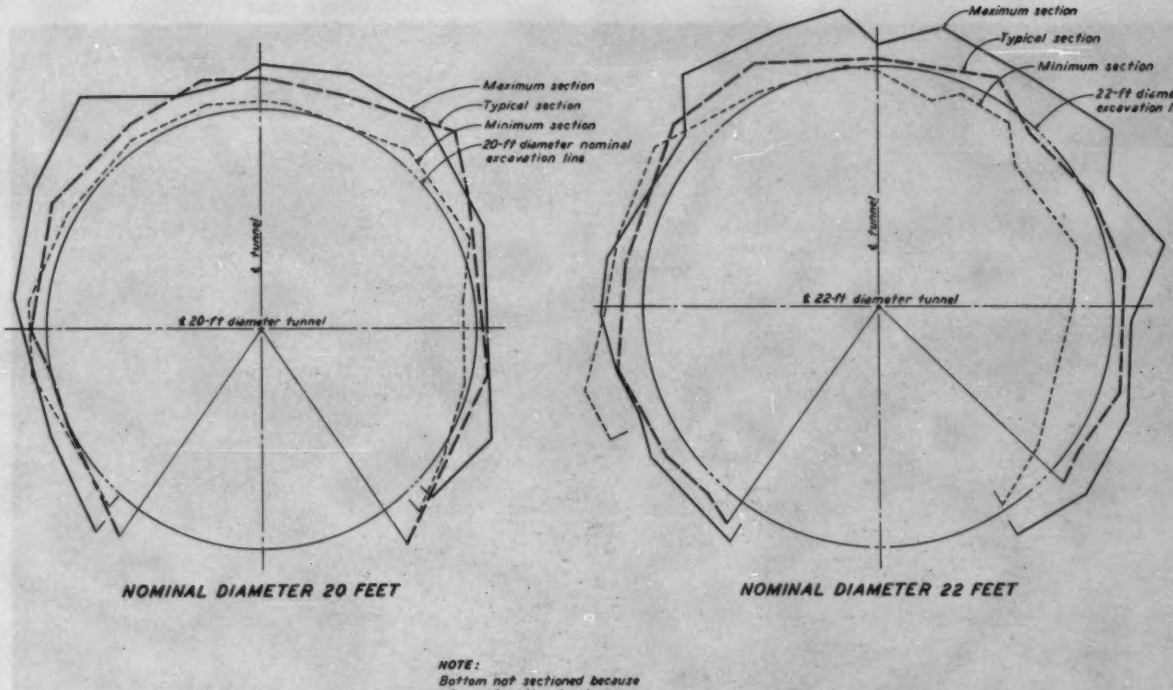

DIMENSIONS FOR UNLINED TUNNEL SECTIONS

Fig. 5. Dimensions for Unlined Tunnel Sections

Fig. 6. Normal 1954 Coating Showing Reproduction of Major Surface Shapes and Peeled Area

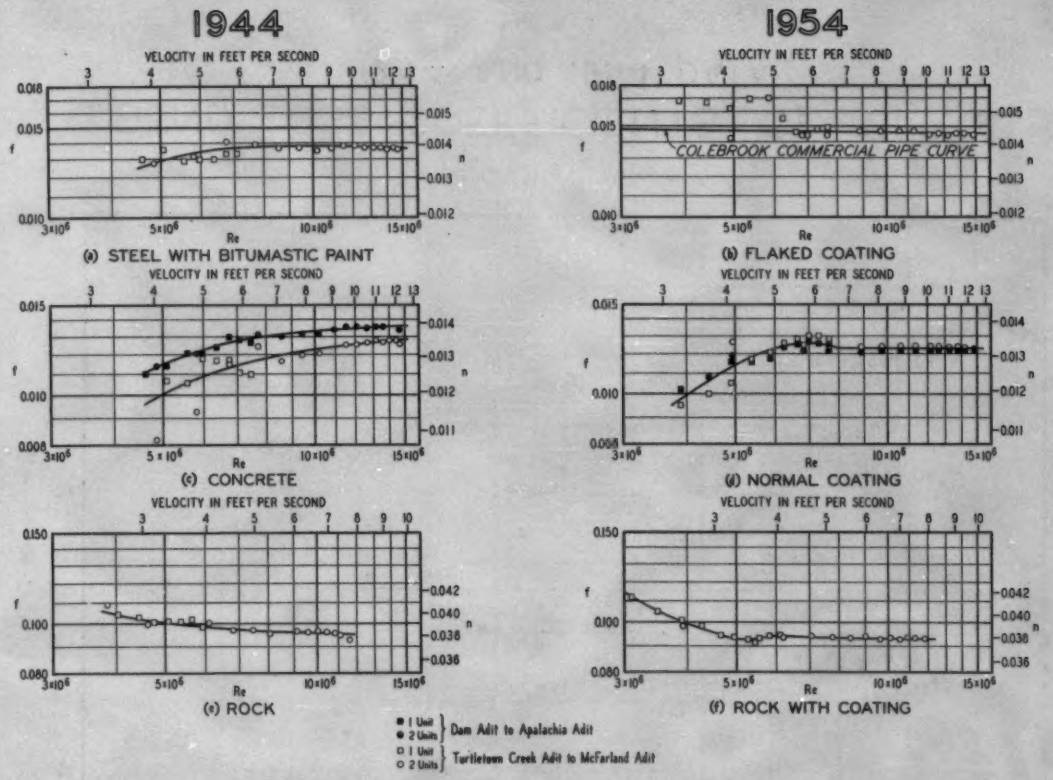

TUNNEL FRICTION COEFFICIENTS-1944 AND 1954 DATA

Fig. 7

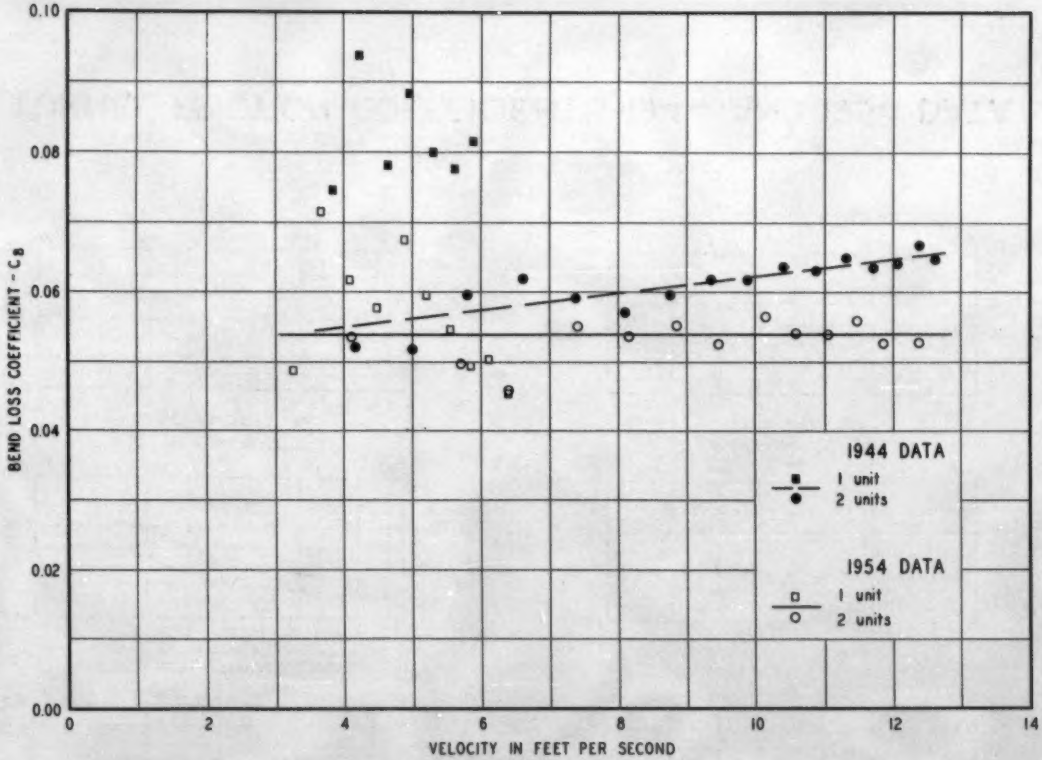

BEND LOSS COEFFICIENTS - C_B - BEND I
1944 AND 1954 DATA

Fig. 8

Paper 1008 HY3

Journal of the
HYDRAULICS DIVISION
Proceedings of the American Society of Civil Engineers

THE USE OF STATISTICS IN RESERVOIR OPERATIONS

Victor A. Koelzer,* A.M. ASCE
(Proc. Paper 1008)

SYNOPSIS

Statistics can be a very useful tool in reservoir operations, by furnishing a proper assessment of the operational chances involved, particularly with respect to water supply. Operating plans must consider the probability of a variation in water supply from that considered to be most likely, in fact the extreme variations frequently form the controls for a particular operation, rather than the most probable supply. The development of annual operating plans for reservoir systems deriving their primary water supply from snowmelt, as well as progressive seasonal modifications to these plans, is demonstrated in this paper. Particular emphasis is given to the important part that probability analyses play in determining limits for the development of the operational plans.

INTRODUCTION

The successful operation of any storage reservoir involves consideration and anticipation of a number of factors. Some of these factors are economic, such as power rates and water rental rates, which, for a given period of operation, are generally predictable within close limits. Others may be physical, such as reservoir, plant, and channel capacities, and are usually fixed. Legal and contractual obligations, generally also of a fixed nature, are frequently involved. Still other factors involve climatic conditions, which are not usually predictable far in advance, and are subject to relatively wide variations. These latter are of two types, water use requirements and water supply.

Water use requirements often involve both economic and climatic factors, and as a result, generally are not random occurrences. On the other hand, the occurrence of streamflow, if unregulated, is a natural phenomenon and, as such, is a random occurrence. It can thus be expected to follow the laws

Note: Discussion open until November 1, 1956. Paper 1008 is part of the copyrighted Journal of the Hydraulics Division of the American Society of Civil Engineers, Vol. 82, No. HY 3, June, 1956.

*Hydr. Eng. Bureau of Reclamation, U. S. Dept. of the Interior, Washington, D. C.

of probability, even though its probability curve is generally skewed rather than following the normal law. Therefore, it is in estimating water supply that the use of statistical procedures has the widest application.

Some engineers are reluctant to use statistical procedures because they feel them to be academic or too difficult to apply. It may seem more inviting and more concrete to use specifically observed figures, such as a historical maximum or a historical minimum. Yet hydrologists know that this procedure can sometimes be very misleading, particularly if no consideration is given to whether the experienced extremes are out of proportion to the length of record.

Admittedly the expression of water supply potential in terms of probabilities may seem somewhat vague to the engineer accustomed to having a more solid foundation under his calculations. But since we are dealing with an element that is fundamentally unpredictable on a long-range basis, it is not surprising if the best method of expression is something less tangible than used in most engineering practice. Most water use projects will be in existence for many years, and the aim should be a general high level of successful operation during the life of the project. The probability approach does not guarantee protection against occasional mistakes, but it does seem to offer the best assurance of a general high level of success over a long period of time. If such is the case the approach is not academic–it is extremely practical.

The emphasis placed on the proper evaluation of operational chances does not mean that common sense, good judgment and observance of fixed operational requirements can be ignored. These must be basic in the determination of any reservoir operations schedule. On the other hand, the so-called "feel-of-the-river" is a valuable asset only if it refers to an intimate knowledge of physical and hydraulic characteristics of a river, but is probably much overrated if this expression is intended to imply an intuitive knowledge of how a river will perform.

Concerning difficulty of use, only the simplest of statistical methods are needed. The time and effort spent in making the analyses represent only a minute part of the work involved in reservoir operations.

The intent of this paper is to demonstrate the use of statistical procedures, rather than to present arguments in favor of any specific type of analysis. Much good information is readily available on this subject,[1] and it is considered outside the scope of the paper to justify the specific method of analysis chosen.

Description of Reservoir System

The probability approach has been used as a basis for estimating water supply in scheduling reservoir operations for one of the Bureau of Reclamation's multiple-purpose systems. Physically this system includes facilities of the Colorado-Big Thompson Project in Colorado, the North Platte and Kendrick Projects in Wyoming and Nebraska, and certain features of the Missouri River Basin Project in these same states. The major features of the system are shown in Fig. 1, and pertinent data are shown in Table 1. Not shown is the extensive transmission grid which permits interconnected system operation of all powerplants. The primary water supply for the system is derived from snowmelt from the Rockies. Early in the spring this water supply can be forecasted on the basis of the winter accumulation of snow and precipitation.

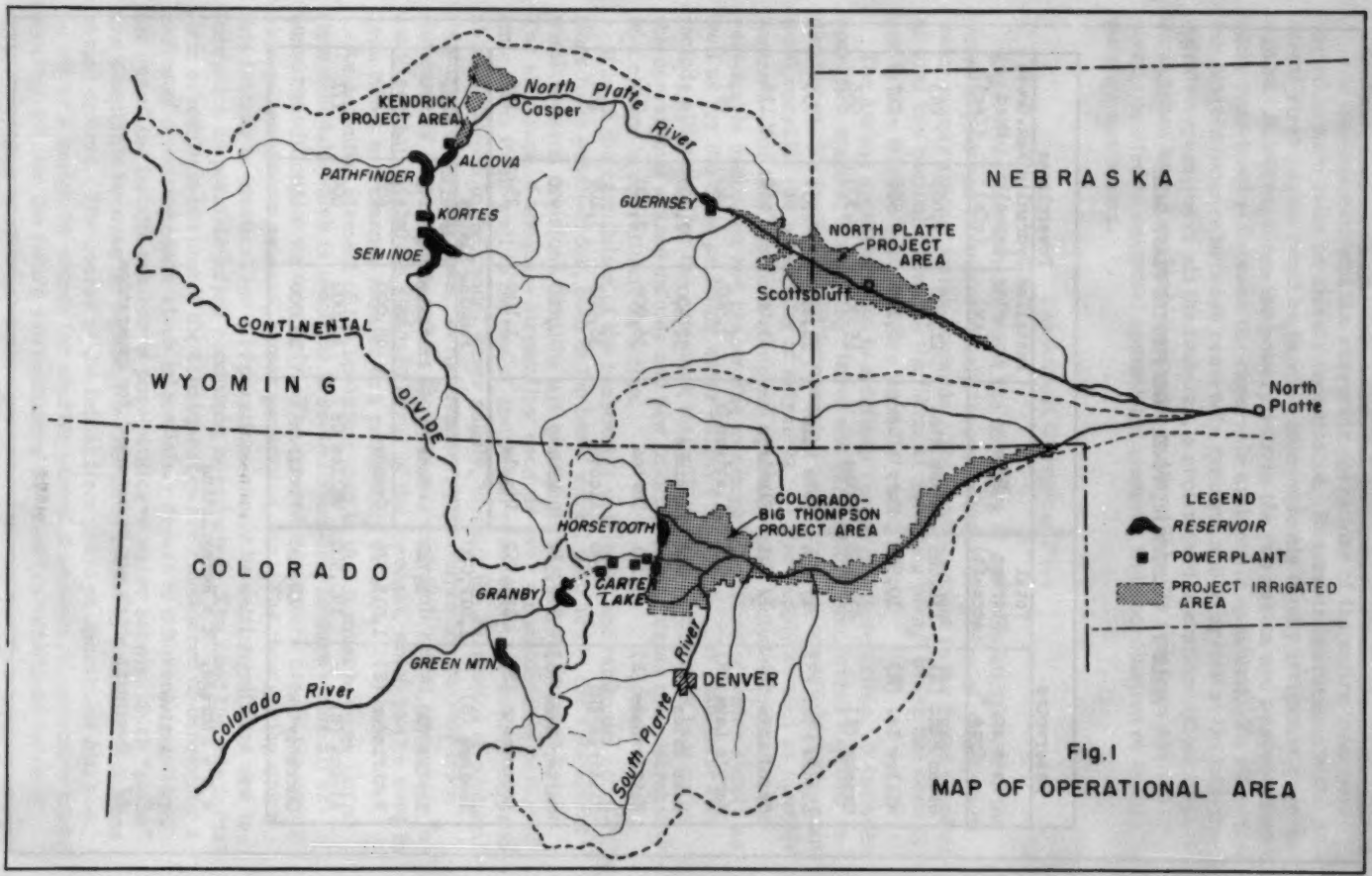

Fig.1
MAP OF OPERATIONAL AREA

TABLE 1. RESERVOIR, POWER, AND PUMPING PLANT DATA

Reservoirs		Powerplants			
Name and Type *	Total Storage (acre-ft)	Name	Installed Capacity (kw)	Hydraulic Capacity (cfs)	Max. Gross Head (feet)
Green Mtn. (S)	154,645	Green Mtn.	21,600	1,660	263
Willow Cr. (R)	10,553	Mary's Lake	8,100	550	217
Granby (S)	539,758	Estes	45,000	1,300	568
Shadow Mtn. (R)	17,354	Pole Hill	33,250	550	838
Grand Lake (R)	1/ 511	Flatiron	63,000	960	1,118
Mary's Lake (R)	927	Flatiron 2/	8,500	440	297
Lake Estes (R)	3,068	Seminoe	32,400	2,850	217
Rattlesnake (R)	2,181	Kortes	36,000	2,700	205
Flatiron (R)	760	Alcova	36,000	3,100	168
Carter Lake (S)	112,382	Guernsey	4,800	920	90
Horsetooth (S)	151,752	Lingle	1,400	230	106
Seminoe (S)	1,012,000	Pumping Plants			
Kortes (R)	4,744	Name	Installed hp	Hydraulic Capacity (cfs)	Max. Lift (feet)
Pathfinder (S)	1,015,876	Granby	18,000	600	186
Alcova (R)	190,500	Willow Cr	10,000	400	171
Guernsey (R)	44,800	Flatiron	13,000	440	297

* S = Storage. R = Reregulating

1/ Active

2/ Pump unit which may be reversed for generation

For maximum benefit the reservoir operations of the entire interconnected system must be closely coordinated. Reservoir operations in the different river basins could be handled independently if only irrigation were involved. However, since the powerplants in the two basins are interconnected, close coordination between the reservoir systems is essential. To effectuate the desired balance between reservoir systems and to arrive at the best integrated operation of all the features, a centralized operations office was established near Loveland, Colorado, in May 1951. Its functions are primarily related to essential operational planning and coordination of multipurpose operations.

The Annual Operating Plan

Experience has indicated that the objective of optimum utilization of the water supply can be achieved only through careful budgeting of anticipated water supply against water demands. This water budget is the basic element of what has become known as the "Annual operating plan," which has been in use in this Bureau system since the 1952 water year.

The annual operating plan is a defined course of future action. It includes operation studies, supporting charts and explanatory text, which together indicate how the facilities will be operated under various conditions. The plan must consider the possibility of extremes in water supply as well as in water demand. For this reason a complete operating plan includes provision for reasonable maximum and reasonable minimum conditions of water supply as well as for the most probable water supply conditions. The plan must also include allowance for the revisions that will be made from time to time as the operational season unfolds and new information indicates the desirability of a change in operational direction.

It is in the calculation of the reasonable maximum and minimum conditions to be provided for, both in the basic annual plan and in the subsequent within-season revisions, that the use of statistical analysis is most helpful. The existence of adequate streamflow records over a considerable period of time lends itself well to the use of statistical procedures for estimating probable variations in the annual water supply, through the derivation of probability curves of annual flows. In like manner, procedures for shorter term forecasts of streamflow, such as for seasonal snowmelt runoff, generally include computation of the standard error of the forecast, which can be used in such cases in a manner similar to a probability curve.

An essential element of the operating plan is that it must have an initial firm schedule which is identical in some controlling feature under all assumed conditions of water supply. The controlling feature can be reservoir storage, reservoir release, power generation, etc. The time during which this feature is identical for all operations should be until significant new information on possible inflow conditions is expected. The need for this initial firm schedule is obvious if the consequences are considered of developing a series of operating plans which immediately depart in different directions, for any of the infinite number of possibilities of water supply. Such "plans" are unsuitable because no dependable course of action is established for any period of time. The course of the initial firm phase of operations can best be set by a month-by-month (or shorter period if necessary) operation study, which looks into the future and considers the possible variations in water

supply, water uses, and other controlling factors. The actual mechanics become somewhat of a trial and error process.

From the above it can be seen that the operating plan has a firm schedule for the initial period only, and that after this initial period the operating plan is more a series of plans under the varying conditions that can occur, rather than being a single set plan. It can also be visualized that the course of the initial firm schedule is controlled by consideration of possible future extremes, rather than being dictated by the most probable occurrence of the future. For example, under assumed minimum inflow conditions, it will generally be desirable to fill a reservoir by the end of the snowmelt runoff season. At the same time, if maximum inflow conditions should occur, it will be desirable to pass all the water through the power plant. These two objectives, requiring consideration of opposite conditions, are the determining factors in establishing the operational position that will be gained during the initial period of the plan. Thus the extremes, rather than the most probable occurrence, form the guide lines of operation, and it becomes essential to have reliable methods of computing the probability of the extremes.

In actual operations, the firm schedule developed as described above is followed until significant new information on water supply, water use or other controlling elements are available. A new plan is then developed which extends the firm schedule beyond the one previously developed, and considers various possibilities of the future As the operational picture unfolds this process is repeated and repeated, using the same procedures. This process can perhaps best be demonstrated graphically, as in Fig. 2.

In Fig. 2, the element of the operating plan that remains constant for all conditions of inflow is reservoir storage. In such a case, the outflow must of necessity vary with different conditions of inflow during the initial period. At the beginning of the water year, at point A, operating plan A is developed which has an initial firm schedule through March, and then has limits of storage as necessary to accommodate the computed probable range of inflow. At point B, new inflow forecast information is available which indicates that a revision in plan is desirable. This plan, identified as Plan B, has a set schedule extending into May, which then changes to limits of operation to accommodate the probable range of inflow. The probable range in Plan B is the same as in Plan A in terms of percentage change, 1-in-20, but is smaller in terms of acre-feet, because of increased forecast accuracy as the season progresses. The same process is repeated in Plans C and D, until the critical operation time, that of peak storage, is reached.

Examples of Use of Probability Analyses in Developing a Reservoir Operating Plan

General Considerations

Previously, the various factors that must be considered in scheduling reservoir operations were discussed, with emphasis on their variability. The examples selected have been chosen for purposes of demonstrating the use of probability studies of water supply, and therefore may not emphasize all the economic, legal, physical and use requirement considerations that would normally be involved. The somewhat simplified examples shown are not intended to detract from the consideration that must be given to such factors.

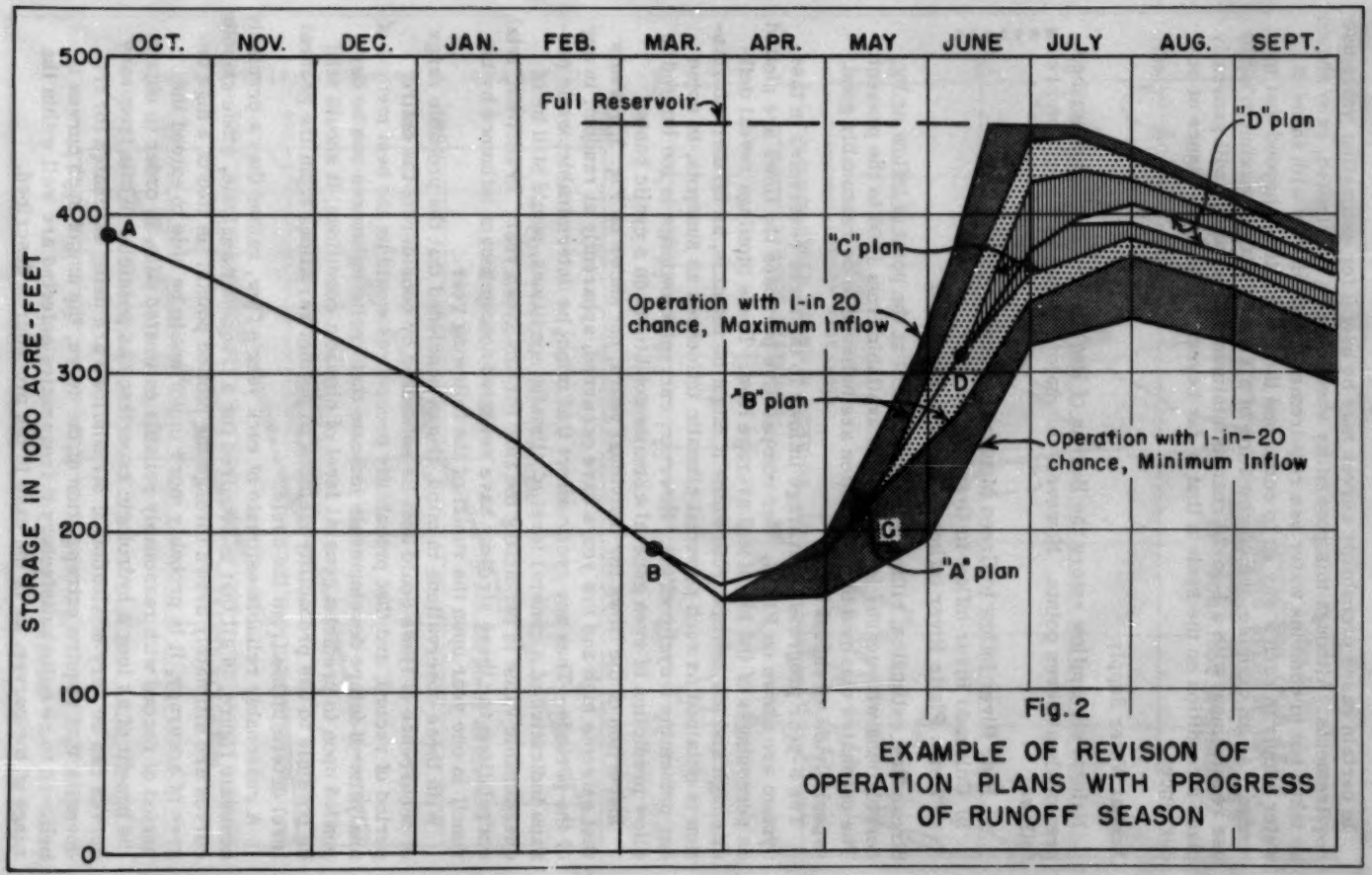

Fig. 2

EXAMPLE OF REVISION OF OPERATION PLANS WITH PROGRESS OF RUNOFF SEASON

In certain cases probability curves may be useful for estimating water use requirements. Although this possibility should not be overlooked, care should be taken not to combine water use requirement probabilities with those of water supply in such a way as to compound the probabilities beyond that intended. As an example, the combination of a 1-in-20 chance maximum water use requirement with a 1-in-20 chance minimum water supply will generally place a condition on the system that is far beyond the 1-in-20 chance of occurrence.

Annual Water Supply

Natural streamflow enters the Bureau of Reclamation system described previously at seven points. However, the major inflows to the system are as follows:

a) Blue River inflow to Green Mountain Reservoir
b) Colorado River inflow to Granby Reservoir
c) North Platte River inflow to Seminoe Reservoir

Streamflow estimates, either by measurement at the point of inflow or by correlations with nearby locations, are available from 1906 to the present. The estimates obtained by correlation are believed to be reasonably good, especially on an annual basis.

The 5-year progressive average inflows to the three reservoirs in the system are shown on Fig. 3. For comparative purposes the flows are plotted as percentages of the historical average flow. These plottings reveal definite high and low swings from which it might be feasible, as further information is obtained on such potential climatic influences as sunspots, to some day determine a cyclic effect. However, current knowledge is too limited to allow prediction of even general climatic conditions on a cyclic basis.

Inspection of the flows for individual years, not shown on Fig. 3, reveals that extreme high and low years have occurred, apparently at random, in any of the periods. Thus any cyclic effect that might be determinable, while perhaps indicative of a general level of climatic conditions, would still be of questionable value in predicting the flow for any given year. In addition, trial correlations for these streams have revealed no significant influence by the runoff in one year upon the runoff of the following year.

With these observations in mind, it was concluded that the probable range of occurrence of flows could best be estimated by considering the entire period of record, and that probability procedures would be the best method of analysis. If future developments indicate that cyclic influences can be depended upon to predict a general level of climatic conditions, it should still be possible to use probability methods to predict variations from the general level determinable from the cycle.

A reasonably reliable estimate of each year's flow, rather than a precisely accurate figure, is all that is required for a frequency analysis, since smooth curves are ultimately drawn through the plotted points. In lieu of a high degree of accuracy, it is probably more important to be able to extend the period of record with reasonably reliable estimated data, in order to obtain the benefit of as long a hydrologic experience as possible. While frequency curves can be very misleading if streamflows are being estimated for frequencies that require extrapolation of the curve, the use of such curves is believed to be quite satisfactory if frequencies selected are well within the range of the curves, as is the case in the procedures described.

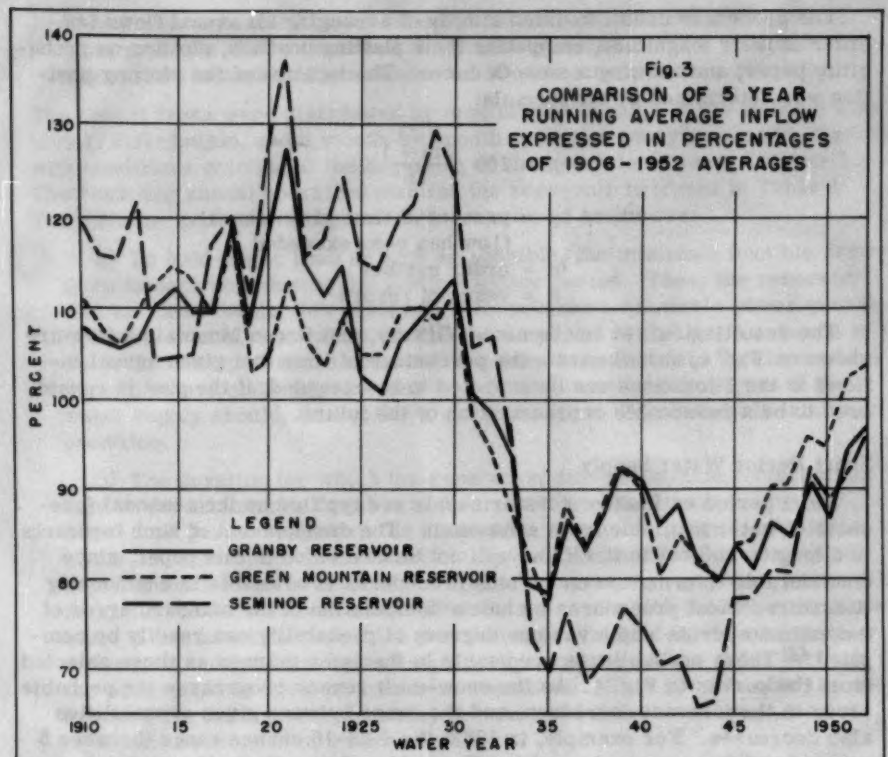
Fig. 3
COMPARISON OF 5 YEAR RUNNING AVERAGE INFLOW EXPRESSED IN PERCENTAGES OF 1906-1952 AVERAGES
PERCENT
WATER YEAR
LEGEND
GRANBY RESERVOIR
GREEN MOUNTAIN RESERVOIR
SEMINOE RESERVOIR

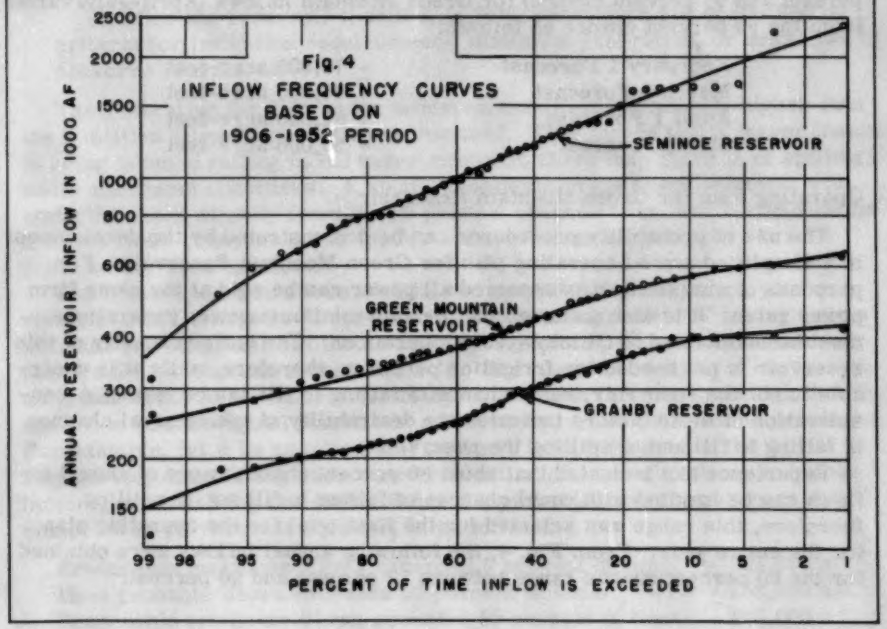
Fig. 4
INFLOW FREQUENCY CURVES BASED ON 1906-1952 PERIOD
ANNUAL RESERVOIR INFLOW IN 1000 AF
PERCENT OF TIME INFLOW IS EXCEEDED
SEMINOE RESERVOIR
GREEN MOUNTAIN RESERVOIR
GRANBY RESERVOIR

The procedure used consisted simply of arranging all annual flows in order of their magnitude, computing their plotting position, plotting on probability paper, and drawing a smooth curve. The location of the plotting position was determined by the formula:

$$p = 100 \left(\frac{2m - 1}{2n}\right)$$

where p = percent of time given annual flow has been exceeded
m = order number
n = years of record

The resulting curves for Seminoe, Granby, and Green Mountain inflow are shown on Fig. 4, and illustrate the percentage of time that given annual inflows at the 3 locations can be expected to be exceeded, if the past is considered to be a reasonable representation of the future.

Short Period Water Supply

Short period estimates of water supply are typified by the seasonal forecasts of water available from snow-melt. The development of such forecasts is a lengthy subject in itself and will not be described in this paper, since considerable information on various procedures is available in engineering literature. Most procedures include a computation of the standard error of the estimate, from which various degrees of probability can readily be computed.(2) These probabilities are usable in the same manner as those selected from the curves in Fig. 4. As the snow-melt season progresses the probable error in the forecast decreases, and the range between given probabilities also decreases. For example, in 1953, the 9-in-10 chance range (between 5 percent and 95 percent chance) for Green Mountain inflows (April-July) varied from the 50 percent chance as follows:

February 1 Forecast	± 70,000 acre-feet
March 1 Forecast	± 67,000 acre-feet
April 1 Forecast	± 62,000 acre-feet
May 1 Forecast	± 55,000 acre-feet

Operating Plan for Green Mountain Reservoir

The use of probability procedures can be demonstrated by the development of a simplified annual operating plan for Green Mountain Reservoir. For purposes of simplicity it is assumed all power can be sold at the same firm power rates. It is also assumed that certain minimum power generations must be maintained to fit into system operations. The entire capacity of this reservoir is not needed for irrigation purposes, therefore, while it is desirable to fill the reservoir, some chance of failing to fill can be taken. A consideration of these factors indicates the desirability of taking equal chances of failing to fill and of spilling the reservoir.

Experience has indicated that about 80 percent chance range of annual inflows can be handled with equal chances of failing to fill and of spilling, therefore, this range was selected for the first trial for the operating plan for the entire year. From Fig. 4, the following annual inflows were obtained for the 80 percent chance range between 10 percent and 90 percent:

Reasonable maximum (flows exceeded 10 percent of time)	560,000 a.f.
Most probable (flows exceeded 50 percent of time)	405,000 a.f.
Reasonable minimum (flows exceeded 90 percent of time)	300,000 a.f.

The annual flows were distributed by months on the basis of the average historical distribution, and a month-by-month operation study was made, starting with conditions existing at the beginning of the operational year, October 1. The resulting annual operation plan for the reservoir is shown in Table 2. The different phases of the plan were determined as follows:

a) To hold power head as high as possible, the minimum feasible drawdown is desirable during the lowflow winter period. Thus, the reservoir was operated during this period to meet minimum allowable power generations under minimum inflow conditions, as shown in the last 4 columns of Table 2. This procedure establishes a drawdown schedule that is used for the two other conditions of water supply, and is satisfactory even if the water supply should, during the winter, change to the reasonable minimum condition.

b) The duration for which the generation under minimum conditions is held to the minimum allowable is determined by operations during the snow-melt period to control the reasonable maximum inflows. Operation of the "maximum condition" in reverse, working backward at powerplant capacity from a full reservoir in July, will assure that no power water will be spilled under this condition. Thus the point at which the two operations meet is the latest date at which generation can be held to the minimum under minimum conditions and still be able to pass all the water through the powerplant in event of maximum conditions. This point is also the one at which the initial firm schedule, in terms of reservoir storage, begins to deviate to meet later inflow conditions.

c) After the reservoir is filled, in July, operations are controlled by criteria for irrigation requirements, minimum generation, or drawdown to conserve rain floods.

The generation for July under minimum conditions is slightly higher than the 5 million kilowatt hours that is required. This means that a lesser chance is being taken of failing to fill under minimum flows than there is of spilling under maximum conditions. A small adjustment in the flows selected, widening the range slightly from the 80 percent chance range, and recomputation with the same procedure, will modify the operations as necessary to fully equalize the chances taken.

The above operation shows the planned operation for the entire year as visualized on October 1. It contains the required ingredient of having a firm schedule for all conditions for an initial period, i. e., an identical reservoir storage for all conditions until April 30. The plan can be firm, if necessary, until that date. At any time prior to April 30 that a forecast indicates that the operation in the original plan is not satisfactory, a new plan can be developed. For example, let it be assumed that on April 1 the forecast for the April-July period, considering snow water content, winter precipitation, and other factors, and including the evaluation of the probabilities of occurrence as computed in the forecast equation, is as follows:

Reasonable maximum (flows exceeded 5 percent of time)	$\pm$ 328,000 a.f.
Most probable (flows exceeded 50 percent of time)	$\pm$ 268,000 a.f.
Reasonable minimum (flows exceeded 95 percent of time)	$\pm$ 208,000 a.f.

TABLE 2. ANNUAL OPERATION PLAN FOR GREEN MOUNTAIN RESERVOIR

(Water Units 1,000 A.F., energy units 1,000,000 kwh)

Month	Reasonable Maximum Conditions (90%)				Most Probable Conditions (50%)				Reasonable Minimum Conditions (10%)			
	Inflow	Outflow	Storage	Generation	Inflow	Outflow	Storage	Generation	Inflow	Outflow	Storage	Generation
Sept.	--	--	111.9	--	--	--	111.9	--	--	--	111.9	--
Oct.	19.0	21.9	109.0	4.2	13.8	16.7	109.0	3.2	10.2	13.1	109.0	2.5
Nov.	13.4	19.4	103.0	3.6	9.7	15.7	103.0	3.0	7.2	13.2	103.0	2.5
Dec.	11.2	18.8	95.4	3.5	8.1	15.7	95.4	2.9	6.0	13.6	95.4	2.5
Jan.	10.1	18.7	86.8	3.3	7.3	15.9	86.8	2.8	5.4	14.0	86.8	2.5
Feb.	9.0	18.7	77.1	3.2	6.5	16.2	77.1	2.8	4.8	14.5	77.1	2.5
Mar.	11.2	26.7	61.6	4.4	8.1	23.6	61.6	3.8	6.0	21.5	61.6	3.5
April	25.2	36.8	50.0	5.6	18.2	29.8	50.0	4.5	13.5	25.1	50.0	3.8
May	105.8	110.5	45.3	16.9	76.5	30.0	96.5	5.0	56.7	32.0	74.7	5.0
June	186.5	92.3	139.5	18.0	134.9	81.4	150.0	17.3	99.9	25.6	149.0	5.0
July	96.3	81.2	154.6	18.6	69.7	65.1	154.6	15.0	51.6	45.0	154.6	9.0
Aug.	46.5	51.1	150.0	11.4	33.6	38.2	150.0	8.5	24.9	39.0	140.0	8.7
Sept.	25.8	25.8	150.0	5.5	18.6	23.6	145.0	5.0	13.8	31.8	122.0	6.6
Total	560.0	521.9	438.1	98.2	405.0	371.9	433.1	73.8	300.0	289.9	410.1	54.1

Since such forecasts have narrower limits of error than the annual estimates, it is possible to operate with a greater assurance of either filling or avoiding spill, therefore, the broader probability limits shown above were selected for trial purposes.

The revised operating plan, based on the April 1 forecast, is shown in Table 3. A firm schedule is chosen for the initial stages of the plan, again in terms of reservoir storage, which is identical for all types of inflow until May 20. A firm plan of operation is thus assured that can be followed well through the development of the next inflow forecast, which will be prepared from snow survey and precipitation data observed as of May 1.

The operational schedules in this revision are developed in the same manner as in the original annual plan; that is, by working the minimum condition operation with minimum power requirements until it meets the maximum condition operation, worked in reverse from full reservoir at plant capacity. The process of revision of operating plans can be repeated as often as significant changes in forecasted conditions occur. Thus a revised operating plan can be made after the May 1 and June 1 streamflow forecasts, and as often during the rapidly changing heavy inflow period as may be required by changing conditions.

It will be noted that the operations shown in Tables 2 and 3 were controlled by the minimum and/or maximum conditions selected. These conditions form the guide lines that control the initial firm schedule, and the operation to meet such conditions is obviously satisfactory for the most probable conditions as well. This emphasizes the importance that the probability studies, which determine the minimum and maximum inflows, have in the operational scheduling.

While the scheduling procedures described will assure successful operations for the conditions cited, it should be borne in mind that the limits chosen represent only a reasonable range, and not the full range of possibilities. Occurrence of flows outside these limits are not only possible, but should be expected to occur with the frequency indicated. Emergency operating plans should always be available to meet these conditions when they occur. While use of probability procedures will yield dividends over a long history of operations, their use should not be "oversold" to the point of creating an impression that positive assurance is being given that the flows will be within the limits selected for analysis.

North Platte Flood Control Operation

Another valuable application of the use of statistical methods in evaluating the chances involved occurred in 1952 on the North Platte River, when high flows of potential flood magnitude were considered a strong possibility. Instructions were received from appropriate administrative officials that the operational objective should be to prevent, if possible, uncontrolled damaging spills throughout the system and at the same time assure that all reservoirs would fill. These instructions were issued, of course, with the full knowledge that absolute guarantees could not be given of accomplishing both objectives. Such a guarantee was not possible because, in order to assure flood control capability, advance releases to provide flood control space would be required, which would cause some risk of failing to fill if the actual flow was substantially less than forecasted. Since there is no flood control allocation in the system, and therefore no formal flood control regulations, it was understood

TABLE 3 - OPERATIONAL PLAN FOR GREEN MOUNTAIN RESERVOIR AFTER APRIL 1 FORECAST

(Water Units 1,000 A.F., Energy Units 1,000,000 Kwh.)

Date	Reasonable Maximum Conditions (95%)				Most Probable Conditions (50%)				Reasonable Minimum Conditions (5%)			
	Inflow	Outflow	Storage	Generation	Inflow	Outflow	Storage	Generation	Inflow	Outflow	Storage	Generation
March 31			61.6				61.6				61.6	
Apr. 10	4.0	9.5	56.1	1.4	3.2	8.7	56.1	1.3	2.5	8.0	56.1	1.2
20	5.9	10.2	51.8	1.5	4.8	9.1	51.8	1.4	3.7	8.0	51.8	1.2
30	10.5	12.3	50.0	1.8	8.6	10.4	50.0	1.5	6.9	8.7	50.0	1.3
May 10	17.4	17.4	50.0	2.6	14.2	14.2	50.0	2.1	11.0	11.0	50.0	1.7
20	28.9	21.9	57.0	3.3	22.8	15.8	57.0	2.4	17.7	10.7	57.0	1.7
31	40.8	26.1	71.7	4.4	33.2	18.5	71.7	3.1	25.8	11.1	71.7	1.8
June 10	57.6	31.1	98.2	5.8	47.1	20.6	98.2	3.8	36.6	10.1	98.2	1.8
20	52.4	13.9	136.7	3.0	42.9	16.9	124.2	3.5	33.1	10.2	121.1	2.0
30	41.3	26.1	151.9	6.0	33.8	16.2	141.8	3.5	26.2	9.6	137.7	2.0
July 10	28.2	25.5	154.6	6.0	23.9	15.7	150.0	3.5	18.5	9.1	147.1	2.0
20	24.6	24.6	154.6	5.8	20.1	15.5	154.6	3.6	15.6	12.7	150.0	2.8
31	16.4	21.0	150.0	4.8	13.4	18.0	150.0	4.1	10.4	10.4	150.0	2.3
Aug 31	37.8	37.8	150.0	8.7	30.8	30.8	150.0	7.1	24.0	40.0	134.0	8.9
Sept 31	20.9	22.2	148.7	5.0	17.1	28.0	139.1	6.4	13.2	35.0	112.2	7.0
Total	386.7	299.6	+87.1	60.1	315.9	238.4	+77.5	47.2	245.2	194.6	50.6	37.7

that the operational chances to be taken should be consistent with the primary purposes of the reservoirs and with the benefits to be gained.

The situation was ideal for use of statistical procedures. The basic streamflow forecasts were made in normal fashion, through multiple correlation procedures, and included in their derivation a computation of the probable chances of missing the forecast by given amounts. Three basic types of operation studies were made, each using the operational scheduling procedure described previously. The three studies were:

a) A purely conservation operation, in which no reservoir releases in excess of powerplant capacity were allowed until the two reservoirs involved were filled. Such an operation indicated that damaging spills would very probably occur.

b) Operation to assure that reservoir outflows with 1-in-5 chance maximum inflows would be held to acceptable limits.

c) Operations to assure that reservoir outflows with 1-in-20 chance maximum inflows would be held to acceptable limits.

The latter operations involved taking some chance of failing to fill both reservoirs and consequently of wasting water for both irrigation and power.

Four factors were evaluated to determine the chances being taken of certain losses occurring because of operations under (b) and (c) above, these losses being:

a) Firm energy loss
b) Dump energy loss
c) Power revenue loss
d) Water lost to system (amount reservoirs fail to fill because of advance releases to provide flood control space)

An appraisal of the chances that would be taken of incurring various losses (in excess of the losses in a purely conservation operation), to assure control of the 1-in-5 and 1-in-20 chance maximum inflows, is indicated graphically in Fig. 5. The chances are shown for two types of seasonal distribution, and a "critical" or rapid, concentration of the seasonal inflow.

The results as presented in Fig. 5 were well suited to allow an administrative policy decision to be made on the chances that should be taken. The results indicated that substantial chances would be taken of losing water, energy, and power revenues if operations were initiated to assure control of the 1-in-20 chance maximum inflows. Although these chances were less than 50-50, it was decided that the chances involved in controlling the 1-in-20 chance maximum flood could not be taken, since there is no flood control allocation and conservation of water has priority of use. On the other hand, it will be noted that operation to assure control of the 1-in-5 chance flood could be initiated and the chances of any losses occurring would exceed 1-in-20 only if a critical distribution of inflow occurred. Other percentage chances could be analyzed in the same manner, but it appeared that operation to control the 1-in-5 chance flood involved about the maximum risk that could be taken of losing water. Therefore, based on these calculated risks, a decision was reached that operations should be geared to assuring control of the 1-in-5 chance flood to the desired flows.

With this decision having been made, the job of scheduling reservoir operations was greatly simplified. As the flood season unfolded, successive

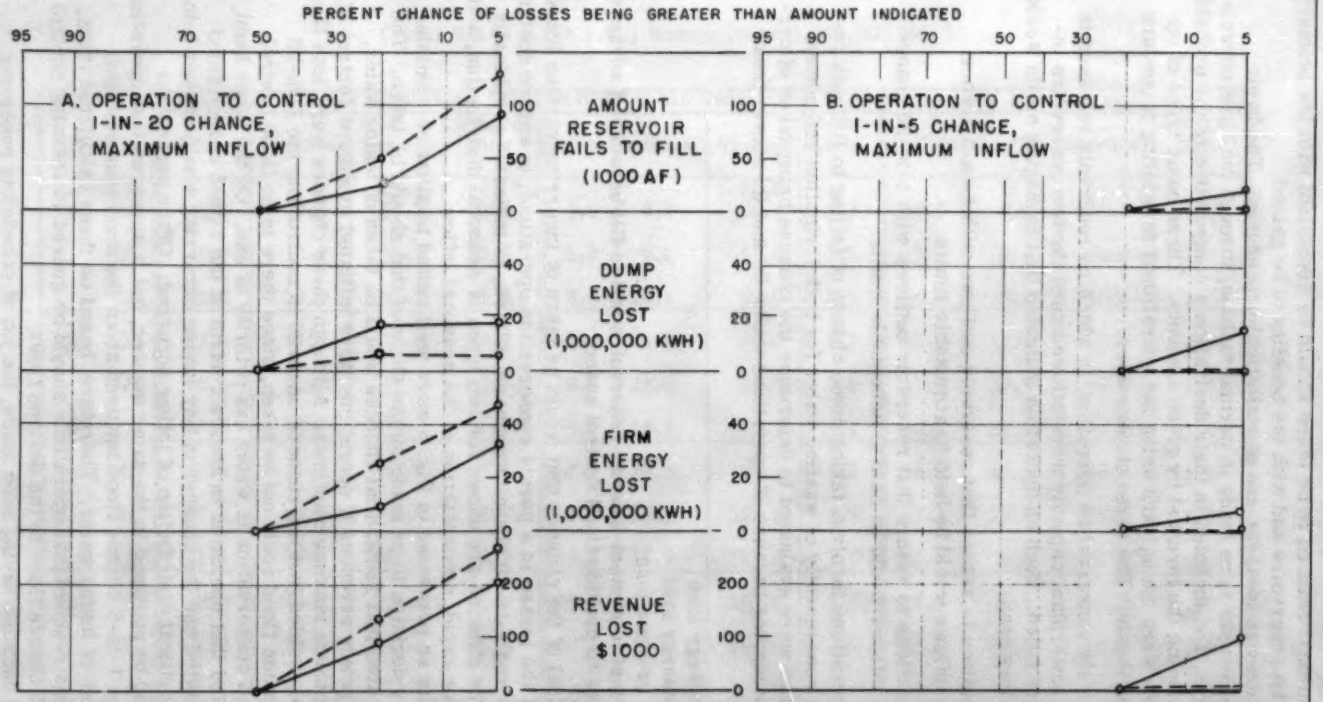

Fig.5 PROBABLE LOSSES RESULTING FROM GIVEN DEGREES OF FLOOD CONTROL PROTECTION NORTH PLATTE SYSTEM - USBR - 1952

forecasts of progressively increasing accuracy were made, which formed the basis on which operation studies could be performed. Using the general principles of scheduling discussed previously, operating plans were developed which, in each instance, were aimed at assurance of controlling the 1-in-5 flood, with maximum filling in event of low flows.

Actual operations were carried out without mishap. Precipitation during the snowmelt season was about normal, which contributed toward a high degree of accuracy in the streamflow forecasts. All reservoirs filled and releases were controlled within the desired amounts.

System Operational Planning

In the Green Mountain example cited, economic considerations have been excluded by assuming all power generated is sold at the same rate. This simplification is rarely possible in actual practice. An excellent method of utilizing statistical analysis for economic evaluation has been presented by Blanchard.[3] He compared the economics of two types of operations by determining, for various flow probabilities, the difference in net revenue between the two types of operation. The difference was then multiplied by the percent interval of probability represented, for each probability limit for which evaluations were made. The algebraic sum of these products represented the probable economic advantage of one plan over the other.

The examples of operational planning that have been cited also considered only the operation of one or two reservoirs and were thus further simplified, for purposes of illustration. The integration of a number of reservoirs into system operation becomes much more complex; however, the same basic principles may be used. In such system planning the number of combinations of different conditions that can occur becomes almost infinite. The necessity of considering economics also increases the number of operating combinations that should be considered.

Present manual methods of performing operation studies limit the number of operating combinations that can be considered, and it is generally necessary to perform a small number of operations, with the adopted method of operations being selected partially by interpolation. The variety of possible combinations stresses the importance of developing economical, high-speed methods of performing integrated system operation studies. Such methods are not readily available at the present time. However, other Bureau of Reclamation engineers and statisticians are currently working on procedures by which such studies may be processed on high-speed electronic computers, and some progress has been made. The methods under development, if successful, will allow quick processing of repeated operations, with simple changes in operating criteria. This method of processing will satisfy an all important need in operational planning, by allowing a very large number of studies to be made rapidly at comparatively low cost. The development of such methods will allow the optimum potential of probability procedures to be realized in operational planning.

Use of Statistics in Operation of Other Reservoirs

Probability methods inherent in forecast procedures form the basis for development of operational plans for other Bureau of Reclamation reservoirs

in addition to those described previously. For example, the operation of Hoover Dam and Lake Mead for flood control is based on protection against a maximum forecasted inflow of a given probability of occurrence.[4] The flood control regulations currently in force provide that this maximum forecasted flow shall be that which, on the average, will not be exceeded 19 times out of 20.

Forecasting methods, based on multiple correlation and statistical procedures, also are the basis for tentative operating agreements for Arrowrock and Anderson Ranch Reservoirs in the Boise Basin in Idaho, and for Hungry Horse Reservoir in Western Montana. Similar use of such methods is under consideration for a number of other major Bureau of Reclamation reservoirs in the West.

SUMMARY AND CONCLUSIONS

Statistical procedures can be very helpful in scheduling reservoir operations, by furnishing an evaluation of the operational chances that are taken. The techniques are particularly applicable to evaluation of water supply probabilities.

Reservoir operating plans must consider all the potentialities for variation in water supply and must properly evaluate the probability of occurrence of extremes. The extremes of water supply frequently form the guides for a given operation, rather than the normal, or most probable, water supply. This emphasizes the need for proper evaluation of the probability of occurrence of the extreme.

A complete operating plan must have an initial firm schedule which can be followed until significant new operating information can be anticipated. After the initial firm schedule, the plan should designate different courses of action for the various possibilities of water supply.

Adaptation of low-cost, high speed electronic computing methods to the processing of operational studies will be an invaluable aid to development of fully coordinated operating plans, and will allow the optimum potential of probability procedures to be realized.

ACKNOWLEDGMENTS

The work described was performed while the writer served in the capacity of Chief of River Operations, Upper Platte System, Region 7, Bureau of Reclamation, Loveland, Colorado. H. R. Brown, Power Operation and Maintenance Officer, was in immediate charge of the work performed. Jesse L. Honnold, Chief, Hydrology Branch, Region 7, had technical cognizance of hydrologic phases of the work.

REFERENCES

1. "Review of Flood Frequency Methods." Final report of the Subcommittee of the Joint Committee on Floods. ASCE Separate No. 110, December 1951.

2. "Multiple Correlation in Forecasting Seasonal Runoff" by Perry M. Ford, Engineering Monograph No. 2, U. S. Bureau of Reclamation, Denver, Colorado, pp. 12-13, 17.

3. "Operational Economy Through Applied Hydrology" by Francis B. Blanchard, Proceedings of Western Snow Conference, Portland, Oregon, April 1955. (being processed for publication)

4. "Use of Inflow Forecasts in Operation of Hoover Dam and Lake Mead for Flood Control" by Frantz R. Lupton, Proceedings 18th Annual Meeting, Western Snow Conference, April 1950, pp. 35-47.

Journal of the
HYDRAULICS DIVISION
Proceedings of the American Society of Civil Engineers

FREE OUTLETS AND SELF-PRIMING ACTION OF CULVERTS

Wen-Hsiung Li,[1] A.M. ASCE, and Calvin C. Patterson,[2] J.M. ASCE
(Proc. Paper 1009)

SYNOPSIS

In this paper, the following observations on scale models of culverts are reported: (1) When the outlet end of a full-flowing culvert is free from submergence, the effective position of the hydraulic grade-line at the outlet section is mainly a function of the Froude Number, and is above the centroid of the section in many practical cases; and (2) A culvert, acting as a sluice, may prime itself in three different manners. Data on conditions for self-priming of square box-culverts and circular pipes with a sharp-cornered entrance are presented. An impulsive pressure-drop in the culvert was observed during priming.

NOTATION

The letter symbols adopted for use in this paper are defined where they first appear, and are arranged alphabetically, for convenience of reference, in the Appendix.

INTRODUCTION

In this paper, some hydraulic characteristics of culverts of practical interest are discussed. The following observations on scale models of culverts are reported:

1) When the outlet of a full-flowing culvert is free from submergence, the effective position of the hydraulic grade-line at the outlet is usually assumed to be located at the centroid of the outlet section. However, it has been observed(1) that this position is higher than the centroid at low values of $\frac{Q}{\sqrt{g}\, D^{5/2}}$ (where Q is the discharge through the culvert, D is the vertical

Note: Discussion open until November 1, 1956. Paper 1009 is part of the copyrighted Journal of the Hydraulics Division of the American Society of Civil Engineers, Vol. 82, No. HY 3, June, 1956.

1. Associate Prof. of Civ. Eng., The Johns Hopkins Univ., Baltimore, Md.
2. Research Asst., The Johns Hopkins Univ., Baltimore, Md.

dimension of the culvert, and g is the gravitational acceleration). Since the allowable head-difference across the culvert in most cases is not much greater than its vertical dimension, an assumed position of the hydraulic grade-line at the centroid of the outlet section will lead to a design on the unsafe side. It seems that a closer examination of this problem is appropriate.

2) A culvert does not necessarily flow full when the entrance is submerged, unless the entrance is of special design. It has been observed that a culvert, acting as a sluice, may prime itself automatically under suitable conditions. It is of practical interest to know more fully about this self-priming action so as to design culverts with a proper hydraulic control. Culverts with a sharp-cornered entrance are chosen for study in this investigation.

Equipments

The scale models used in this investigation consisted of an intake-box and a transparent pipe (circular or square in cross-section). When submergence of the outlet was desired, an outlet-box was added to the downstream end of the pipe, as shown in Fig. 1. The whole assembly was mounted on a steel channel-section, the longitudinal slope of which could be varied from zero to five percent.

The circular culvert models were Lucite pipes of 2-7/8 in. inside diameter. The square box-culvert models were made of Plexiglas and were 2.54 in. in width each side. The calibrated values of Manning's coefficient n were 0.009 and 0.010 for the circular pipes and the square box-culverts respectively. The floor of the approach channel was level with the invert of the culvert entrance. The outlet apron, if used, was level with the invert at the outlet. The headwall was vertical as shown in Fig. 1. Wing-walls at the entrance were used in some of the tests with box-culverts, as shown in Fig. 2. The entrances of all the culvert models were sharp-cornered and flush with the vertical headwall.

The elevations of the head-water and tail-water surfaces were measured with point gages. The head-water elevation was also read from a water column connected to one side of the intake-box. The water supply was measured with a calibrated orifice-meter in the supply-line. The pressure of the air inside a partly full culvert was observed with a U-tube connected to the invert of the culvert at a distance of 2D from the entrance. It was observed that the pressure of the air was not different from atmospheric by any significant amount even for culvert models 50D in length under a head-water depth of 10D.

Effective Position of Hydraulic Grade-Line at Free Outlets

In the one-dimensional approach to the pipe-flow problem, it is assumed that the pressure at each section is hydrostatically distributed so that the sum of the pressure head (p/w) and the elevation z is the same for every fluid element at a cross-section. The value of this sum at the centroid of the section can therefore be used as the mean value for the whole flow passing the section. However, at the free outlet of a culvert, the pressure is not hydrostatically distributed. The actual distribution must depend on the characteristics of the flow as well as the geometry of the culvert section and the

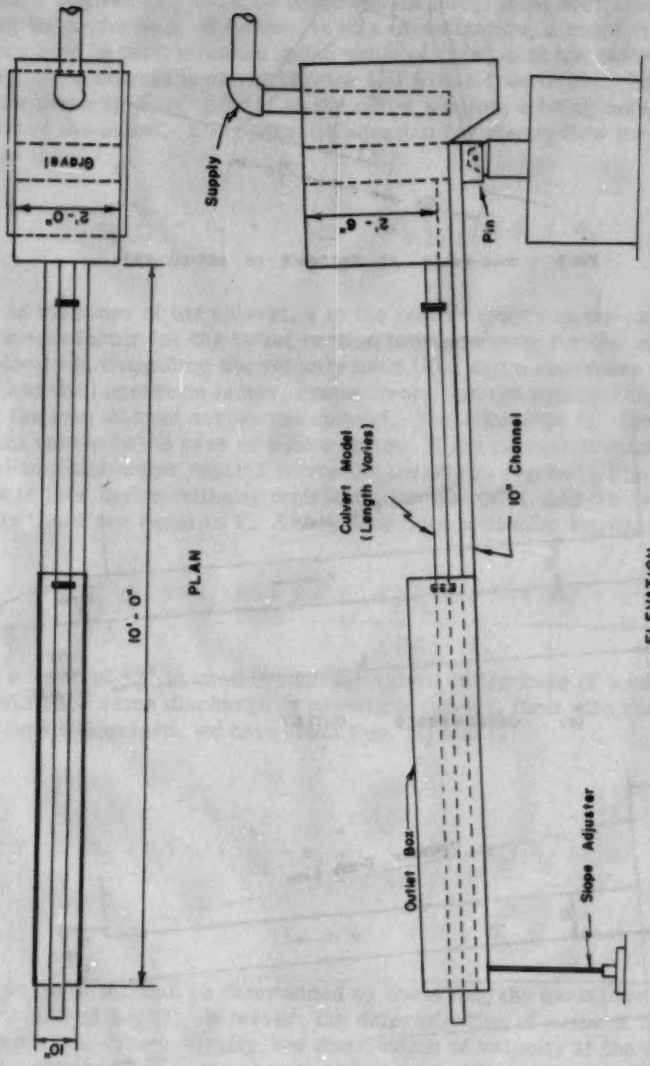

FIG 1 ADJUSTABLE - SLOPE MODEL CULVERT

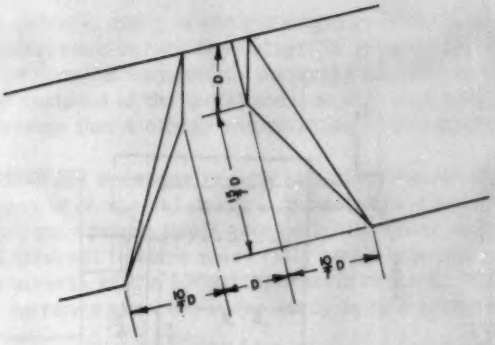

FIG.2 WING-WALLS AT ENTRANCE OF BOX-CULVERT

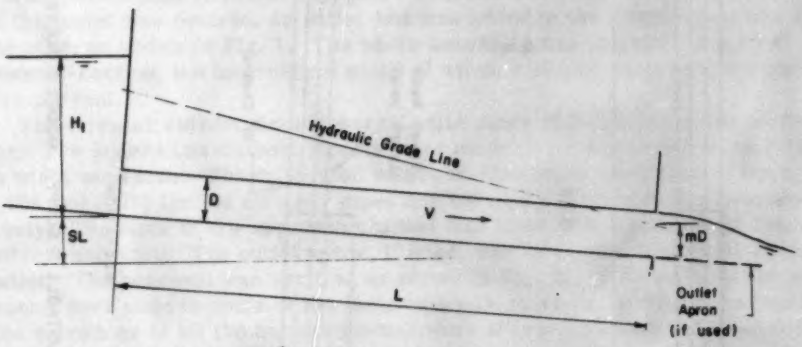

(a) UNSUBMERGED OUTLET

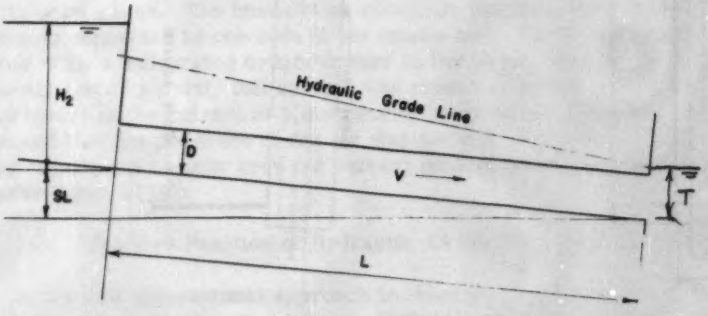

(b) SUBMERGED OUTLET

FIG.3 HYDRAULIC GRADE LINES

presence of wing-walls and apron at the outlet. The sum (p/w)+z at the centroid, therefore, cannot be used to represent the mean value for the whole flow passing the section. To find the total head at the outlet, the distribution of pressure and velocity must be found and an integration over the whole section must be performed. However, in this investigation, a more direct method is used to determine the mean value of (p/w)+z at the outlet.

In Fig. 3a, a culvert is shown flowing full with a free outlet. Let mD represent the mean value of (p/w)+z at the outlet section, z being measured from the invert of the outlet. The hydraulic equation for steady flow through this culvert is then

$$a_1 \frac{u_1^2}{2g} + H_1 + s\,L = \alpha_1 \frac{v^2}{2g} + m\,D + \Delta_1 \qquad (1)$$

where s is the slope of the culvert, v is the mean velocity in the culvert, α is the correction factor for the outlet section to compensate for the use of the mean velocity in computing the velocity head,(2) u and a represent the mean velocity and the correction factor, respectively, for the approaching stream, and Δ is the loss of head across the culvert. The subscript "1" here is used to indicate values in the case of a free outlet. If the culvert is submerged at the outlet to a tail-water depth T above the invert, as shown in Fig. 3b, the pressure is then hydrostatically distributed at the outlet, and the value of (p/w)+z is therefore equal to T. The appropriate hydraulic equation is then

$$a_2 \frac{u_2^2}{2g} + H_2 + s\,L = \alpha_2 \frac{v^2}{2g} + T + \Delta_2 \qquad (2)$$

Here the subscript "2" is used to indicate values in the case of a submerged outlet. When the same discharge is passing a culvert, first with the outlet free and then submerged, we have from Eqs. (1) and (2)

$$m\,D = T - (H_2 - H_1) + \left(a_1 \frac{u_1^2}{2g} - a_2 \frac{u_2^2}{2g}\right) - (\alpha_1 - \alpha_2) \frac{v^2}{2g} - (\Delta_1 - \Delta_2) \qquad (3)$$

Thus the value of mD can be determined by observing the quantities at the right-hand side of Eq. (3). However, the determination of some of these quantities is not easy. Theoretically, the distribution of velocity at the outlet section will be changed due to the change of outlet condition. The values of α_1 and α_2 will therefore be theoretically different. There is also a theoretical difference between Δ_1 and Δ_2 due to the different rates of head-loss in the vicinity of the outlet caused by the change in velocity distribution. However, these small differences are of no great practical importance at the present, since the values of the correction factor and the head-loss themselves can only be approximately known in practice. The values of α_2 and Δ_2 for the case of hydrostatically distributed pressure at each cross-section have been

investigated to some extent by past investigators.(3) For practical convenience, let the effective value of mD be defined as the value computed from Eq. (1) with the values of α_1 and Δ_1 assumed to be the same as the better known values of α_2 and Δ_2 respectively. Thus

$$\text{Effective mD} = T - (H_2 - H_1) + \left(a_1 \frac{u_1^2}{2g} - a_2 \frac{u_2^2}{2g}\right) \qquad (4)$$

Since the hydraulic grade-line can be defined as the plot of the mean value of (p/w)+z above the z = 0 datum, the effective value of mD as defined in Eq. (4) gives the effective position of the hydraulic grade-line at the free outlet, as shown in Fig. 3a. This effective value of mD for long culverts can also be obtained by projecting the observed hydraulic grade-line to the outlet section.

In this investigation, culvert models of 20D in length were tested with full flow at different slopes and discharges. At each discharge, the values of H_1 and H_2 were observed respectively with the outlet free and with the outlet submerged to a tail-water depth T greater than D. The velocity head of the approach flow in the model was found to be negligible. Tests were carried out with and without an apron at the outlet. When an apron was used, it was put at the level of the invert of the outlet section (Fig. 3a). The test results of the circular pipe are shown in Fig. 4, and those of the square box-culvert in Fig. 5. The value of m, computed according to Eq. (4), was found to be mainly a function of the Froude number $\frac{v}{\sqrt{gD}}$. The presence of an apron increased the value of m, but the increase was insignificant in the case of the circular pipe where the apron had only point contact with the jet at the outlet section. Although there was some change in the values of m with the culvert slope, this change is significant only in the case of the box-culvert with an outlet apron.

At values of $\frac{v}{\sqrt{gD}}$ less than about unity, the jet became detached from the top of the culvert. It can be reasoned that, when the jet is detached from the top of the culvert, the value of m is also affected by the characteristics of the culvert barrel, since the effect of gravity is then no longer limited to the vicinity of the outlet. For cases with $\frac{v}{\sqrt{gD}}$ greater than unity, Figs. 4 and 5 will furnish proper values of m for design.

It should be mentioned that the value of m may be quite different for culverts not included in this investigation. The following outlet conditions give rise to higher values of m: (1) an outlet apron is used with box-culverts, the total width of which is much greater than its height; and (2) there are parallel wing-walls as well as an apron at the outlet. For these two cases, the value of m can be as high as unity. In case of doubt, it is safe to use a value of unity for m for a free outlet.

Self-Priming Action of Culverts with Sharp-Cornered Entrance

A culvert does not necessarily flow full when the entrance is submerged unless the entrance is of special design. Because of the separation of the

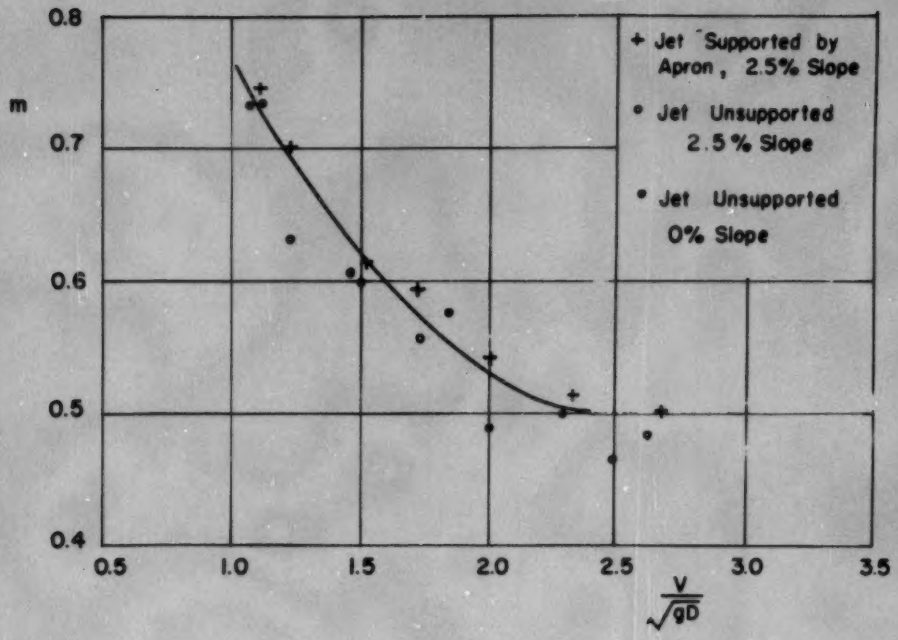

FIG.4 EFFECTIVE POSITION OF THE HYDRAULIC GRADE-LINE AT OUTLET OF ROUND CULVERTS.

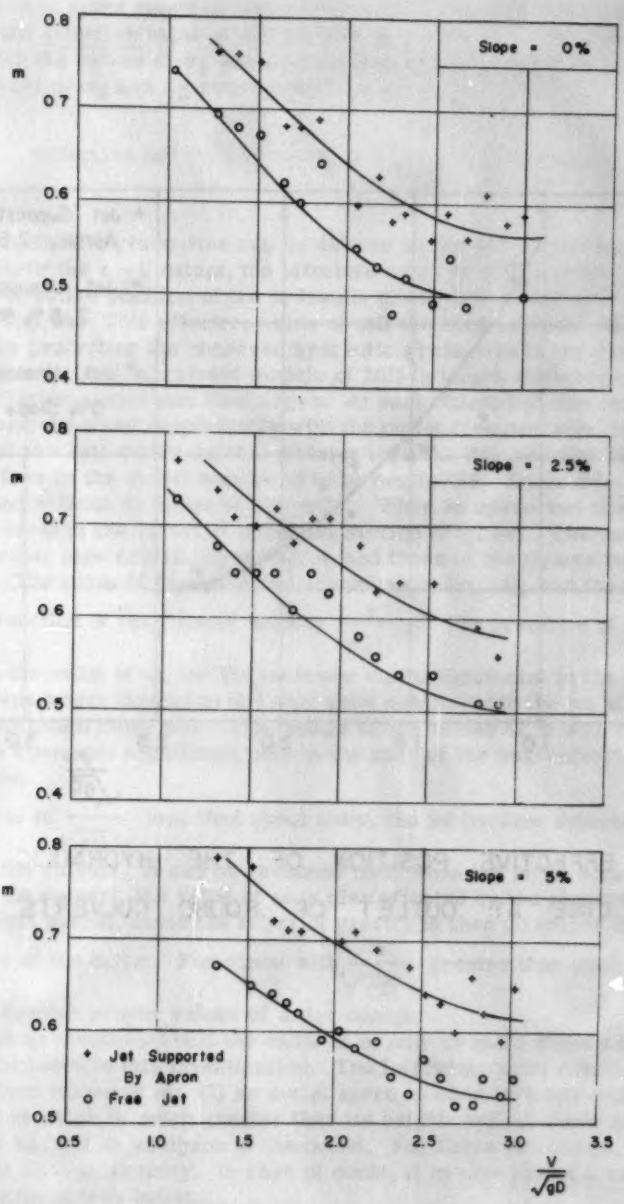

FIG.5 EFFECTIVE POSITION OF THE HYDRAULIC GRADE-LINE AT OUTLET OF SQUARE BOX-CULVERTS

water from the sides and top of the entrance section, the entrance may act as a sluice (Fig. 10). However, under suitable conditions, the culvert may prime itself automatically. In this investigation, this self-priming action of culverts with a sharp-cornered entrance is studied. Entrances flush with a vertical head-wall, with and without wing-walls, are included. The outlet is to be free from submergence and the water is not supported by an outlet apron.

Culvert models of various lengths, ranging from 4D to 50D, were tested at slopes varying from zero to five percent under head-water depths up to 12D. The calibration curves of the culverts before priming, with the entrance acting as a sluice, are shown in Fig. 6. For each culvert model, the slope was varied by small increments. At each slope, the discharge was increased very slowly with small increments until the culvert primed itself. (Different results were obtained when the discharge was increased more rapidly. The culverts became full more readily due to the surging waves thus created). When priming took place, the section where the culvert first became full was noted. (This section will be called the "section of priming" in this paper.) The head-water elevation was read at that instant. After priming, the head-water would fall to a new level of equilibrium for full flow. Upon decrease of discharge, the culvert remained full until air was admitted into the culvert through the entrance.

The observed conditions for priming are shown in Figs. 7, 8 and 9. Conditions above and to the right of each curve will not produce full flow in a culvert of a length corresponding to that curve. Three distinctive types of self-priming action were observed and may be described as follows:

(1) Self-priming after a hydraulic jump (Fig. 10a):

At extremely mild slopes, a culvert with a sharp-cornered entrance may prime itself with the water-surface reaching the top of the culvert after a hydraulic jump. This action takes place at low values of head-water depth H. The distance from the entrance to the jump increases with the discharge (less than 10D when self-priming action took place in the models). Between the entrance and the jump, the water-surface is covered with weak diamond-shaped standing surface-waves generated at the sides of the entrance section. The magnitude of these waves increases with the discharge.

In order to have a self-priming action of this manner, the culvert must not only have a very mild slope but must also be of sufficient length. The shorter the culvert, the milder must be the slope. For culverts less than about 8D in length, self-priming in this manner will not take place even when the culvert is at a zero slope.

(2) Self-priming with a divergent flow (Fig. 10b):

When a culvert cannot prime itself in the manner described above, a relatively long culvert (about 35D or longer) may become full by rising to the top near the outlet with a divergent flow (conventionally known as M3 and S3 curves).(4) When a culvert is long enough for this action to take place, the steeper the slope, the larger the discharge required. This priming action takes place at medium values of H, up to about 10D for the square culverts and up to about 7D for the circular culverts.

The surface of the divergent flow is covered with standing surface-waves which increase in magnitude with increase of discharge. (These waves were

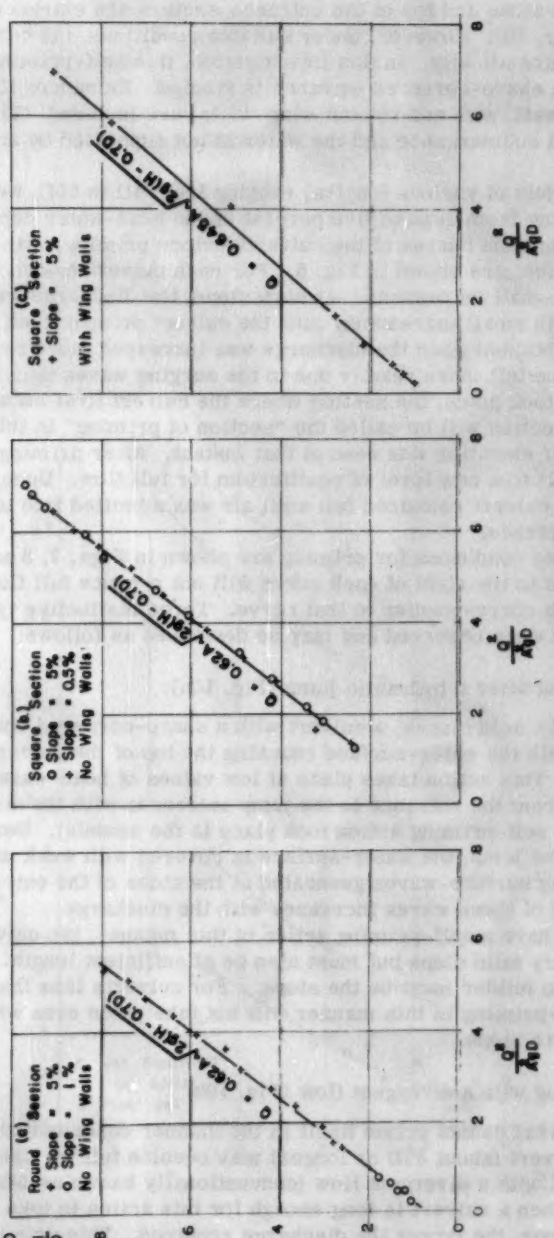

FIG. 6 CALIBRATION CURVES OF CULVERT MODELS WITH ENTRANCE ACTING AS A SLUICE.

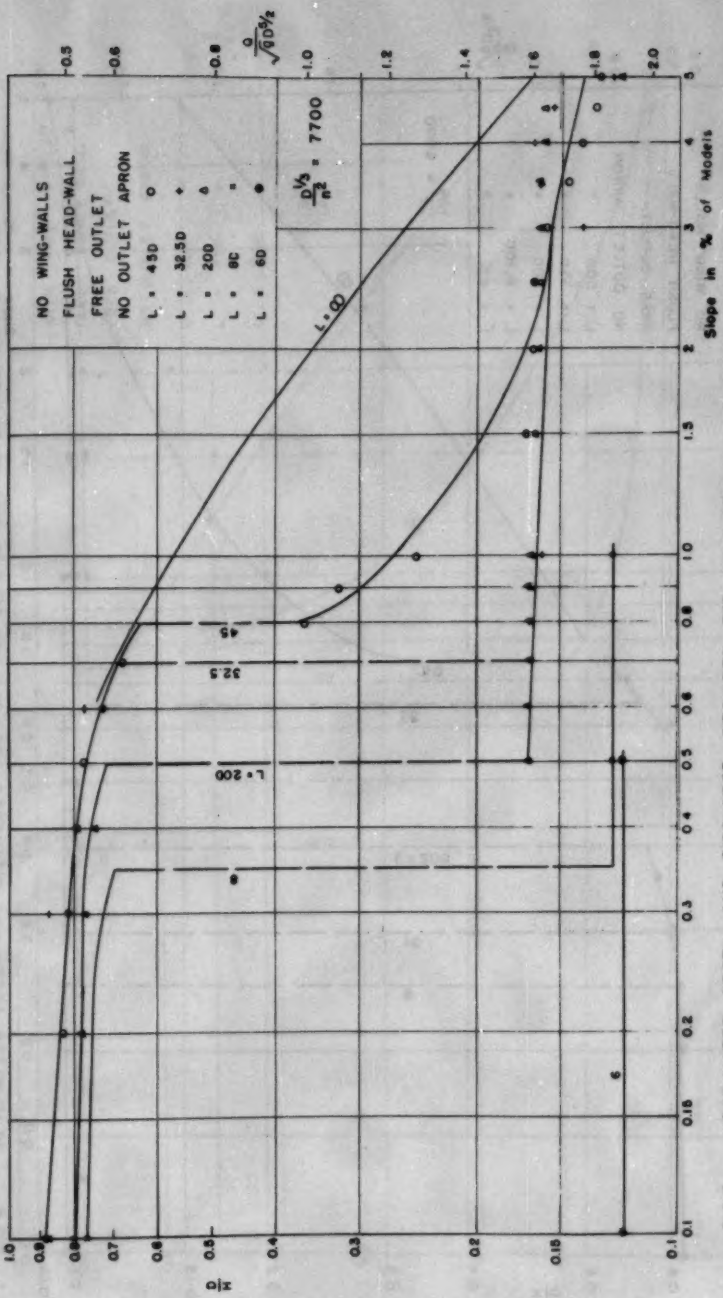

FIG 7 HEAD-WATER DEPTH AND DISCHARGE REQUIRED FOR SELF-PRIMING OF ROUND CULVERTS

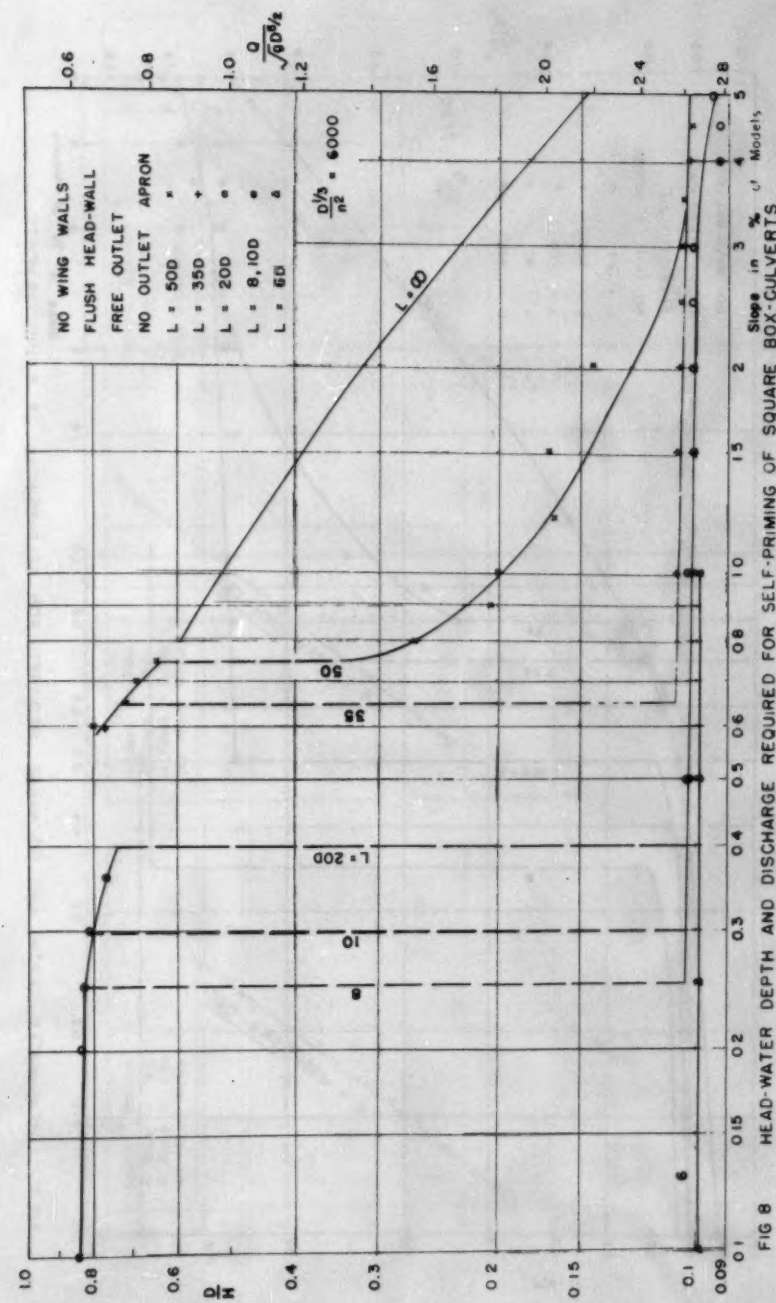

FIG 8 HEAD-WATER DEPTH AND DISCHARGE REQUIRED FOR SELF-PRIMING OF SQUARE BOX-CULVERTS

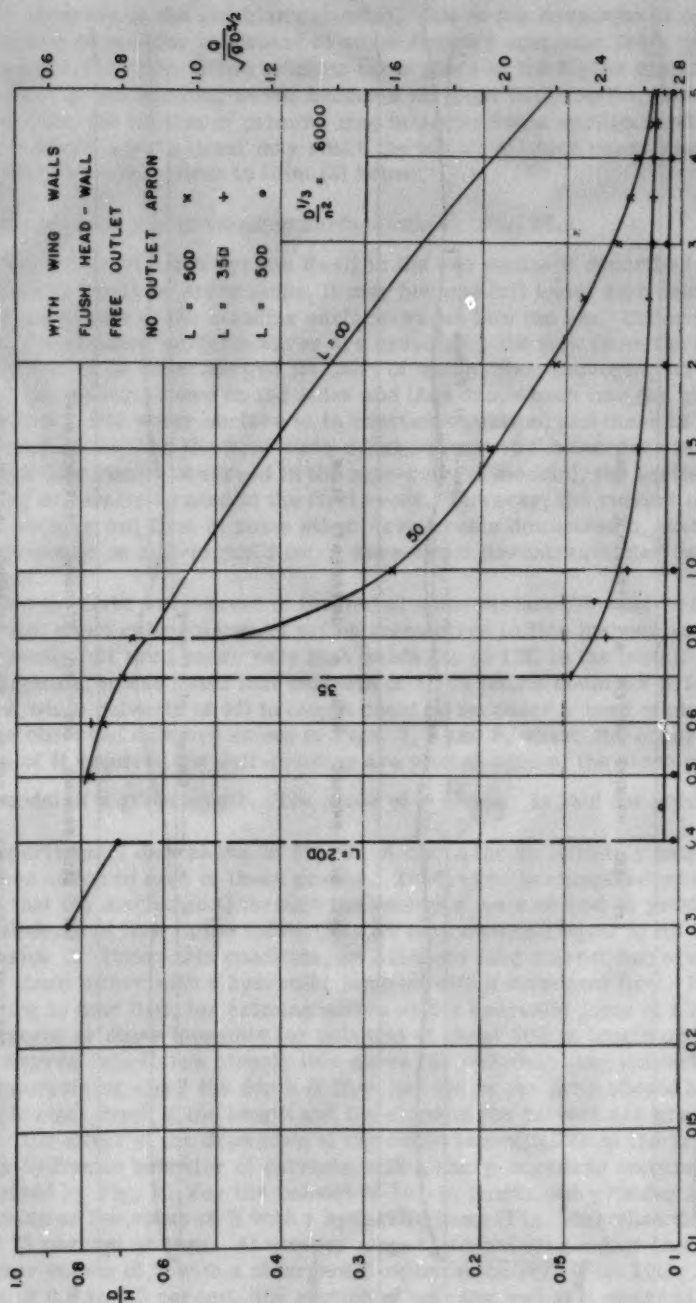

FIG. 9 HEAD WATER DEPTH AND DISCHARGE REQUIRED FOR SELF-PRIMING OF SQUARE BOX-CULVERTS.

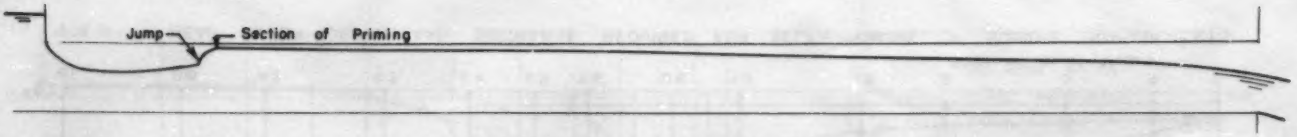

(a) SELF-PRIMING AFTER A HYDRAULIC JUMP.

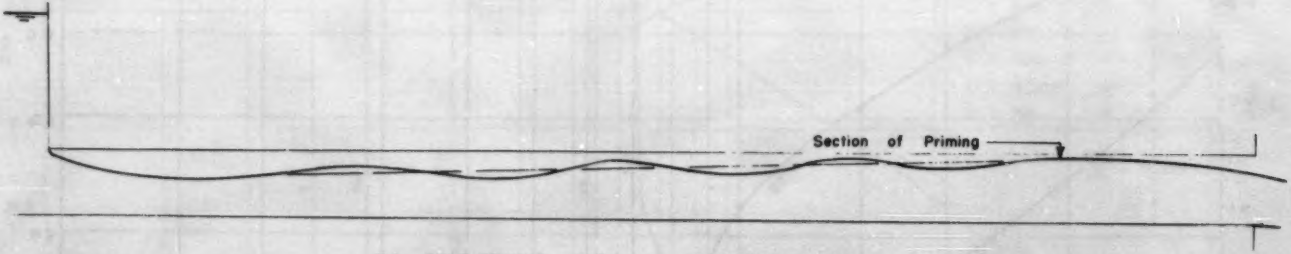

(b) SELF-PRIMING WITH A DIVERGENT FLOW.

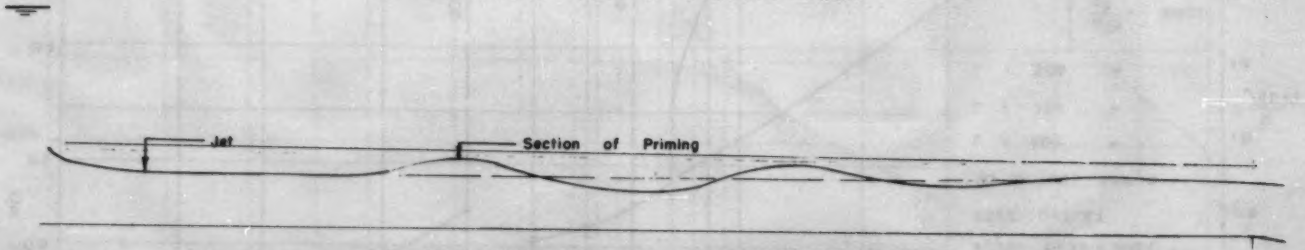

(c) SELF-PRIMING DUE TO STANDING SURFACE-WAVE

FIG 10 . SKETCHES SHOWING TYPICAL SELF-PRIMING ACTION

easily observed in the circular culverts). Due to the drawdown at the outlet, the section of priming is located at some distance upstream from the outlet, as shown in Fig. 10b. When priming takes place at the higher discharges, the magnitude of the standing waves becomes so large that, for the same condition of flow, the section of priming may be located at a section further upstream where a wave crest may reach the top first. Such cases may be considered to be a transition to item (3) below.

(3) Self-priming due to standing surface-waves (Fig. 10c):

When a culvert cannot prime itself in the two manners described above due to its short length or steep slope, it may become full under high heads when one of the crests of the standing surface-waves hits the top. Under these high heads, the standing surface-waves are created by the flow from the entrance in the form of an unsubmerged jet, part of which, upon impinging on the bottom of the culvert, flows up the sides and then drops back into the main part of the flow. The water surface is in constant agitation, and there is rapid entrainment of air. As the first wave-crest nearest to the entrance is largest in magnitude (easily observed in the pipe-culvert models), the section of priming is usually located at the first crest. However, the culvert may sometimes become full first at some other wave-crests downstream, since, being superimposed on a divergent flow, a wave-crest downstream may reach the top first.

Since the first wave-crest is located at some distance downstream of the entrance, short culverts cannot prime themselves in this manner and will remain partly full even under very high heads (up to 12D in the tests). In this investigation, it was found that culverts of 4D in length could not prime themselves, while culverts of 6D in length could do so under a head of about 10D.

The observed data are shown in Figs. 7, 8 and 9, where the observed values of H required for self-priming are plotted against the slope of the culvert model of a given length. The scale of $\frac{Q}{\sqrt{g}\,D^{5/2}}$ is laid out according to the experimental data shown in Fig. 6. A curve for an infinitely long culvert has been added to each of these graphs. This curve is computed with the condition that the discharge Q through the entrance (as a sluice) is producing a normal depth of flow in the culvert (as an open channel) equal to its vertical dimension D. Under this condition, an infinitely long culvert can always prime itself either with a hydraulic jump or with a divergent flow. It is interesting to note that, for priming action with a hydraulic jump at a slope of 0.6 percent or more (possible for culverts of about 30D in length or longer), the observed data follow closely this curve for infinitely long culverts. This is not surprising since the depth of flow just below the jump should be close to the normal depth if the length and the slope of the culvert are great enough so that the effect of the drawdown at the outlet is negligible at the jump.

The hydraulic behavior of culverts with a sharp-cornered entrance may be illustrated by Fig. 8. For the culvert of 50D in length, the priming action took place at low value of H with a hydraulic jump (Fig. 10a) when the slope was 0.75 percent or less. At steeper slopes, the priming action took place at higher values of H with a divergent flow in the culvert (Fig. 10b). For slopes of 0.8 to 3.5 percent, the section of priming was at a distance of from 3D to 9D upstream of the outlet. At 4.5 and 5 percent slopes, the section of priming was at about the mid-section of the culvert. This condition indicated

a transition to the priming action as described under item 3 (Fig. 10c). For the culvert of 35D in length, the behavior was qualitatively similar, except that at all slopes between 0.65 and 5 percent, the priming action was a transition from that described under item 2 (Fig. 10b) to that described under item 3 (Fig. 10c). The section of priming was located near either the outlet or the mid-section of the culvert. The behavior of shorter culverts of 8D or more in length was qualitatively the same. The shorter the culvert, the closer the priming action under high heads to that described under item 3. For the culvert of 6D in length, no priming action with a hydraulic jump was observed even at a zero slope. At all slopes, this culvert primed itself under high heads as described under item 3. For the culvert of 4D in length, no priming action was observed with H up to 12D.

In this investigation, only smooth pipes were used. The effect of surface roughness of the culvert has to be investigated. By dimensional consideration, it can be shown that the length L of culvert required for priming action can be expressed as

$$\frac{L}{D} = \text{function of } \left(\frac{Q}{\sqrt{g}\, D^{5/2}} , \frac{D^{1/3}}{n^2} , s \right) \qquad (5)$$

Since, before the priming action, we have (see Fig. 6)

$$\frac{Q}{\sqrt{g}\, D^{5/2}} = \text{function of } \frac{H}{D} \qquad (6)$$

Thus

$$\frac{L}{D} = \text{function of } \left(\frac{D}{H} \text{ or } \frac{Q}{\sqrt{g}\, D^{5/2}} , \frac{D^{1/3}}{n^2} , s \right) \qquad (7)$$

The value of $\frac{D^{1/3}}{n^2}$ for the circular culvert models was 7700 (in ft.-sec. units) and that of the square box-culverts was 6000. The curves in Figs. 7, 8 and 9 can therefore be used for culverts with the same values of $\frac{D^{1/3}}{n^2}$, Manning's formula being accepted as applicable.

Using Manning's formula for describing the frictional effect, we can simplify Eq. (7). For the convenience of discussion, take the case of priming with a divergent flow (Fig. 10b). The "backwater" equation gives[5]

$$\frac{sL_{12}}{D} = \emptyset\left(\alpha, \frac{y_2}{D}\right) - \emptyset\left(\alpha, \frac{y_1}{D}\right) - \frac{Q^2}{D^5}\left[\psi\left(\alpha, \frac{y_2}{D}\right) - \psi\left(\alpha, \frac{y_1}{D}\right)\right] \qquad (8)$$

where

$$\alpha^2 = 0.45 \left(\frac{D^2}{A}\right)^2 \left(\frac{D}{R}\right)^{4/3} \frac{n^2}{sD^{1/3}} \cdot \frac{Q^2}{D^5} \tag{9}$$

y_1 is the depth of flow at the contracted section of flow near the entrance, and y_2 is the depth of flow at the section of priming. L_{12} is the distance between these two sections. ϕ and ψ are the backwater functions for closed conduits. For a given cross-sectional shape and entrance geometry, we have by dimensional consideration

$$\frac{y_1}{D} = \text{function of } \frac{Q}{\sqrt{g}\, D^{5/2}} \tag{10}$$

and

$$\frac{y_2}{D} = \text{function of } \frac{Q}{\sqrt{g}\, D^{5/2}} \cong 1 \tag{11}$$

Since, for a given cross-sectional shape,

$$\alpha^2 = \text{const.} \frac{n^2}{sD^{1/3}} \cdot \frac{Q^2}{D^5} \tag{12}$$

we have, from Eqs. (6), (8), (10), (11) and (12),

$$\frac{sL_{12}}{D} = \text{function of } \left(\frac{Q}{\sqrt{g}\, D^{5/2}} \text{ or } \frac{D}{H}, \frac{sD^{1/3}}{n^2}\right) \tag{13}$$

Similar expression can be written for the flow downstream of the section of priming. Thus

$$\frac{sL}{D} = \text{function of } \left(\frac{Q}{\sqrt{g}\, D^{5/2}} \text{ or } \frac{D}{H}, \frac{sD^{1/3}}{n^2}\right) \tag{14}$$

The function in Eq. (14) depends on the cross-sectional shape and the entrance and outlet conditions, and can be determined experimentally. For square box-culverts as described in Fig. 8, Fig. 11 has been plotted according to the data shown in Fig. 8. Similar graphs can be prepared in a similar manner for culverts of other description. Since the application of Manning's formula to divergent supercritical flow may be questioned, Eq. (14) should not be considered to be theoretically exact. However, in the absence of a better theory for turbulent flow, the correctness of Eq. (14) and Fig. 11 is consistent with the present knowledge.

The data presented in Figs. 7, 8 and 9 have been obtained from culvert models with a flush head-wall, a relatively wide approach-channel level with the invert of the entrance, a sharp-cornered entrance, and a free outlet

without an apron. If the entrance is projecting, or if the approach-channel is at an elevation lower than the invert of the entrance, the contraction of flow at the entrance will be greater, and the culvert will probably prime itself less readily. (A special exception is a projecting entrance with a hood).(6) On the other hand, if the corner of the entrance is tapered or rounded to a certain extent, or if an apron is put at the outlet, or if the approach-channel is relatively narrow, the culvert will probably prime itself more readily. It is not the purpose of this paper to present data for many types of entrances which can be studied in the same manner. It is believed that the data shown in Figs. 7, 8, 9 and 11 can be used, without introducing errors on the unsafe side, in the design of culverts with a flush head-wall and an approach-channel level with the invert. In using Figs. 7, 8 and 9, the value of $\frac{D^{1/3}}{n^2}$ of the culverts should not depart too far from those of the models.

Impulsive Pressure-Drop in Culverts During Priming

It was observed in this investigation that, during the priming of the culverts, either by self-priming action as described above or by submergence of the outlet, there was an impulsive pressure-drop inside the culverts. The preliminary data indicate that the adverse effect of this impulsive pressure-drop on the stability of thin-walled structures can be significant in some cases.

The creation of this impulsive pressure-drop may be explained as follows: A flow with a free surface has a certain capacity of air entrainment which depends on the characteristics of the flow. Before priming, the air in a partly full culvert is continuously being entrained by the water and replenished by air flowing in from the outlet. During priming (see Fig. 12a), the supply of air from the outlet is blocked off while the air trapped inside the culvert, upstream of the section of priming, continues to be entrained. Unless the evacuated space is rapidly filled with water, a partial vacuum will be created. During priming, the culvert becomes full with a surface wave moving from the section of priming toward the entrance section. Seemingly, this surface-wave cannot, due to inertia, move fast enough to fill the evacuated space. As a result, there is an impulsive pressure-drop inside the culvert. The duration of this pressure-drop is very short (only a fraction of a second in the models). When the culvert becomes completely filled with water, the pressure in the culvert rises rapidly to settle at the equilibrium pressure for full flow (see Fig. 12b).

The magnitude and duration of the pressure-drop depend on many factors. To determine this pressure-drop accurately, a thorough investigation must be undertaken. In the present study, only preliminary tests were carried out with piezometric connections at the bottom of the culverts near the entrance. The observed values of the pressure-drop due to self-priming of the circular culverts are shown in Fig. 12c. Because of the inertia effect in the measuring device and scale effect, these values are approximate and should not be used for design purposes. These data are presented to call attention to this fact. The authors offer this phenomenon as a possible explanation of the collapse of some thin-walled culverts during floods.

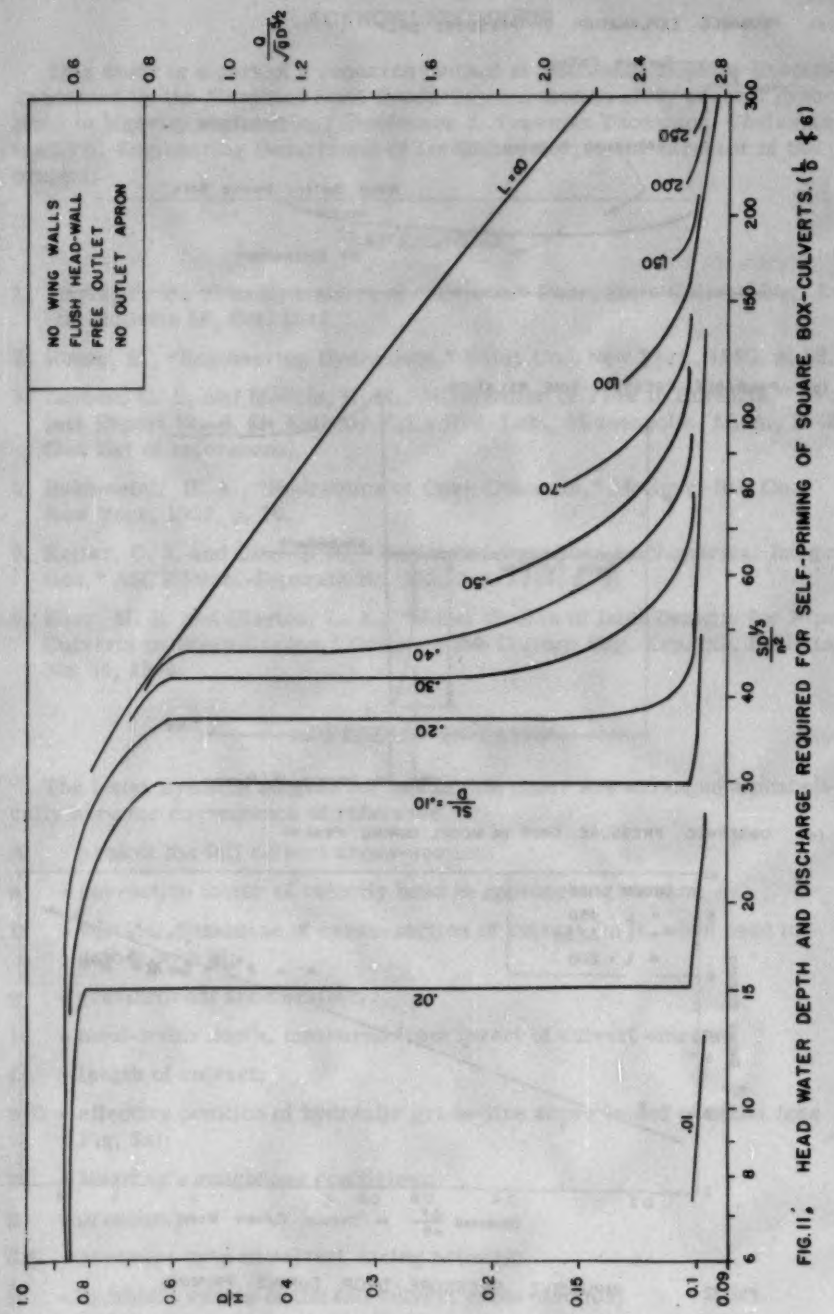

FIG.11, HEAD WATER DEPTH AND DISCHARGE REQUIRED FOR SELF-PRIMING OF SQUARE BOX-CULVERTS.($\frac{1}{6}$ to 6)

(a) PROBABLE EXPLANATION OF PRESSURE DROP

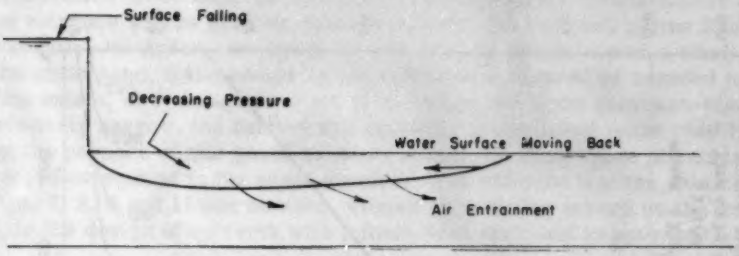

(b) PROBABLE PRESSURE-TIME RELATION

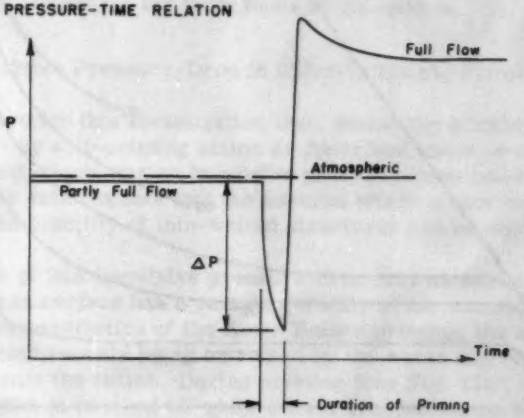

(c) OBSERVED PRESSURE DROP IN MODEL DURING PRIMING

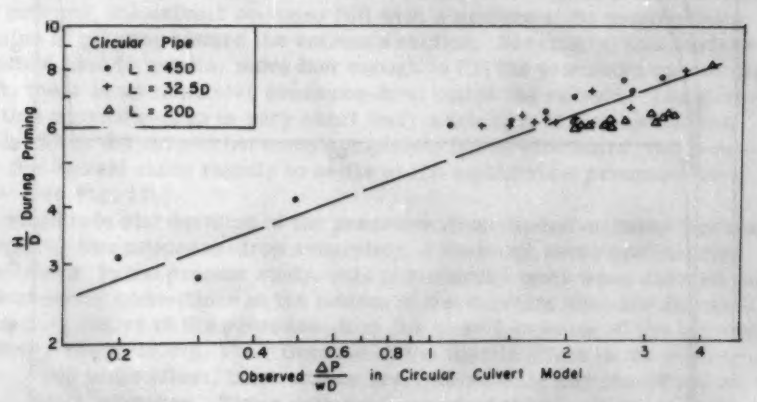

FIG. 12 IMPULSIVE PRESSURE-DROP DURING PRIMING

ACKNOWLEDGMENTS

This study is a part of a research project at The Johns Hopkins University sponsored by the Maryland State Roads Commission to study several problems in highway engineering. Professor J. Trueman Thompson, Chairman of the Civil Engineering Department of the University, is the Director of the project.

REFERENCES

1. Mavis, F. T., "The Hydraulics of Culverts," Penn. State College Eng. Exp. Sta. Bulletin 56, Oct. 1942.
2. Rouse, H., "Engineering Hydraulics," Wiley Co., New York, 1950, p. 58.
3. Larson, C. L. and Morris, H. M., "Hydraulics of Flow in Culverts," Project Report No. 6, St. Anthony Falls Hyd. Lab., Minneapolis, Minn., 1948 (See list of references).
4. Bakhmeteff, B. A., "Hydraulics of Open Channels," McGraw-Hill Co., New York, 1932, p. 76.
5. Keifer, C. J. and Chu, H. H., "Backwater Functions by Numerical Integration," ASCE Proc.-Separate No. 383, Jan. 1954, p. 5.
6. Karr, M. H. and Clayton, L. A., "Model Studies of Inlet Designs for Pipe Culverts on Steep Grades," Oregon State College Eng. Exp. Sta. Bulletin No. 35, 1954.

APPENDIX - NOTATION

The letter symbols adopted for use in this paper are arranged alphabetically here for convenience of reference.

A = area of the full culvert cross-section;

a = correction factor of velocity head in approaching stream;

D = vertical dimension of cross-section of culvert (in ft. when used together with n);

g = gravitational acceleration;

H = head-water depth, measured from invert of culvert entrance;

L = length of culvert;

mD = effective position of hydraulic grade-line above invert of outlet (see Fig. 3a);

n = Manning's roughness coefficient;

p = pressure;

Δp = pressure drop in culvert during priming;

R = hydraulic radius of the full culvert cross-section;

s = longitudinal slope of culvert (ft. per ft.);

T = tail-water depth, measured from invert of outlet;

u = mean velocity of approaching stream;

v = mean velocity in a full-flowing culvert;

w = weight per unit volume of water;

y = depth of flow in culvert;

z = elevation, measured from invert of outlet;

α = correction factor of velocity head in a full-flowing culvert; or a flow parameter as defined in Eq. (9);

Δ = total head-loss in flow through culvert.

Journal of the
HYDRAULICS DIVISION
Proceedings of the American Society of Civil Engineers

CONTENTS

DISCUSSION
(Proc. Paper 1010)

Note: Paper 1010 is part of the copyrighted Journal of the Hydraulics Division of the American Society of Civil Engineers, Vol. 82, No. HY 3, June, 1956.

Discussion of "A MORE SIMPLIFIED VENTURI TUBE"

by J. C. Stevens
(Proc. Paper 678)

J. C. Stevens,[1] M. ASCE.—The discussion by R. B. Dowdell brings up a few points that deserve clarification. Since he is on the engineering staff of Builders Providence it is only natural that he should defend the practices that have grown up over many years among those organizations that manufacture Venturi meters.

Mr. Dowdell states that the coefficient for the Herschel-type Venturi tube can be predicted with $\pm$ 3/4%, tantamount to claiming a 3/4% accuracy for that type of tube. He then states that the "scatter points in the author's Fig. 3 amounts to 4%.

One must be careful not to confuse precise determinations of flow coefficients with precise computations of flow coefficient determinations.

If the Stevens Simplified Venturi tube will give results within 4% the author will be content and so will Leupold and Stevens Instruments Inc., under whose auspices this Simplified Venturi Tube was developed and who bore the expense of the experiments described in this paper, and so will thousands of customers who care little about tubes whose coefficients can be predicted within 3/4 per cent if less expensive ones are available with an accuracy of 4%.

However the accuracy of the entire meter, tube and registering device, is the real criterion by which efficacy of such devices are judged by the discriminating customer.

As stated in the author's paper the Venturi head is made up of the difference in the energy between the approach and the throat. That energy comprises the difference in velocity heads plus friction between those points and that only applies to one pound or other unit of water as it passes through the tube.

The friction is negligible in the Simplified Tube because of the low velocities, e.g., tap manifolds 7 and 17 only 10 inches apart in Fig. 3 where the coefficient is 1.00. Where the manifolds are farther apart and under the high velocities, the coefficient accounts for the friction factor.

Velocity heads enter so importantly into the computations of Venturi tube flow that unless one determines the energy coefficient α in the equation

$$h_v = \alpha \frac{v^2}{2g}$$ [2]

(1) Cons. Engr. Leupold & Stevens Instruments Inc., Portland, Oreg.
(2) "Velocity Head correction for Hydraulic Flow" by Morrough P. O'Brien and Joe W. Johnson, Engineering News—Record Aug. 16, 1934, p. 214.

very substantial errors may creep into precise calculations of flow. That coefficient is not unity unless the velocity is uniform throughout the cross sections.

Thus the actual flow through a Venturi tube is given by—

$$Q = cKd^2 \sqrt{\alpha_2 h_2 - \alpha_1 h_1} \quad (3)$$

If the velocity distribution patterns are alike at both sections this becomes

$$Q = cKd^2 \sqrt{\alpha \Delta h}$$

Of course in the laboratory where Q is measured this coefficient and that of friction are automatically taken into account. In commercial installations however that depart from the conditions under which the coefficient determinations were made, and they generally do, the laboratory determined coefficients can seldom be applied rigidly to such commercial installations, without introducing substantial errors in the flows indicated by the meter.

Unfortunately in commercial installations there is rarely any means of checking the Venturi tube flow. The customer therefore takes the laboratory coefficients for gospel truth and goes blithely on year after year unwittingly tabulating flows that may be quite erroneous.

The coefficient α is given by

$$\alpha = \frac{\int_0^A V^3 dA}{V_m^3 A}$$

Where V is the mean velocity in the sub areas into which the cross sectional area is arbitrarily divided,
A is the area of the cross section, and
V_m the mean velocity in the entire area = Q/A

It will be found that the coefficient α may vary normally between 1.03 to 1.20 and up to 2.00 or more if there are sharp bends or other disturbances in the approach line. A field determination(4) by the author on flow through a siphon in which there were bends resulted in values of α up to 1.78.

In order to illustrate the importance of this velocity head coefficient Table (3) has been prepared. The errors indicated are in the meter indicated flows which are based on calculations using coefficients from laboratory experiments.

Two tubes are considered, both being in a standard 12-inch pipe line. A flow of 5 cfs is used for both. One tube is a Herschel type tube having a throat diameter to produce, for that flow, a differential head of 1 foot of mercury. The other is the Simplified tube whose smaller diameter is such as to

(3) "Handbook of Hydraulics" by Horace Williams King, 3d Ed. page 471. McGraw-Hill Book Company, New York.

(4) "Siphons as Water Level Regulators" by J. C. Stevens. Transactions ASCE Vol. 104 (1939) p. 1787.

produce a differential head of 1 foot of water.

It is assumed that both meters are commercial installations that depart from the laboratory conditions under which the coefficients were determined.

The Herschel tube permits a slight change in direction of the velocity filaments at the throat. In other words the pattern of velocity distribution at the throat manifold is different and more turbulent than in the approach pipe. Therefore different values of α at the two cross sections are inherent in this type of tube, and the value of α is greater at the throat section than at the approach section.

In the Simplified tube the velocity patterns are alike at both manifolds since both are in the reducer and involve only converging flow. There are no eddies. The values of α therefore are the same for both cross sections. The manifolds used were No. 7 and one 9 inches farther down on the reducer (See Fig. 3. Separate 678).

The constants of the two tubes are as follows:

		Herschel Tube	Simplified Tube
Approach diam.	d_1	1.01 ft	.950
Throat diam.	d_2	.461 ft	.771
Approach area	A_1	.800 ft^2	.707
Throat area	A_2	.165 ft^2	.468
Approach Velocity	V_1	6.25 fps	7.07
Throat Velocity	V_2	30.25 fps	10.68
Approach Vel. head	h_1	.61 ft	.78
Throat Vel. head	h_2	14.15 ft	1.78
Differential	Δh	13.54 ft	1.00
Coefficient		.98	1.00[5]
Ratio	d_2/d_1	.46	.813
Constant[3]	K	6.45	8.35
$Q = cKd\sqrt{\Delta h}$	cfs	$136\sqrt{13.54}$	$5.00\sqrt{1.00}$
Q	cfs	5.00	5.00

(5) See Taps 7-17, Fig. 3, Separate 678.

Table 3

Herschel Tube	α_1	α_2	$\alpha_1 h_1$	$\alpha_2 h_2$	$\Delta \alpha h$	Indicated Q	% Error
	1.03	1.05	.63	14.88	14.25	5.15	3.0
	1.05	1.10	.64	15.57	14.93	5.26	5.2
	1.10	1.15	.67	16.30	15.63	5.39	7.8
	1.15	1.25	.70	17.70	17.00	5.62	12.4
Simplified Tube	1.03	1.03	.80	1.83	1.03	5.08	1.6
	1.05	1.05	.82	1.87	1.05	5.14	2.8
	1.10	1.15	.86	1.96	1.10	5.25	5.0
	1.15	1.15	.90	2.04	1.15	5.37	7.4

It is well to repeat that these errors may result from carefully calculated flow through commercial Venturi meters when their installations depart even slightly from the conditions in the laboratory under which the flow coefficients were determined. In flagrant cases for instance, a bend in the approach pipe a short distance up stream; can easily produce errors of 30% or more in both types of tubes and such cases are not at all uncommon.

F. Paderi[6] has presented some interesting data on his experiments made 14 years ago at the University of Pisa. He made 38 manifolded piezometric taps in the reducer of a Venturi tube.

One interesting feature is that he found it necessary to put one manifolded piezometer set above the 7-1/2 inch diameter throat and in the reducer itself in order to stabilize the meter indications. This evidences that there were eddies in the throat section.

(6) Journal of the Hydraulics Division, HY 1, Feb. 1956, p. 25.

Discussion of
"FLOW GEOMETRY AT STRAIGHT DROP SPILLWAYS"

by Walter Rand
(Proc. Paper 791)

WALTER RAND,[1] A.M. ASCE.—The writer wishes to express his appreciation for the discussion presented by Messrs. A. J. Peterka and J. N. Bradley. He fully shares their concern relative to the use of shallow flow depths in a model to predict the performance of large prototype structures. The interest of the discussers was mainly directed to the determination of scale effect on the length of hydraulic jump. Unfortunately, the available data on this subject is not well suited for numerical comparisons, and the length of hydraulic jump was not a part of writer's investigations because of secondary importance for sill controlled stilling basins. The writer did not even plot any experimental points of other investigators in Fig. 4, because of the large differences in the available data, probably due to different test installations, and ways of measurement. The graph was completed with the plot of Eq. 19, that roughly averages the measurements of Bakhmeteff, Matzke, and Moore. The coefficient "6" in this equation has been used earlier by A. T. Ippen.[2] In using this coefficient, the writer considered also the possibility that Eq. 19 might be used to determine the length of a stilling basin without an end sill of sufficient height. He had knowledge of the experiments of M. Heintz,[3] where the length of the jump was measured on a 19.7 in. wide apron, that was followed by a sand bed downstream, and where the determination of the jump length was also based on the observations of the flow action on this erodable bed. The effective length of the jump was found to be as small as $L = 4.55(d_2 - d_1)$. With this in mind and without going into the discussion of the determination of dimensions of a stilling basin, the writer adopted the Eq. 19 as an acceptable approximation for the length of hydraulic jump.

The writer does not believe that Eq. 19 can be used to demonstrate the scale effect as has been done by Messrs. Peterka and Bradley in Table 1 and Fig. 2 of their discussion. Eq. 19 does not represent any particular set of model experiments. The choice of the coefficient "6" and the assumption, that it is a constant for a variable Froude number were rather arbitrary. In fact, this coefficient, that represents the ratio $L/(d_2 - d_1)$, is a variable according to the data given by Messrs. Peterka and Bradley:

(1) Lecturer in Civ. Eng., The City College, New York, N.Y.
(2) "Channel Transitions and Controls," by A. T. Ippen in "Engineering Hydraulics," edited by Hunter Rouse, John Wiley and Sons, Inc., New York, 1950, p. 572.
(3) M. Heintz, "Die Berechnung der Absturzbauwerke," doctoral thesis submitted to the Technical University of Karlsruhe in Germany in 1940.

F	d_1	d_2	d_2-d_1	L	$L/(d_2-d_1)$
8.9	2.5'	30'	27.5'	183'	6.65
4.76	3.8'	24'	20.2'	144'	7.13
2.40	6.0'	17'	11.0'	83'	7.55

This is why the % difference of L/h in Table 1 of the discussers is increasing with decreasing Froude number, and not decreasing, as could be expected on the basis of increasing frictional resistance with higher model Froude numbers, and as shown in Fig. 1 of the discussers. The disagreement between Table 1 and Fig. 1 could not be explained on the basis of scale effect alone.

The differences in L/d_2 values of different investigators, as given in Fig. 1 of the discussers, may be the result of scale effect. However, if the results of Moore were plotted in Fig. 1, they would generally agree with the results of Messrs. Peterka and Bradley for higher F values, even though the experiments were performed on very different models (the width of flume: Moore—11 in., Peterka and Bradley—to 4.9 ft.)

Computation of L/d_2 values on the basis of Moore data:

F	$L/(d_2-d_1)$	d_1/d_2	$L/d_2 = \frac{L}{d_2-d_1}(1-d_1/d_2)$
6.69	6.75	0.1117	6.0
4.95	7.60	0.153	6.44
4.24	6.90	0.181	5.65
4.06	4.06	0.190	4.70

The close agreement between $L/d_2 = 6.0$ at $F = 6.69$ of Moore and the curve of Messrs. Peterka and Bradley in Fig. 1 is remarkable. However, the depth d_1 in the case of Moore's experiment was only about 0.04 ft. that is of the same order as Bakhmeteff and Matzke's 0.032 ft. for $F = 8.9$, as referred by the discussers.

On the basis of these observations, it seems that the numerical computations of the discussers do not represent the scale effect too well. The available data on the length of hydraulic jump is probably affected by some other factors besides the scale effect. Also, Eq. 19 can not be used to determine the scale effect of the models. The experimental results of Messrs. Peterka and Bradley are valuable, and the plot in Fig. 2 could be used to determine the maximum visible length of the hydraulic jump.

No data was given by the discussers to estimate the scale effect on the other length terms at a straight drop spillway. It would be very desirable if Fig. 4 could be completed with data on the measurements on actual drop structures or on large models. Fortunately, some conclusions can be drawn as to the model effect on the values d_1/h and d_2/h. The ratio d_1/h may be somewhat smaller for actual drop structures than given in Fig. 4. However, it can not approach d_{01}/h too closely, and due to the fact that there is no flow along the bottom of the flume upstream of the location of d_1, and that the smooth glass sidewalls do not affect the nappe too much, the prototype values

of d_1/h should be relatively close to the model values.

The depth d_2 and d_2/h may be affected of the excessive friction on the bottom and along the sides of the model flume. However, the d_2 values, computed from the d_1 values by Eq. 8 correspond practically to the measured d_2 values, and d_2/h can not approach d_{02}/h too closely. Probably due to the fact that the drop length l_d is not excessively long as compared to other length terms, and because of the absence of extensive friction areas along the bottom, the data of different investigators, gathered on different test installations, could be as close as that given in Fig. 4.

Before concluding this discussion, the writer wishes to correct the typographical errors in the Proceedings Paper No. 791.

As printed:	Should be:
page 791-1, line 4 from below: "Die Sturtzbett ausbildung. . .	"Die Sturtzbettausbildung. . .
page 791-2, line 17 from above: . . . supercritical flow on the apron at the distance. . .	. . . supercritical flow on the apron. The point at which the tangent to the upper nappe will become parallel to the apron, at the distance. . .
page 791-4, line 12 from below: the distance I_j	the distance l_j
page 791-7, last column of numerical values, the last figure: 2.11	3.11
page 791-8, line 9 from above: For D 0.001 the difference. . .	For D < 0.001 the difference. . .
page 791-9, line 7 from below: . . . and permitted me to conduct. . .	. . . and permitted him to conduct. . .

Discussion of "LUNAR-CYCLE MEASUREMENT OF ESTUARINE FLOWS"

by Irvin M. Ingerson
(Proc. Paper 836)

JOHN A. ROBERSON,[1] A.M. ASCE.—As described by the author, the method of flow measurement is novel and the technique for computation is ingenious. It is the writer's opinion that one limitation of the flow measurement method may be present for certain conditions. The author states that the "moving boat method" of flow measurement "is recommended for any continuously flowing stream or channel where velocities of less than one-half foot per second are to be measured anywhere in the section." Errors of the same order of magnitude as the actual stream velocities may occur if one does not consider the velocity field of the measuring boat itself. The following is an explanation of possible sources of error.

As a solid, such as a boat, is propelled through the water, a velocity field is created about the body and this field travels with the body. One may visualize the steady state condition by referencing the coordinate system to the boat, then a streamline pattern may be drawn where the flow is indicated with respect to the boat. A streamline sketch of the flow past a two dimensional ship hull is shown in Figure I.

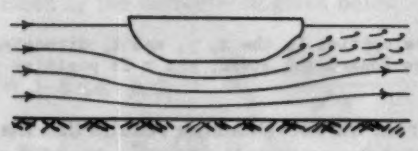

Fig. I. Steady State Flow Pattern Around a Two Dimensional Vessel.

It may be noted that deceleration of water occurs near the bow of the ship where the water is pushed ahead of the ship while a higher velocity occurs beneath the ship where the flow is induced toward the rear of the ship. The phenomena has been measured many times for fleet and merchant vessels.

A three dimensional quantitative estimate of the same phenomena may also be evaluated by means of hydrodynamic methods. A ship's hull is approximated by potential theory where the ship's hull is replaced by a one-half volume of a Rankine solid, which is the combination of a source and equal sink with a uniform stream, and the boundary conditions such as river bottom and water surface are satisfied by the method of images.[2] To

(1) Hydr. Engr., U.S. Dept. of the Navy, Mine Defense Lab., Panama City, Fla.
(2) A detailed theoretical treatment of this subject is given in Milne-Thomson "Theoretical Hydrodynamics," Second Edition, The MacMillan Company, New York, N.Y.

determine the velocity at a desired point in the water, the velocity components of the sources and sinks are added algebraically to the undisturbed field velocity. It has been verified in laboratory and field tests that such an approximation for determination of induced velocities produces fairly reliable results for velocities at considerable distance from the boat and for speeds less than 0.4 critical speed ($V_c = \sqrt{gd}$ where d is depth).

To indicate the magnitudes of induced velocity that might be encountered for a measuring boat 40 ft. long, 12 ft. beam, 6 ft. draft, and traveling at a speed of 5 ft./second in still water, theoretical solutions for velocity were made considering measuring points at the bow and amidships, 6 ft. transverse distance from ship's ℄ , and at depths of 5 ft. and 20 ft. (0.2 and 0.8 d) in 25 ft. of water. The results are shown in Table I.

TABLE I.

VELOCITIES RELATING TO MEASUREMENTS FROM A HYPOTHETICAL BOAT.

Depth of Meter (ft)	Actual Vel. (ft/sec.)	Vel. That Should Be Indicated by meter (ft/sec)	Induced Velocities (ft/sec)*						Total Vel. Sensed by Meter (ft/sec)		Apparent Vel. Indicated by Meter (ft/sec)	
			Bow			Amidship						
			u	v	w	u	v	w	Bow	Amidship	Bow	Amidship
5	0	5	-.206	.487	-.394	.260	0	0	4.835	5.260	-.165	.260
20	0	5	.019	.032	-.054	.122	0	0	5.020	5.122	.020	.122

* u, v, and w, are velocities in the x, y, and z, directions respectively, where x is positive toward the stern, and z is positive upward.

It may be noted from the above sample results that the induced velocities are significant and that the magnitude and sign change depending upon the location of measurements with respect to the ship. The possible discrepancies presented herein could be minimized or eliminated by field and/or laboratory calibration. Undoubtedly this was done in the tests described by the author as he has stated that "Field tests were made in still water and in flowing streams, and these tests indicated that high accuracies are readily obtainable." It is the writer's opinion that the "moving boat method" be adopted only after the limitations of the system are understood and taken into consideration.

Discussion of
"INTEGRATING THE EQUATION OF GRADUALLY VARIED FLOW"

by Ven-Te Chow
(Proc. Paper 838)

R. SILVESTER,[1] —As the author has stated "the preference of a method depends more or less upon the individual taste." This probably refers to preference between one direct integration method and another, but it is pertinent to question the preference of such methods over the step method.

Although the former may provide a unique answer to the problem this does not make it any more accurate than the step method which appears to have the added advantages of

a) providing depth information along the entire length of the backwater curve

b) being much easier to learn and apply

c) being self checking by indicating the shape of the curve as computations progress

d) being applicable, for first approximations, to non-prismatic channels, i.e., channels varying slowly in bottom width.

For the sake of completeness the solution to the given example by the step method with aids introduced by the writer[1] is given below. The graphs of

$$K' = 1.486\, AR^{2/3} = \frac{1.486\, A^{5/3}}{P^{2/3}}$$

$$\text{and } Z = \sqrt{\frac{A^3}{T}}$$

for the trapezoidal channel of side slopes 1:2 are included in Fig. 1. Similar graphs for the parabolic channel are shown in Fig. 2. The nomograph (Fig. 3) is suitable for the solution of parts of the equation

$$\frac{dy}{dx} = \frac{S_o - \left(\frac{Qn}{K'}\right)^2}{1 - \frac{Q^2}{gZ^2}} = \frac{S_o - S_f}{1 - S_r}$$

Solution

(i) $Q = \frac{K'}{n}\sqrt{S_o}$ by substitution or nomograph (by putting $S_f = S_o$)

$K' = 250$ hence from Figure 1 $y_n = 3.4$ ft.

(1) Senior Lecturer in Civ. Eng., Univ. of Western Australia, Crawley, Western Australia.

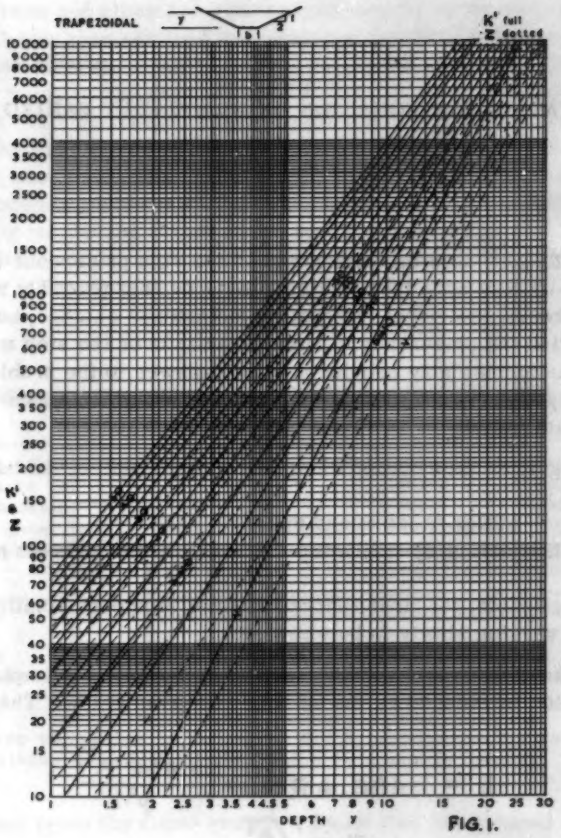

FIG. 1.

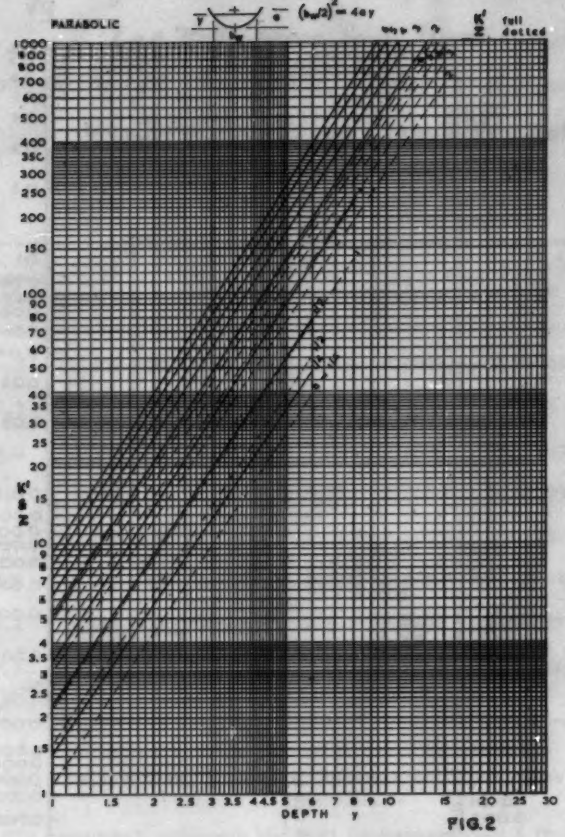
PARABOLIC
$\frac{T}{e} = \frac{(h_w/2)^2}{4ay}$
K' full
$\frac{K'}{Z}$ dotted
1000
900
800
700
600
500
400
350
300
250
200
150
100
90
80
70
60
50
40
35
30
25
20
15
10
9
8
7
6
5
4
3.5
3
2.5
2
1.5
1
$\frac{K'}{Z}$
1 1.5 2 2.5 3 3.5 4 4.5 5 6 7 8 9 10 15 20 25 30
DEPTH y

FIG. 2

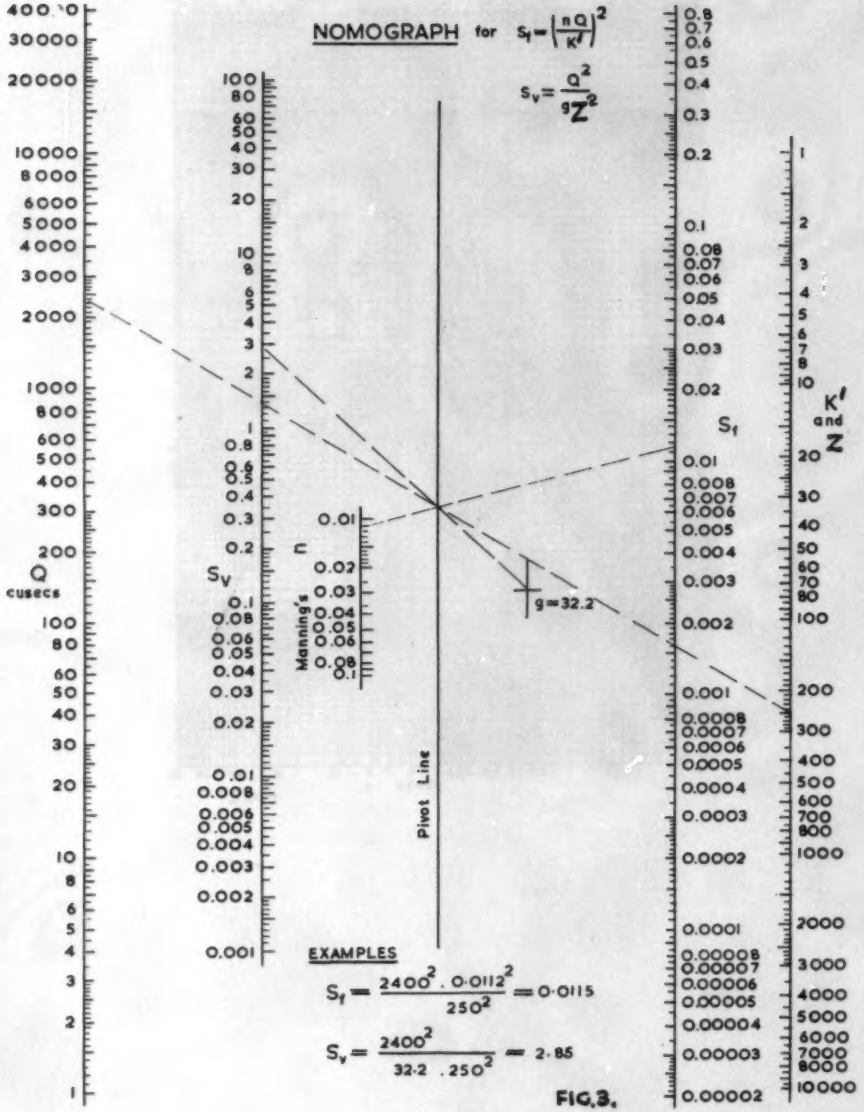
NOMOGRAPH for $S_f = \left(\frac{nQ}{K'}\right)^2$
$S_v = \frac{Q^2}{gZ^2}$
Q cusecs
S_v
n
Manning's
S_f
K' and Z
g=32.2
Pivot Line
EXAMPLES
$S_f = \frac{2400^2 \cdot 0.0112^2}{250^2} = 0.0115$
$S_v = \frac{2400^2}{32.2 \cdot 250^2} = 2.85$

FIG.3.

(2) $Z_c = \frac{Q}{\sqrt{g}}$ by substitution or nomograph (by putting $S_v = 1$)
$Z_c = 70.5$ hence from Figure 1 $y_c = 2.16$ ft.

(3) Commencing at the 5.0 ft. depth and working upstream we have results as tabulated below.

TABLE I

Depth y in ft.	Increment dy in ft.	K'	Z	S_f	S_v	$S_o - S_f$	dy/dx (a)	Increment d_x in ft.
5.0	0.3	505	305	0.00039	0.056	0.00121	0.00128	234
4.7	0.3	455	265	0.00049	0.076	0.00111	0.0012	250
4.4	0.2	395	235	0.00065	0.10	0.00095	0.001055	190
4.2	0.2	365	215	0.00078	0.12	0.00082	0.000932	214
4.0	0.2	337	198	0.00086	0.145	0.00074	0.000865	231
3.8	0.2	307	182	0.00106	0.165	0.00054	0.000646	310
3.6	0.1	276	166	0.0013	0.2	0.0003	0.000375	267
3.5	0.1	258	156	0.0015	0.22	0.0001	0.000128	780

(a) dy/dx is positive, therefore increase in depth downstream. 2476

It is readily seen that, although the last increment of 0.1 ft. is only 6% of the surface drop, the backwater curve for this drop constitutes over 30% of the total length.

This raises the question "For what is a backwater curve required?" Generally it is required to assess depths so that side wall levels can be determined. A certain amount of freeboard above the calculated water level is fixed at say 0.75 ft. to cope with wave formation, in which case $\pm$ 0.1 ft. is of little consequence, especially in view of the fact that the design quantity cannot be accurately predicted. Even where exact quantities for immediate use may be known there is always the unpredictable future load.

The most difficult type of problem in open channel varied flow is that in which the quantity is unknown. It would be interesting to see the author's solution to the cited example when end conditions of the profile are defined and it is required to compute the discharge. A similar problem was introduced by the writer in Reference 1 and subsequently a more expedient solution provided,(2) although still on a trial and error basis.

REFERENCES

1. "New Graphs Aid Open Channel Calculations," R. Silvester, Water Power, September 1954, p. 338.

2. Letter to the Editor, R. Silvester, Water Power, November 1954, p. 428.

ALFRED S. HARRISON,(1) J.M. ASCE.—The writer congratulates Professor Chow for his valuable solution to the problem of integrating the differential equation of gradually varied flow. His contribution is two-fold. First he has manipulated the differential equation into a form where the integral arising from the friction loss term and the integral arising from the velocity head term can both be evaluated using the well-known varied flow function of Bakhmeteff. Furthermore, he has prepared simple curves which make it convenient quickly to find values of the parameters M, N, Z and $AR^{2/3}$ for most of the cross sections commonly encountered. These simplifications may encourage engineers to take advantage of the time savings afforded in many cases by the analytical method of integration as compared with the more tedious step method which is now more generally in use.

In two special cases, when the channel bottom is either horizontal or has an adverse grade, the computation method presented by the author cannot be used. In these cases, the normal depth y_n is not definable because the value of K_n from Eq. 6 must be either infinite or imaginary. For beds with horizontal grades, Bakhmeteff[13] has developed one method of integration in which it is assumed that the gradient in the velocity head term is constant throughout a reach. The readers may be interested in the following method in which this assumption need not be made.

If we define S_c as the slope that will produce a discharge Q at a normal depth equal to critical depth y_c, Eq. 4 becomes

$$Q = K_c \sqrt{S_c} \qquad (A)$$

where K_c is the conveyance corresponding to y_c. Combining Eq. 4 and Eq. A,

$$S = \frac{K_c^2 S_c}{K^2} \qquad (B)$$

Substituting Eq. B and Eq. 13 into Eq. 3 and letting $S_c = 0$ for a horizontal bed,

$$\frac{dy}{dx} = \frac{-\frac{K_c^2}{K^2} S_c}{1 - \frac{Z_c^2}{Z^2}} \qquad (C)$$

(1) Head, Hydraulics and Sediment Sec., Omaha District, Corps of Engineers. Omaha, Nebr.

or,

$$\frac{dy}{dx} = \frac{-(y_c/y)^N S_c}{1 - (y_c/y)^M} \qquad (D)$$

Let $p = y/y_c$. Solving the dx and integrating,

$$x = \frac{y_c}{S_c}\left[\left(\frac{1}{N-M+1}\right)p^{N-M+1} - \left(\frac{1}{N+1}\right)p^{N+1}\right] \qquad (E)$$

The length of the water surface profile from section 1 (upstream) to section 2 (downstream) is

$$L = X_2 - X_1 = \frac{y_c}{S_c}\left[P_{(p_2,M,N)} - P_{(p_1,M,N)}\right] \qquad (F)$$

where $P_{(p,M,N)} = \left[\left(\frac{1}{N-M+1}\right)p^{N-M+1} - \left(\frac{1}{N+1}\right)p^{N+1}\right]$

Example. Assume a horizontal channel with the same cross section as the author's example. A vertical drop controls the water surface at critical depth at the downstream end of the channel. Determine how far upstream the depth will be 3.0 feet.

Solution.

1. From the author's example $y_c = 2.16$ ft., N = 3.65 and M = 3.43.

2. For $\frac{y_c}{b} = 0.108$, $\frac{(AR^{2/3})c}{b^{8/3}} = 0.025$ from Fig. 4 and $(AR^{2/3})c = 2950 \times 0.025 = 73.8$.

$$K_c = \frac{1.49}{0.025} \times 73.8 = 4396$$

3. $S_c = \left(\frac{400}{4396}\right)^2 = 0.00818$ from Eq. A.

4. The values of the function $P_{(p,M,N)}$ are evaluated in the following table:

Section	y	p	$\frac{1}{N-M+1}p^{N-M+1} =$ $0.820p^{1.22}$	$\frac{1}{N+1}p^{N+1} =$ $0.215p^{4.65}$	P
2 (downstream)	2.16	1.00	0.820	0.215	0.605
1 (upstream)	3.00	1.39	1.225	0.993	0.232
				$P_{(p_2)} - P_{(p_1)} =$	0.373

5. $L = \frac{2.16 \times 0.373}{0.00828} = 97$ Ft. from Eq. F.

For a wide rectangular channel in which the depth is always small compared with the width, M = 3.0 and N = 3.33 at all water depths. For this section,

$$P_{(p)} = 0.750p^{1.33} + 0.231p^{4.33} \qquad (G)$$

The function $P_{(p)}$ for wide rectangular channels is plotted in Fig. (A). By use of Fig. (A) one can compute the length for a given change in depth as in the previous example. Furthermore, the change in depth for a given length can be computed directly by using Eq. F in the following form:

$$\frac{LS_c}{y_c} = P_{(p_2)} - P_{(p_1)} \qquad (H)$$

Example. Assume a wide rectangular channel with a horizontal bed grade and a sluice gate which occupies the width of the channel. Manning's n = 0.025. The discharge is 10 c.f.s. with the sluice gate raised one foot from the bed. What will be the water depth 15 feet downstream of the sluice?

Solution.

1. $y_c = \sqrt[3]{\frac{10^2}{32.2}} = 1.46$ Ft.

$K_c = \frac{1.49}{.025}(1.46)^{5/3} = 112$

$S_c = \frac{10^2}{112^2} = 0.00798$ from Eq. (A)

L = 15 Ft.

2. Computation of the downstream depth y_2 is illustrated in the following tabulation:

y_1	p_1	$P_{(p_1)}$ (Fig. A)	$\frac{LS_c}{y_c}$	$P_{(p_2)}$ (Fig. H)	p_2 (Fig. A)	y_2 (ft.)
1.00	0.685	0.400	0.082	0.482	0.860	1.26

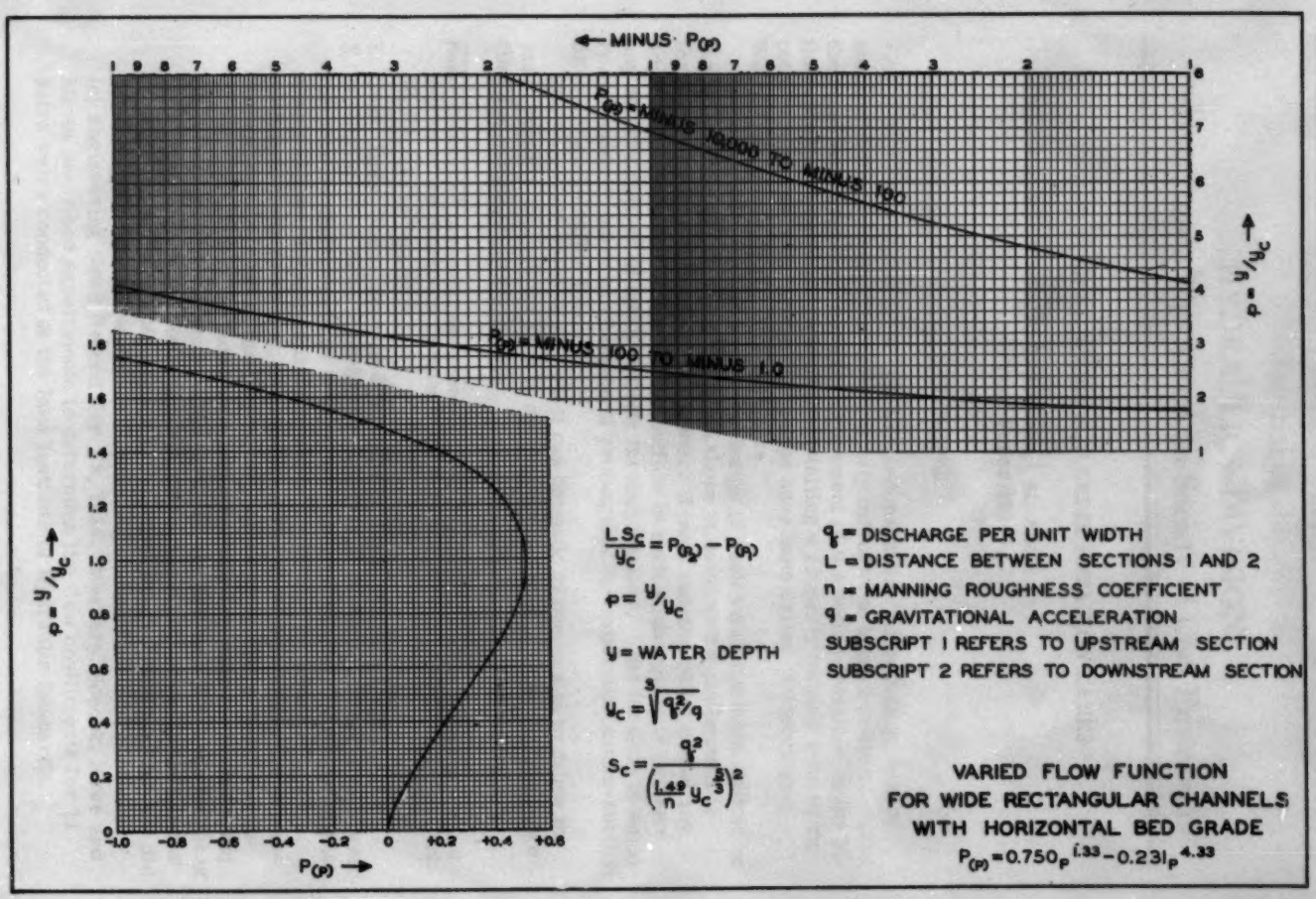

$$\frac{L S_c}{y_c} = P_{(2)} - P_{(1)}$$

$p = y/y_c$

y = WATER DEPTH

$$y_c = \sqrt[3]{q_s^2/g}$$

$$S_c = \frac{q_s^2}{\left(\frac{1.49}{n} y_c^{\frac{2}{3}}\right)^2}$$

q_s = DISCHARGE PER UNIT WIDTH
L = DISTANCE BETWEEN SECTIONS 1 AND 2
n = MANNING ROUGHNESS COEFFICIENT
g = GRAVITATIONAL ACCELERATION
SUBSCRIPT 1 REFERS TO UPSTREAM SECTION
SUBSCRIPT 2 REFERS TO DOWNSTREAM SECTION

VARIED FLOW FUNCTION FOR WIDE RECTANGULAR CHANNELS WITH HORIZONTAL BED GRADE

$$P_{(p)} = 0.750_p{}^{1.33} - 0.231_p{}^{4.33}$$

Paper 1015 HY 3

Journal of the
HYDRAULICS DIVISION
Proceedings of the American Society of Civil Engineers

PROPORTIONAL WEIRS FOR SEDIMENTATION TANKS

J. C. Stevens,[1] M. ASCE
(Proc. Paper 1015)

SYNOPSIS

For grit channels or other types of sedimentation tanks it is desirable automatically to control the mean velocity through the tank in order to obtain the most favorable conditions for settlement of the solids contained in the influent. This can readily be done by installing a properly formed weir in the outlet end of the tank. Weirs of the type have been called "Proportional Weirs," herein designated as "P-Weirs."

As far as the writer is aware the design of such weirs has been limited to those for rectangular tanks.[2] Herein there is developed a mathematical formula for the profile of a P-weir which if built into the outlet end of any sedimentation tank will control the outflow in such a manner as to produce any desired pattern of mean velocity through the tank. This formula is equally applicable to tanks or channels of rectangular or trapezoidal cross-section or to any combination thereof.

One important velocity pattern it can be made to produce is to cause the mean velocity through the tank to decrease with depth in order to give more time for the solids to settle out.

Note: Discussion open until November 1, 1956. Paper 1015 is part of the copyrighted Journal of the Hydraulics Division of the American Society of Civil Engineers, Vol. 82, No. HY 3, June, 1956.

1. Cons. Hydr. Engr., Stevens & Thompson, Cons. Engrs., Portland, Ore.

2. (a) Engineering News June 25, 1914. Prof. E. W. Rettgar described a weir the head on which would be directly proportional to flow. The base of such a weir is theoretically of infinite width.
(b) Engineering News Aug. 27, 1914, p. 463. E. W. Pratt gave the mathematical development of the Sutro weir, named after Henry Sutro who invented it in 1908. The Sutro weir had a rectangular weir for its base and the proportionality of head to flow obtained above a datum 1/3 the height of the rectangular weir above its crest. By this "trick" however the base of the proportional weir coincided with the top of the rectangular weir and did not become of infinite width.
(c) Engineering News Record Nov. 12, 1936. Messers. Soucek, Howe and Mavis described experiments to determine the flow coefficients for 11 Sutro weirs conducted at the Iowa Institute of Hydraulic Research.

For weirs of this type free flow conditions can not always be assured. The effect of submergence on them is presented with a nomagram for the solution of the Villemonte(8) submerged weir formula.

Proportional Weirs of the Portland Sewage Treatment Plant

The problem of outlet P-weirs arose with the design of the grit channels for the Treatment Plant of the Portland (Oregon) Sewerage Project.[3] There are four of these channels each built to the shape shown in Fig. 1. This problem was assigned to the writer. The first design of the channel shape differed from that shown in Fig. 1 and the weirs were designed to fit the earlier design. They were not symmetrical but the right boundary was curved, the left was straight. Each had an adjustable plate at the back by which the width of the weir and the inclination of the left edge could be altered. Because of this adjustable feature the weirs, models of which had been previously tested, were installed in the channels as finally built. Referring to Fig. 1, the weirs were designed and tested for channels having numerical values of B = 4.0; d = 0.5, s = 1.0, a = 1.0, e = 1.5 a trapezoid above a depth of 1.5 to the top; but the channels were finally built to make d = 1.17 ft. and b adjustable from 2.0 to 3.0 ft.

NOTATION

The dimensional notation will be found in Fig. 1. In addition the following are used

Q , total flow through the sedimentation tank, cfs.

Q_1, total flow through the surcharged rectangular weir which forms the base of the P-weir

Q_2, total flow through the P-weir exclusive of Q_1

Q_t, calculated theoretical flow

F , flow through the trapezoidal section of the channel where $h < k$, cfs

F_1, flow through the surcharged base weir where $h < k$

F_2, flow through P-weir for $h < k$ exclusive of F_1

A , cross-sectional area of the channel sq. ft.

A_1, area of the trapezoidal portion of the channel

A_2, area of the upper rectangular portion of the channel

A_o, area at $h = k$

V , mean velocity in the grit channel = Q/A, fps.

V_o, = mean velocity in grit-channel due to flow through the base rectangular weir only ie for $h = O$

3. The design and advisory supervision of construction of this project was done jointly by Stevens & Koon (predecessors to Stevens & Thompson) and J. W. Cunningham and Associates. A. W. Rawn Mem. ASCE was Consulting Engineer.

V_1, mean velocity in grit channel through area below h = k

V_2, mean velocity in the rectangular section of the grit channel where h > k

c , the coefficient of discharge ie Q/Q_t

m , constant in the equation for mean velocity; also an exponent, also a subscript signifying "model."

α , a + k

θ^n, $= \alpha^n - j^n$

s_λ, slope of sides of trapezoidal cross-section ie s horizontal to 1 vertical inclination of the left edge of the P-weirs

p and q, constants in the equation for areas

p is also a subscript signifying "Prototype"

H_a, head on upstream side of weir crest for submerged flow, feet

H_b, head on downstream side of weir crest

Q_a, flow corresponding to H_a

Q_b, flow corresponding to H_b

The cross-section area of the tank may readily be expressed in terms of h, the head on the top of the base weir, see equation (19) and (20).

$$A_1 = p + qh + sh^2 \qquad \text{for } h < k \tag{1}$$

$$A_2 = wj \qquad \text{for } h > k \tag{2}$$

If we decide to provide velocities varying inversely as the depth the mean velocity in the channel below any value of h

$$V = V_0 - mh \tag{3}$$

In the trapezoidal section where h < k

$$F = A_1 V = (V_0 - mh)(p + qh + sh^2) \tag{4}$$

and in the rectangular section where h > k

$$F_1 = A_2 V_2 = (V_1 - mj)(wj) \tag{5}$$

The flow through the surcharged rectangular weir depends solely on the depth of water on its crest and is found thus, (refer to the notation in Fig. 1)

$$Q_1 = bc\sqrt{2g}\int_h^{a+h} \sqrt{y}\, dy = bc\sqrt{2g}\,\tfrac{2}{3} y^{\frac{3}{2}}\Big]_h^{a+h} = \tfrac{2}{3} bc\sqrt{2g}\left[(a+h)^{3/2} - h^{3/2}\right] \tag{6}$$

This is the flow through the base weir as surcharged by the depth of water

above it and considered apart from the flow through the P-weir. This condition may be likened to a flume with an orifice in the bottom. The flow down stream of the orifice could be measured in the flume with a current meter, and the flow through the orifice must be added to obtain the total flow in the flume.

When h = O the base weir is no longer surcharged and (6) reduces to

$$Q_1 = \tfrac{2}{3} bc\sqrt{2g}\ a^{3/2}$$

in which the effect of the end contractions is neglected as being an unnecessary refinement.

In a similar manner the flow through the P-weir is given by

$$Q_2 = c\sqrt{2g}\int_0^h (h-y)^{1/2} x\, dy \qquad (7)$$

Where x = f(y) which is to be determined

Coefficient of Discharge

We have used a coefficient of c = 0.60 herein. In justification the following may be cited.

1) Foot note (2c) refers to experiments on models of Sutro Weirs made at the Iowa Institute of Hydraulic Research. For these experiments the coefficients of flow for 11 experiments averaged .615 with a range between .619 and .605.

2) The average of 3 models, to 1/4 scale first considered for the P-weirs was tested in a hydraulic laboratory with the following results. (Dimensions below are for prototypes see Fig. 1 for dimensional notation).

2.1) Weir 2A, width b = 2.5 with an unsymmetrical profile similar to that in Fig. 1 and designed for an all trapezoidal channel with dimensions B = 4.0 d = 1.0, s = 1 on 1 and e = 0. Max. c = .62, min. 52. average .57

2.2) Weir 3C similar to 2A except base adjusted to b = 3.16 ft. and d = 0.5. Max. c = .77, min .61, average .68 bottom contractions were incomplete.

2.3) Weir 4A a rectangular notch with b = 2.0, d = 0.5 Max. c = .63, Min .52 average .59

The average from tests of the above 3 weirs = 61%

An average value of 60% was therefore adopted for this paper.

Flow Through the Trapezoidal Section

The total flow through the outlet weir including the base weir for h < k is given by

$$F = F_1 + F_2 = \tfrac{2}{3} bc\sqrt{2g}\left[(a+h)^{3/2} - h^{3/2}\right] + c\sqrt{2g}\int_0^h (h-y)^{1/2} x\, dy$$
$$= (V_0 - mh)(p + qh + sh^2) \qquad (8)$$

From which

$$c\sqrt{2g}\int_0^h (h-y)^{1/2} x\,dy = (V_0 - mh)(p+qh+sh^2) - \tfrac{2}{5}bc\sqrt{2g}\left[(a+h)^{3/2} - h^{3/2}\right] \quad (9)$$

In order to evaluate the left hand member of (9) we must find an expression for x in terms of y. To do this we first expand $(h - y)^{1/2}$ into a series and integrate

$$\int_0^h (h-y)^{1/2} y^n dy = \int_0^h y^n \left(h^{1/2} - \tfrac{1}{2}h^{-1/2}y - \tfrac{1}{8}h^{-3/2}y^2 - \tfrac{1}{16}h^{-5/2}y^3 - \cdots\right) dy \quad (9.1)$$

$$= \frac{h^{1/2}y^{n+1}}{n+1} - \frac{h^{-1/2}y^{n+2}}{2(n+2)} - \frac{h^{-3/2}y^{n+3}}{8(n+3)} - \frac{h^{-5/2}y^{n+4}}{16(n+4)} - \cdots \Bigg]_0^h$$

$$= h^{n+3/2}\left(\frac{1}{n+1} - \frac{1}{2(n+2)} - \frac{1}{8(n+3)} - \frac{1}{16(n+4)} - \frac{5}{128(n+5)} - \frac{7}{256(n+6)} - \frac{21}{1024(n+7)} - \cdots\right)$$

that is

$$\int_0^h (h-y)^{1/2} y^n dy = N h^{n+3/2} \quad (10)$$

Where N is the sum the coefficients in the series. It becomes infinite for n = -1, -2, etc but has finite values for fractional also positive integral values of n. The principal use made of equation (10), as will be seen later, is to determine the relation between the exponents of h in (9) and those of y in (9.1) in evaluating x, thus:

for

$n =$	$-7/2$	$-5/2$	$-3/2$	$-1/2$	$1/2$	1	$3/2$	$5/2$
$n+3/2 =$	-2	-1	0	1	2	$5/2$	3	4

Before proceeding farther it will be well to present Table 1, which gives the complete integrals of the left member of (10) those may be verified from "A Short Table of Integrals" by B. O. Pierce (Ginn & Co.)

The term $(a+h)^{3/2}$ in (9) may be expanded into the series

$$(a+h)^{3/2} = a^{3/2} + \tfrac{3}{2}a^{1/2}h + \tfrac{3}{8}a^{-1/2}h^2 - \tfrac{1}{16}a^{-3/2}h^3 + \tfrac{3}{128}a^{-5/2}h^4 - \tfrac{3}{256}a^{-7/2}h^5 + \cdots \quad (11)$$

Evaluating (9) and collecting coefficients of like powers of h we have

Table 1 Integrals

n	$\int_0^h (h-y)^{1/2} y^n dy$ (4)	Reference (4)
-3/2	$-\pi$	Pierce 219 and 214
-1/2	$\frac{\pi}{2}h$	do
0	$\frac{2}{3}h^{3/2}$	—
1/2	$\frac{\pi}{8}h^2$	Pierce 218 and 214
3/2	$\frac{\pi}{16}h^3$	do
5/2	$\frac{5\pi}{128}h^4$	do
7/2	$\frac{7\pi}{256}h^5$	do
1	$.275h^{5/2}$ (4.1)	Pierce (4.1) 749

(4) The integral $\int_0^h (h-y)^{1/2} y^n dy = \int_0^h (hy-y^2)^{1/2} y^{n-1/2} dy$ It will be noted that $(hy-y^2)=0$ for $y=0$ and $y=h$

(4.1) from (10) in which N for 7 terms = .277; but estimated at .275 for an infinite number of terms

$$c\sqrt{2g}\int_0^h (h-y)^{1/2} x\, dy$$
$$= (\tfrac{1}{6}p - \tfrac{2}{5}bc\sqrt{2g}\,a^{3/2}) + (\tfrac{1}{6}q - mp - bc\sqrt{2g}\,a^{1/2})h +$$
$$+ \tfrac{2}{3}bc\sqrt{2g}\,h^{3/2} + (\tfrac{1}{6}s - mq - \tfrac{1}{4}bc\sqrt{2g}\,a^{-1/2})h^2 -$$
$$- (ms - \tfrac{1}{24}bc\sqrt{2g}\,a^{-3/2})h^3 - \tfrac{1}{24}bc\sqrt{2g}\,a^{-5/2}h^4 +$$
$$+ \tfrac{1}{128}bc\sqrt{2g}\,a^{-7/2}h^5 - \cdots\cdots \quad (12)$$

This is a general expression for flow through the P-weir exclusive of that through the base weir. However we can not find the profile of the weir until we obtain an expression for x in terms of y. Referring to the above listed values of the exponents of y and h following equation (10) we may assume x to be a series of the form

$$x = A_1 y^{-3/2} + A_2 y^{-1/2} + A_3 y^0 + A_4 y^{1/2} + A_5 y^{3/2} + A_6 y^{5/2} + A_7 y^{7/2} + \cdots\cdots \quad (13)$$

Multiply each term of (13) by $\sqrt{h-y}$ and integrate between the limits o and h. Referring to Table 1 we find

$$c\sqrt{2g}\int_0^h (h-y)^{1/2}\,x\,dy = A_1(-\pi) + A_2\frac{\pi}{2}h + \frac{2}{3}A_3h^{3/2} + A_4\frac{\pi}{8}h^2 + A_5\frac{\pi}{16}h^3 + A_6\frac{5\pi}{128}h^4 + A_7\frac{7\pi}{256}h^5 + \cdots \quad (14)$$

Equating coefficients of like powers of h in (12) and (14) we obtain

$$x = -\frac{1}{\pi}\left(-V_0p + \frac{2}{3}bc\sqrt{2g}\,a^{3/2}\right)y^{-3/2} + \frac{2}{\pi}\left(V_0q - mp - bc\sqrt{2g}\,a^{1/2}\right)y^{-1/2} + bc\sqrt{2g} + \frac{8}{\pi}\left(V_0s - mq - \frac{1}{4}bc\sqrt{2g}\,a^{-1/2}\right)y^{1/2} + \frac{16}{\pi}\left(-ms + \frac{1}{24}bc\sqrt{2g}\,a^{-3/2}\right)y^{3/2} - \frac{2}{5\pi}bc\sqrt{2g}\,a^{-5/2}y^{5/2} + \frac{2}{7\pi}bc\sqrt{2g}\,a^{-7/2}y^{7/2} + \cdots \quad (15)$$

It will be observed that the first right hand member of (15) includes two terms that cancel each other. The negative term represents the flow through the channel for h = o and the positive term the flow through the base weir flowing full also for h = o under the head a, both representing the same quantity.

Considerable time was spent in an attempt to eliminate the $y^{-1/2}$ term also, by solving both the $y^{-3/2}$ and the $y^{-1/2}$ terms[5] simultaneously for a and b and by other expedients but the values obtained were impractical for use. The negative exponent of y renders the x-values of such terms infinite. However a bit of legitimate "fudging" of the weir profile at these critical points is justified as will be seen hereafter.

We may now rewrite (15) in the following form[6]

$$x = \frac{2}{\pi}\left(V_0q - mp - bc\sqrt{2g}\,a^{1/2}\right)y^{-1/2} + \frac{8}{\pi}\left(V_0s - mq\right)y^{1/2} - \frac{16}{\pi}msy^{3/2} + bc\sqrt{2g}\left[1 - \frac{2}{\pi}\tan^{-1}\left(\frac{y}{a}\right)^{1/2}\right] \quad (16)$$

which becomes the general expression for the profile of the P-weir for a trapezoidal tank or channel.

Two cross sections of the grit channels have been considered herein.

---

5. The $y^{-3/2}$ term is readily eliminated for a rectangular tank by imposing the condition that a constant mean velocity in the channel shall obtain from a datum $\frac{1}{3}a$ above the crest of the base weir. See reference (2) also see Advanced Mathematics for Engineers by Reddick and Miller p162 - John Wiley & Sons Inc. New York.
6. We extract the following from (15)

$$bc\sqrt{2g}\left(1 + \frac{8}{\pi}\frac{1}{4}a^{-1/2}y^{1/2} + \frac{16}{\pi}\frac{1}{24}a^{-3/2}y^{3/2} - \frac{2}{5\pi}a^{-5/2}y^{5/2} + \frac{2}{7\pi}a^{-7/2}y^{7/2} - \cdots\right)$$
$$= bc\sqrt{2g}\left[1 - \frac{2}{\pi}\left(a^{-\frac{1}{2}}y^{1/2} - \frac{1}{3}a^{-3/2}y^{3/2} + \frac{1}{5}a^{-5/2}y^{5/2} - \frac{1}{7}a^{-\frac{7}{2}}y^{7/2} + \cdots\right)\right]$$
$$= bc\sqrt{2g}\left[1 - \frac{2}{\pi}\tan^{-1}\left(\frac{y}{a}\right)^{1/2}\right] \qquad \text{Pierce 779}$$

Referring to Fig. 1.

I is a hypothetical cross-section in which B= 4.0'; d=.67'; w=14.0'; b=3.22'

$a = 1.0'$; $k = 4.17'$; $c = .84'$; $c\sqrt{2g} = 4.81$; $s = 1.0$; $V_0 = 1.40$

$m = .07$; $p = 7.37$ and $q = 5.66$

This section is used to illustrate the formulas developed herein.

II is the cross-section as built. The only changes in the above numerical values are $b = 2.14'$ and $d = 1.17'$ and since this raises the datum for h

$$k = 3.67'; \quad p = 10.45 \quad \text{and} \quad q = 6.66.$$

In analyzing the weirs as built the crest of the base rectangular weir will have variable lengths instead of $b = 2.14$ since the left edge is adjustable.

In I the value of a is merely a convenient choice. The value of b is then obtained from $\frac{2}{3} bc\sqrt{2g}\, a^{3/2}$ the flow through the base weir for h = o.

The P-Weir Profile

Substituting the above numerical values for cross-section I in (16) we obtain

$$x = -5.15 y^{-1/2} + 2.55 y^{1/2} - .357 y^{3/2} + 15.5 - 9.85 \tan^{-1}\sqrt{y} \qquad (17)$$

The profile of the P-Weir for the trapezoidal portion of the grit channel is shown in Fig. 2—Note the extent of "fudging" at the critical point where x becomes infinite at y = o (Shown dotted in Fig. 2). The tabulation of x is found in Table 4.

A check is readily obtained by substituting (17) in (8) using the series form for the $\tan^{-1}$ term—see footnote (5)

$$F_2 = c\sqrt{2g}\int_0^h (h-y)^{1/2}\, x\, dy = -5.15\frac{\pi}{2}h + 2.55\frac{\pi}{8}h^2 - .357\frac{\pi}{16}h^3$$
$$+ \frac{2}{3}15.5\, h^{3/2} - 9.85\left(\frac{\pi}{8}h^2 - \frac{\pi}{16}\frac{1}{3}h^3 + \frac{5\pi}{128}\frac{1}{5}h^4 - \frac{7\pi}{256}\frac{1}{7}h^5 + \cdots\right)$$
$$= -8.10h + 10.3h^{3/2} - 2.87h^2 + .57h^3 - .24h^4 + .12h^5 - \cdots \qquad (17.1)$$

Also we have

$$F_1 = \frac{2}{3} bc\sqrt{2g}\left[(a+h)^{3/2} - h^{3/2}\right]$$
$$= 10.3\left(1 + \frac{2}{3}h - h^{3/2} + \frac{3}{8}h^2 - \frac{1}{16}h^3 + \frac{3}{128}h^4 - \frac{3}{256}h^5 + \cdots\right)$$

adding F_1 and F_2 to obtain

$$F = 10.3 + 7.40h + h^2 = .07h^3 \qquad (17.2)$$

By substituting the numerical values for I in (8) we find

$F = (V_o - mh)(p+qh+sh^2) = 10.3+7.40h+h^2 - .07h^3$

which checks with (17.2). This method of checking the results avoids computing the terms of the two series to laborious limits.

If other numerical values are used, especially if a is changed, it will change the datum for h and y and consequently the values of other quantities.

Cross-Sectional Areas

It is obvious from Fig. 1 that

$$A_1 = B(d+a+h) + s(d+a-e+h)^2 \qquad (18)$$

from which we may obtain values of

$$p = Bd + s(d-e)^2 + [B+2s(d-e)]a + sa^2 \qquad (19)$$

$$q = B+2s(d-e)+2sa \qquad (20)$$

The value of q in (20) is the first derivative of (19)
Substituting the numerical values of I in (19) we have for I

$$p = 2.71 + 3.66a + a^2 \quad \text{and} \quad q = 3.66 + 2a \qquad (21)$$

and for II

$$p = 4.79 + 4.66a + a^2 \quad \text{and} \quad q = 4.66 + 2a \qquad (22)$$

The areas with which we are most concerned in this paper are given in Table 2 on the following page. The area curves are given in Fig. 3.

Flow Through the Rectangular Section

At first thought it would seem that the simplest expression for the flow through the upper rectangular section would be found by solving

$$c\sqrt{2g}\int_k^h (h-y)^{1/2} \times dy$$

but a trial will show that it will be impracticable to isolate the several powers of h in order to evaluate x. We therefore adopt the expedient of changing the notation for this portion of the channel.

The total area for the channel is

$$A = A_o + wj \qquad (23)$$

and the total flow in the channel is

$$Q = AV = (A_o + wj)[V_2 - m(k+j)] = (A_o + wj)(V_1 - mj) \qquad (24)$$

Table 2 Areas of Grit Channels

Cross-Section II $A_1 = 10.45 + 6.66h + h^2$			Cross Section I $A_1 = 7.37 + 5.66h + h^2$
H	h	A	A
0		4.79	2.71
1.0	0	10.5	7.37
2.0	1.0	18.1	14.0
3.0	2.0	27.8	22.7
4.0	3.0	39.5	33.3
4.67	3.67	48.4	46.0
$A_2 = 48.4 + 14.0j$			48.4
5.0	4.0	53.0	$A_2 = 48.4 + 14.0j$
6.0	5.0	67.0	60.0
7.0	6.0	81.0	74.0
8.0	7.0	95.0	88.0
9.0	8.0	109	102

The total surcharged flow through the rectangular weir is

$$Q_1 = \frac{2}{3} bc\sqrt{2g}\left[(\alpha+j)^{3/2} - (k+j)^{3/2}\right] \qquad (25)$$

and the flow through the P-Weir exclusive of Q_1 is.

$$Q_2 = F_2 + c\sqrt{2g}\int_0^j (j-z)^{1/2} \times dz \qquad (26)$$

Expanding the two series' in (25) we have

$$(\alpha+j)^{3/2} = \alpha^{3/2} + \tfrac{3}{2}\alpha^{1/2}j + \tfrac{3}{8}\alpha^{-1/2}j^2 - \tfrac{1}{16}\alpha^{-3/2}j^3 + \tfrac{3}{128}\alpha^{-5/2}j^4 - \tfrac{3}{256}\alpha^{-7/2}j^5 + \cdots$$

$$-(k+j)^{3/2} = -k^{3/2} - \tfrac{3}{2}k^{1/2}j - \tfrac{3}{8}k^{-1/2}j^2 + \tfrac{1}{16}k^{-3/2}j^3 - \tfrac{3}{128}k^{-5/2}j^4 + \tfrac{3}{256}k^{-7/2}j^5 - \cdots$$

combining and writing θ^n for $\alpha^n - k^n$ we find

$$Q_1 = \frac{2}{3} bc\sqrt{2g}\left(\theta^{3/2} + \tfrac{3}{2}\theta^{1/2}j + \tfrac{3}{8}\theta^{-1/2}j^2 - \tfrac{1}{16}\theta^{-3/2}j^3 + \tfrac{3}{128}\theta^{-5/2}j^4 - \tfrac{3}{256}\theta^{-7/2}j^5 + \cdots\right) \qquad (27)$$

(26) then becomes

$$Q_2 = F_2 + c\sqrt{2g}\int_0^j (j-z)^{1/2} x\, dz = Q - Q_1 = F + (V_1 - mj)\, wj - Q_1$$

or

$$c\sqrt{2g}\int_0^j (j-z)^{1/2} x\, dz = \left[(F-F_2) - \tfrac{2}{3} bc\sqrt{2g}\,\theta^{3/2}\right] + (wV_1 - bc\sqrt{2g}\,\theta^{1/2})\, j - (wm + \tfrac{1}{4} bc\sqrt{2g}\,\theta^{-1/2})\, j^2 - bc\sqrt{2g}\left(-\tfrac{1}{24}\theta^{-3/2} j^3 + \tfrac{1}{64}\theta^{-5/2} j^4 - \tfrac{1}{128}\theta^{-7/2} j^5 + \cdots\right) \quad (28)$$

now

$$F - F_2 = F_1 = \tfrac{2}{3} bc\sqrt{2g}\,\theta^{3/2}$$

the surcharged flow through the rectangular base weir for j = o. Therefore the first right term of (28) equals zero and x may be written

$$x = A_1 z^{-1/2} + A_2 z^{1/2} + A_3 z^{3/2} + A_4 z^{5/2} + A_5 z^{7/2} + \cdots$$

Substituting in the left member of (28) and integrating between the limits o and j (see Table 1) we obtain

$$c\sqrt{2g}\left[\tfrac{\pi}{2} A_1 j + \tfrac{\pi}{8} A_2 j^2 + \tfrac{\pi}{16} A_3 j^3 + \tfrac{5\pi}{128} A_4 j^4 + \tfrac{7\pi}{256} A_5 j^5 + \cdots\right]$$

Equating coefficients of like powers of j we find

$$x = \tfrac{2}{\pi}\left(\frac{wV_1}{c\sqrt{2g}} - b\theta^{1/2}\right) z^{-1/2} - \tfrac{8}{\pi}\frac{wm}{c\sqrt{2g}} z^{1/2} - b\tfrac{2}{\pi}\left(\theta^{-1/2} z^{1/2} - \tfrac{1}{3}\theta^{-3/2} z^{3/2} + \tfrac{1}{5}\theta^{-5/2} z^{5/2} - \tfrac{1}{7}\theta^{-7/2} z^{7/2} + \cdots\right) \quad (29)$$

or otherwise

$$x = \tfrac{2}{\pi}\left(\frac{wV_1}{c\sqrt{2g}} - b\theta^{1/2}\right) z^{-1/2} - \tfrac{8}{\pi}\frac{wm}{c\sqrt{2g}} z^{1/2} - b\tfrac{2}{\pi}\tan^{-1}\left(\frac{z}{\theta}\right)^{1/2} \quad (30)$$

We can now assign the numerical values for I and in addition

$$\alpha = 5.17\ ;\quad k = 4.17\ ;\quad V_1 = 1.4 - .07(4.17) = 1.11\ ;$$

$$F = 53.6\ ;\quad F_1 = 33.6\ ;\quad F_2 = 20.0\ .$$ See Table 5

It will be convenient to have a table of values of $\theta^n = \alpha^n - k^n$ as follows:

Table 3 Values of θ^n

α^n		k^n		θ^n
$5.17^{3/2}$	11.755	$4.17^{3/2}$	8.515	3.240
$5.17^{1/2}$	2.274	$4.17^{1/2}$	2.042	.232
$5.17^{-1/2}$	.440	$4.17^{-1/2}$	.490	-.050
$5.17^{-3/2}$	.085	$4.17^{-3/2}$	.117	-.032
$5.17^{-5/2}$	.017	$4.17^{-5/2}$	.028	-.011
$5.17^{-7/2}$	.003	$4.17^{-7/2}$	.007	-.004

Substitute the foregoing numerical values for I in (28) omitting the first right term and find

$$c\sqrt{2g}\int_0^j (j-z)^{1/2} \times dz = 11.95j - .79j^2 - .021j^3 + .0027j^4 - .00048j^5 + \cdots \quad (31)$$

Also substitute the above numerical values in (29) and obtain

$$x = 1.58z^{-1/2} - .52z^{1/2} - b\frac{2}{\pi}\left[-.05z^{1/2} + \left(\tfrac{1}{3}\right)(.032z^{3/2}) - \left(\tfrac{1}{5}\right)(.011z^{5/2}) + \left(\tfrac{1}{7}\right)(.004z^{7/2} - \cdots)\right] \quad (32)$$

Substitute (32) in (26) and integrate obtaining

$$Q_2 = 20 + c\sqrt{2g}\int_0^j (j-z)^{1/2} \times dz$$

$$= 20 + 11.95j - .79j^2 - .021j^3 + .0027j^4 - .00048j^5 + \cdots$$

Also substitute the values of θ in Table 3 in (27) and find

$$Q_1 = \tfrac{2}{3}bc\sqrt{2g}\left[(\alpha + j)^{3/2} - (k - j)^{3/2}\right]$$

$$= 33.6 + 3.59j - .19j^2 + .021j^3 - .0027j^4 + .00048j^5 - \cdots$$

$$Q_2 + Q_1 = Q = 53.6 + 15.5j - .98j^2 \quad (32.1)$$

Which is also obtained by substituting the numerical values in (24)
In (32) we substitute for the series by writing

$$x = 1.58z^{-1/2} - .52z^{1/2} - 2.05 \tan^{-1}(-.05z^{1/2}) \quad (33)$$

Which is evaluated in Table 4. The profile for the complete P-weir is shown in Fig. 2.

Flow Through the Entire Channel

We may now combine and tabulate the data for the entire channel.

The values of x for both portions are tabulated in Table 4 from which Fig. 2 has been prepared. It shows the profiles of the P-weir for each section extending to infinity when h and j each equal zero. The extent of "fudging" shown dotted is seen to cover very minor portions of the profile. In spite of the mathematical discontinuity the profile of the weir obviously must be continuous, therefore this "fudging" is fully justified.

In Table 5 is tabulated the flows and mean velocities in both sections of the channel.

The areas and flows for the entire channel for both Cross-sections I and II are shown in Fig. 3.

Flow Through P-Weirs as Built in Channel II

It is of interest to know the flow characteristics of the P-Weirs and grit channels of the Portland plant as they were built. The cross-section and a profile of the bed of the channels are shown in Fig. 1. The numerical values differed from those heretofore given. The P-Weirs were designed and built to meet the following

$$B=4.0\ ;\ V=1.0\ ;\ a=1.0\ ;\ d=0.5\ ;\ b=2.5\ ;\ s=1.0$$

$$e=1.5\ ;\ c\sqrt{2g}=3.6\ ^{(7)}$$

As built however there is a rather sharp rise in the channel bed at the outlet end on which the weir plate rests (Fig. 1), in order to get the weir above the influence of the grit scrapers. The channel bed also has a slight downstream slope so the datum is the average elevation of the bed as shown in Fig. 1. Thus the dimension d is actually 1.17 ft. instead of 0.5. However the former value must be used since the weirs were designed for those dimensions.

As heretofore stated the weirs are not symetrical and the back plate is adjustable. The plate in each weir was adjusted to reduce b to 2.14 ft. shortly after the plant was put in operation in 1951.

The problem is to find the flow through the P-Weirs as installed and adjusted in the channels as built, and determine the velocities through them.

The weirs were built to a profile given by

$$x=-.36-.88y^{-1/2}+.71y^{1/2}+2.5\left(1-\frac{2}{\pi}\tan^{-1}\sqrt{y}\right) \quad (35)$$

in which the first right member is added to the original equation since each value of x in the original has been reduced by .36 ft.

7. This value was erroneously used to make the $y^{-3/2}$ term in x disappear—a long story but not germane to this paper.

Table 4

$$x = -5.15y^{-\frac{1}{2}} + 2.55y^{\frac{1}{2}} - .357y^{\frac{3}{2}} + 15.5 - 9.85 \tan^{-1}\sqrt{y} \qquad (17)$$

y (1)	$y^{\frac{1}{2}}$ (2)	$-5.15y^{-\frac{1}{2}}$ (3)	$2.55y^{\frac{1}{2}}$ (4)	$-.357y^{\frac{3}{2}}$ (5)	$\tan^{-1}y^{\frac{1}{2}}$ (6)	$-9.85(6)$ (7)	$\Sigma(3)(4)(5)(7) = x$
0	0	$-\infty$	0	0	0	0	$-\infty$
.1	.316	-16.3	.80	-.011	.305	-3.00	-3.01
.2	.447	-11.5	1.14	-.032	.421	-4.15	+ .96
.4	.632	- 8.14	1.61	-.090	.564	-5.56	3.32
.6	.775	- 6.65	1.98	-.166	.659	-6.49	4.17
.8	.894	- 5.76	2.28	-.255	.730	-7.19	4.58
1.0	1.000	- 5.15	2.55	-.357	.785	-7.74	4.80
2.0	1.414	- 3.64	3.60	-1.01	.955	-9.41	5.05
3.0	1.732	- 2.98	4.42	-1.85	1.047	-10.31	4.78
4.17	2.042	- 2.52	5.21	-3.04	1.115	-10.98	4.17

$$x = 1.58z^{-\frac{1}{2}} - .52z^{\frac{1}{2}} - 2.05 \tan^{-1}(-.05z^{\frac{1}{2}}) \qquad (33)$$

z (1)	$z+k$ (2)	$1.58z^{-\frac{1}{2}}$ (3)	$-.52z^{\frac{1}{2}}$ (4)	$-\tan^{-1}(.05z^{\frac{1}{2}})$ (5)	$-2.05(5)$ (6)	$\Sigma(3)(4)(6) = x$
0	4.17	∞	0	0	0	∞
.25	4.42	3.16	- .26	-.025	+.051	2.95
.50	4.67	2.23	- .37	-.035	.072	1.93
1.0	5.17	1.58	- .52	-.050	.103	1.16
1.5	5.67	1.29	- .64	-.061	.125	.77
2.0	6.17	1.12	- .74	-.070	.145	.52
3.0	7.17	.91	- .90	-.086	.177	.19
4.0	8.17	.79	-1.104	-1.000	.204	-.05

(Col.6) Pierce's Integrals contains an excellent table of trigometric functions in terms of both degrees and radius (p 146)

Table 5

$h<k$ $F=(1.40-.07h)(7.37+5.66h+h^2)$ (4) $Q_1=10.33\left[(1+h)^{3/2}-h^{3/2}\right]$ (6)

h (1)	5.66h (2)	h^2 (3)	A_1 (4)	-.07h (5)	V (6)	F (7)	$(1+h)^{3/2}$ (8)	$h^{3/2}$ (9)	(8)-(9) (10)	10.33(10) Q_1 (11)	(7)-(11) F_2 (12)
0	0	0	7.4	0	1.40	10.3	1.000	0	1.00	10.3	0
.5	2.83	.25	10.4	-.03	1.37	14.3	1.837	.354	1.48	15.3	-1.0
1.0	5.66	1.00	14.0	-.07	1.33	18.6	2.828	1.000	1.83	18.9	-.3
1.5	8.50	2.25	18.1	-.10	1.30	23.5	3.953	1.837	2.12	21.9	+1.6
2.0	11.3	4.00	22.7	-.14	1.26	28.6	5.196	2.828	2.37	24.5	4.1
3.0	17.0	9.00	33.4	-.21	1.19	39.8	8.000	5.196	2.80	29.0	10.8
4.0	22.6	16.0	46.0	-.28	1.12	51.5	11.18	8.000	3.18	32.8	18.7
4.17	23.6	17.4	48.4	-.29	1.11	53.6	11.76	8.515	3.25	33.6	20.0

$h>k$ $Q=AV=(48.4+14.0j)(1.11-.07j)$ (24) $Q_1=10.33\left[(1+h)^{3/2}-h^{3/2}\right]$ (6)

j (1)	h (2)	.07j (3)	V (4)	14.0j A_2 (5)	48.4+(5) A (6)	(4)+(6) Q (7)	$(1+h)^{3/2}$ (8)	$h^{3/2}$ (9)	(8)-(9) (10)	10.33(10) Q_1 (11)	(7)-(11) Q_2 (12)
0	4.17	0	1.11	0	48.4	53.6	11.76	8.51	3.25	33.6	20.0
.5	4.67	-.03	1.07	7.0	55.4	59.3	13.50	10.09	3.41	35.2	24.1
1.0	5.17	-.07	1.04	14.0	62.4	64.9	15.33	11.76	3.57	36.9	28.0
1.5	5.67	-.11	1.00	21.0	69.4	69.4	17.22	13.50	3.72	38.4	31.0
2.0	6.17	-.14	.97	28.0	76.4	74.1	19.20	15.33	3.87	40.0	34.0
3.0	7.17	-.21	.90	42.0	90.4	81.4	23.35	19.20	4.15	42.9	38.5
4.0	8.17	-.28	.83	56.0	104	86.4	27.77	23.35	4.42	45.6	40.8

(Col. 11) The surcharged flow through the rectangular weir depends solely on the head on the weir crest hence the formulas for both sections are alike.

Treating (35) in the same manner as (17) we find the flow through the P-weir in the existing channel to be

$$Q = 6.0 + 4.0h - .86h^{3/2} + h^2 \qquad (36)$$

In which the term $-.86h^{3/2}$ accounts for the reduction in the width of the base weir.

Flows from (36) are not tabulated but the mean velocities based on (36) are shown as curve (2) of Fig. 4. They are seen to increase with depth instead of being constant as planned obviously due to changes in the channels after they were fabricated.

Effect of Inclining the Back Plate

We can make the velocities practically constant or even to vary inversely with depth by making the proper adjustment in the width of the weir base and by inclining the left edge of the P-weir. If we move this plate out of its vertical position we introduce a new factor λ. For example, if we widen the base of the weir from its present value of b = 2.14 to b = 3.0 and incline the top to narrow the weir 2.5 ft. in 7.0 we have

$$\lambda = (3.0 - 0.5)/7 = .356 \qquad (37)$$

the inclination per foot of head.
The profile of the weir then becomes

$$x = .50 - .88y^{-1/2} + .71y^{1/2} - .356y + 2.50(1 - \tan^{-1}\sqrt{y}) \qquad (38)$$

Where the first right term accounts for the increase in the width of the base weir from 2.5 to 3.0 ft. and -.356 y accounts for the inclination of the left edge. Treating equation (38) as was done for (17) and (36) we obtain

$$Q = 6.0 + 4.0h + 1.30h^{3/2} + h^2 - .352h^{5/2} \qquad (39)$$

The mean velocities resulting from the tabulation of (39) are shown by curve (3) in Fig. 4.

In a similar manner if we leave the base weir at the original width of 2.5 ft. and incline the left edge the same amount so the width at the top becomes zero we obtain

$$x = -.88y^{-1/2} + .71y^{1/2} - .356y + 2.5\left(1 - \frac{2}{\pi}\tan^{-1}\sqrt{y}\right) \qquad (40)$$

and

$$Q = 6.0 + 4.0h + h^2 - .352h^{5/2} \qquad (41)$$

The mean velocities from (41) are shown in curve (4) of Fig. 4. They are seen to vary inversely with depth.

Submergence

The effect of submerging the crest of any sharp crested weir is best treated according to the method outlined by Dr. Villemonte[8] M. ASCE. His formula is

$$Q = Q_a \left(1 - \frac{Q_b}{Q_a}\right)^m \qquad (42)$$

In which

Q = the flow resulting from submerging the weir crest

Q_a = free flow for the upstream head on the weir crest, H_a

Q_b = free flow for the downstream head on the weir crest, H_b

The degree of submergence is given by

$$S = \frac{H_b}{H_a}$$

The free fully aerated flow curve or formula as in I or II Fig. 3 is used to obtain both Q_a and Q_b.

The formulas developed herein for the total flow through the P-weir are for free flow conditions. The effect of submerging the outlet weir is to diminish the flow and thus reduce the velocity through the tank or channel.

It is seen from Table 5 and curve (1) Fig. 4 that for the P-weir herein designed for the Channel I in Fig. 1 with B = 4.0, b = 3.22, d = .67 etc. the velocities diminish uniformly from v = 1.40 for h = 0 to .80 for h = 8.5. Submergence will decrease these velocities and the designer must take this factor into account.

In order to determine the effect of submergence a nomogram of Dr. Villemonte's formula (42) is given in Fig. 5 from which the flow for any degree of submergence is readily found.

It was constructed from the free flow curve for channel I of Fig. 3 and tabulated in Table 5.

Dr. Villemonte obtained a value of 0.385 for m in his formula based on his extensive laboratory experiments. The conditions for clearances in his experiments were ideal which are not found in the Portland plant. Because of this departure from the idea an exponent of m=2/5 has arbitrarily been used herein.

For any particular installation an approximate relationship between the upstream and downstream heads can be obtained by observations. The designer then can provide for this pattern of submergence and make the P-weirs so as to obtain the mean velocities desired.

For the Portland plant as built the observed relationship between upstream and downstream heads on the crest of the base weir 2.14 ft. wide are as follows:

---

8. Submerged-weir Discharge Studies—James R. Villemonte Engineering News—Record Dec. 25, 1947.

H_a	3.0	3.5	3.75	4.0	5.0	6.0
H_b	0	.08	.19	.28	.72	1.20

From the flow curve for channel I of Fig. 3 we find the free flow Q_a at a 7-foot head H_a on the crest to be 73 cfs and at 2.50 ft. head 23 cfs. The nomogram of Fig. 5 then shows the outflow becomes 63 cfs a reduction of 15% in the flow. This would reduce the velocity shown in curve (1) Fig. 4 from .97 to .85 feet per second. The 7-foot stage remaining the same.

CONCLUSION

It appears that the mean velocities in sedimentation tanks or channels are entirely under the control of the designer, without the use of mechanical devices to control the outflow. Moreover they may be modified at will by the adaption of a properly designed proportional weir at the outlet and of the tank. The P-weir may also be adjustable, if changing conditions are anticipated, and the effect of any adjustments determined in advance.

It is hoped that some one will be sufficiently interested in the theoretical formulas presented herein to determine the efficacy of a Proportional Wier by laboratory experiments to control the outflow from a channel composed of a combination of rectangles and trapezoids to produce some desirable pattern of mean Velocities in the channel.

The P-Weir does not have to be symmetrical as in Fig. 2 but may have one straight side. Messrs. Soucek, Howe and Mavis(2c) in their experiments with the Sutro Weir, found that the unsymmetrical weir has a discharge coefficient about 1% greater than the symmetrical type due doubtless the greater perimeter of the former.

The discharge coefficients obtained at the Portland plants, on the unsymmetrical P-Weirs there, offer partial confirmation at least of the validity of the formulas herein.

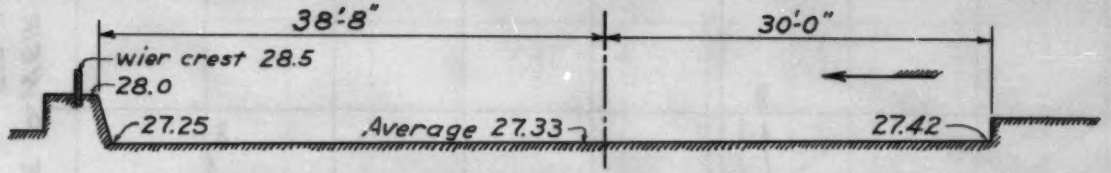

(a.) PROFILE OF BED OF GRIT CHANNELS (distorted)

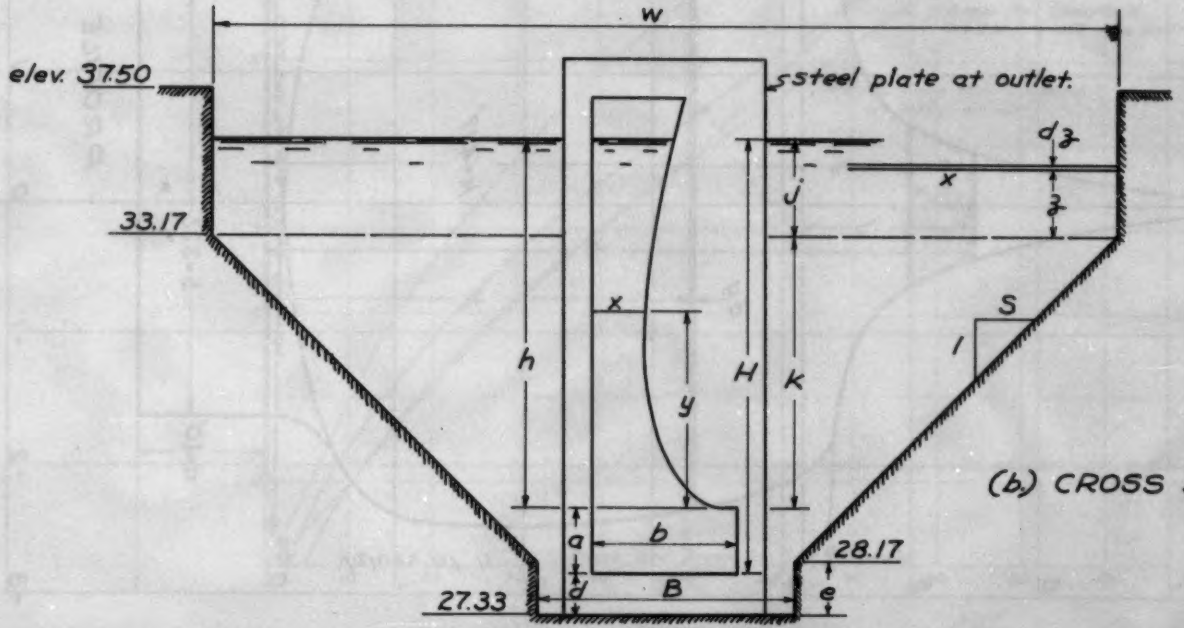

(b.) CROSS SECTION

FIG. 1

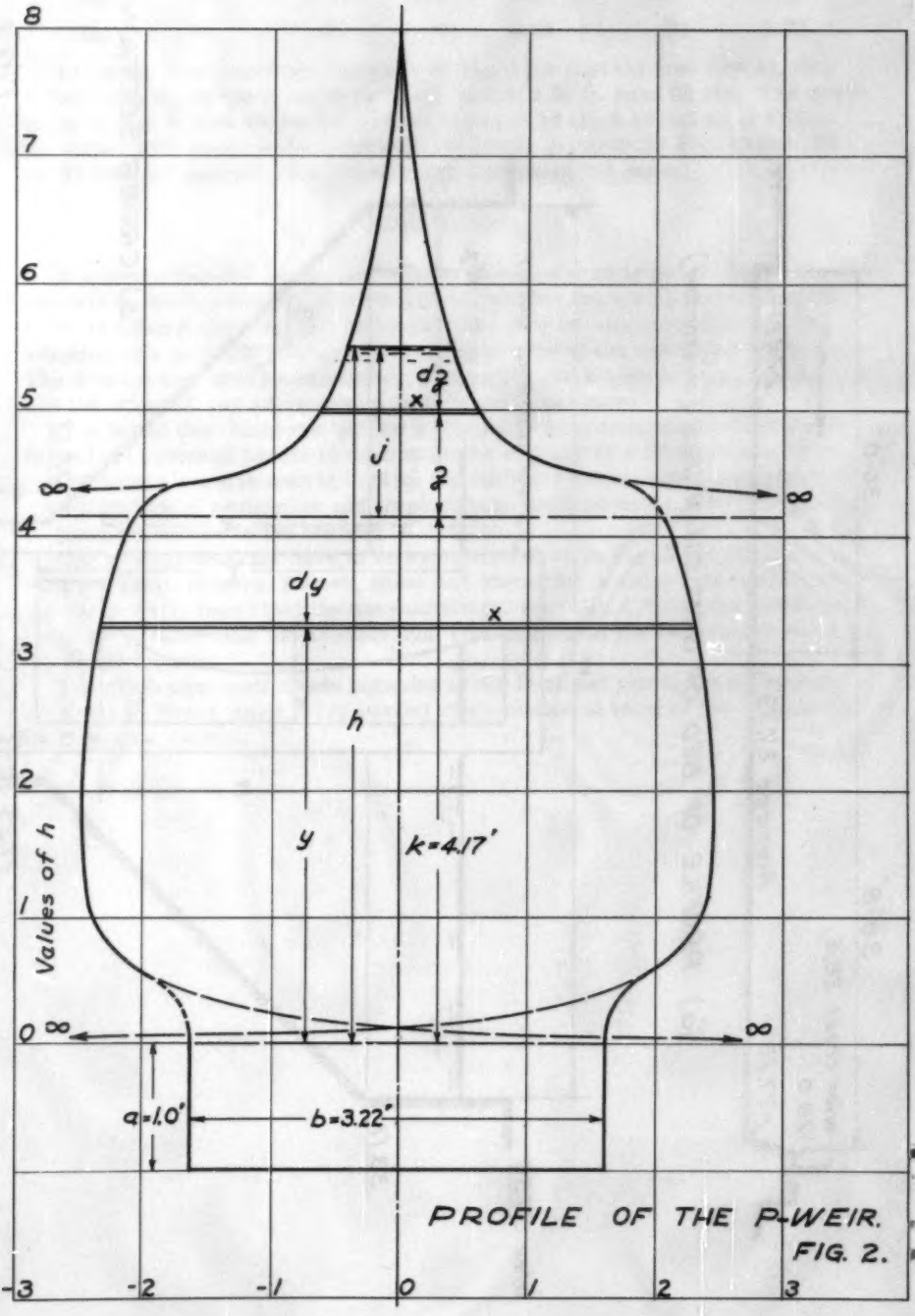

PROFILE OF THE P-WEIR.
FIG. 2.

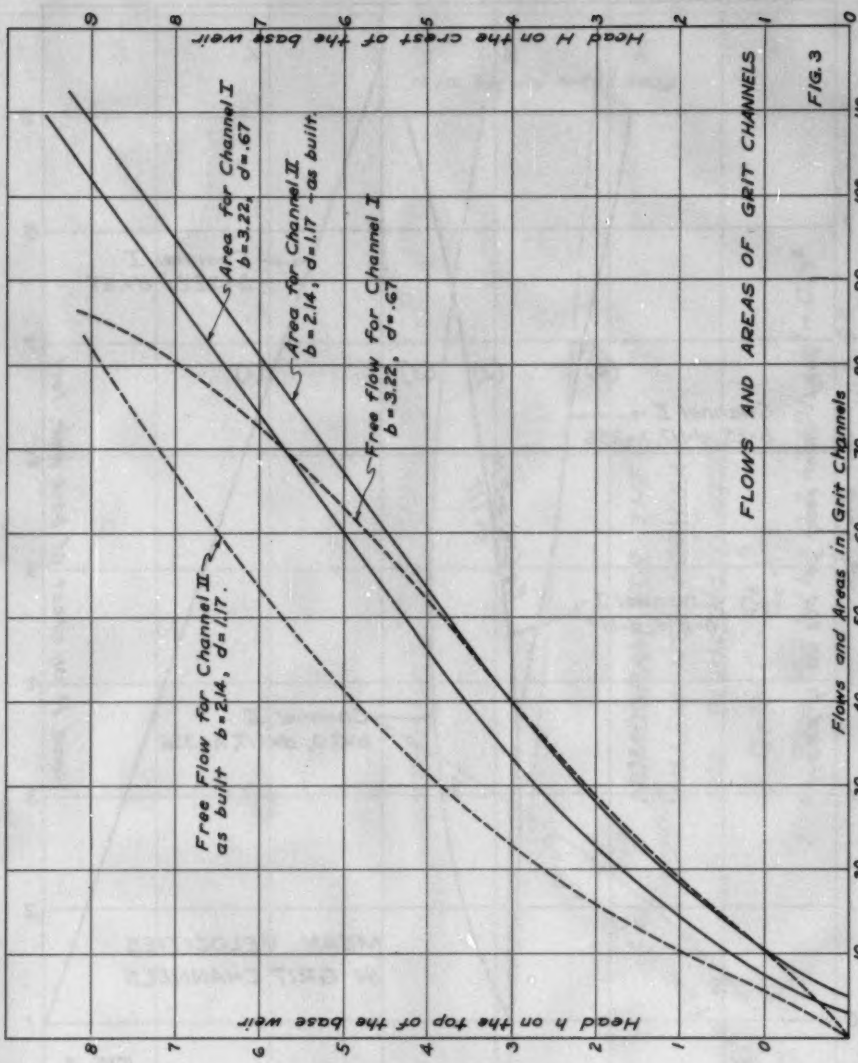
Head H on the crest of the base weir
Head h on the top of the base weir
Flows and Areas in Grit Channels
Area for Channel I b=3.22, d=.67
Area for Channel II b=2.14, d=1.17 -as built.
Free flow for Channel I b=3.22, d=.67
Free Flow for Channel II as built b=2.14, d=1.17.
FLOWS AND AREAS OF GRIT CHANNELS
FIG. 3

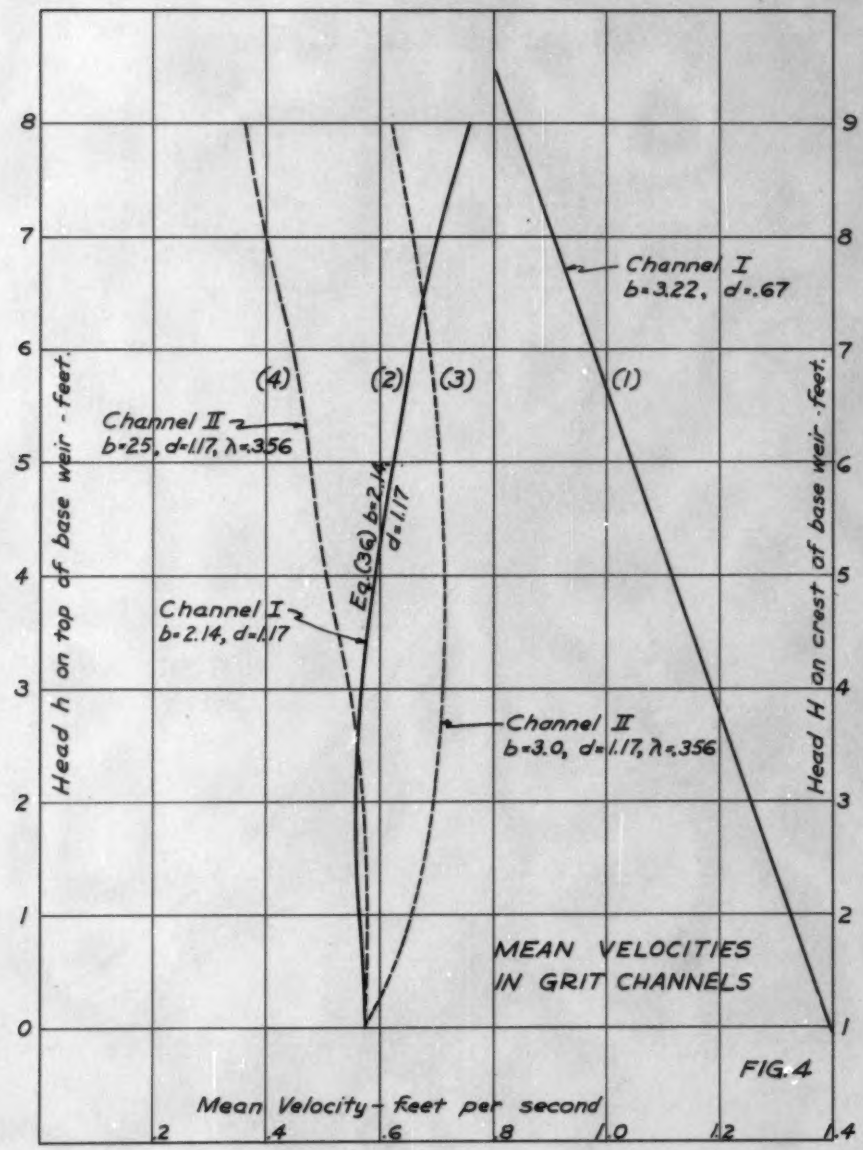
Head h on top of base weir - feet.
Head H on crest of base weir - feet.
Mean Velocity - feet per second
Channel I
b=3.22, d=.67
Channel II
b=2.5, d=1.17, λ=.356
Channel I
b=2.14, d=1.17
Eq.(36) b=2.14
d=1.17
Channel II
b=3.0, d=1.17, λ=.356
(1)
(2)
(3)
(4)
MEAN VELOCITIES
IN GRIT CHANNELS

FIG. 4

Q = Outflow from Basin, cfs.
Free flow for Hb cfs.
Qa = Free flow for He. cfs.
NOMOGRAM FOR THE
VILLEMONTE FORMULA
FOR SUBMERGED WEIRS
$Q = Qa\left(1 - \frac{Qb}{Qa}\right)^{\frac{3}{2}}$
Free flow for $h < k = 10.3 + 7.40h + h^2 - .07h^3$
$h > k = 53.6 + 15.5j - .98j^2$

FIG. 5